Simulation of the Daytime Boundary Layer Evolution in Deep Mountain Valleys

by
David C. Bader
Thomas B. McKee

Department of Atmospheric Science
Colorado State University
Fort Collins, Colorado

Colorado State University

Department of Atmospheric Science

Paper No. 344

SIMULATION OF THE DAYTIME BOUNDARY LAYER

EVOLUTION IN DEEP MOUNTAIN VALLEYS

by

David C. Bader

Thomas B. McKee

Department of Atmospheric Science
Colorado State University
Fort Collins, Colorado
80523

December, 1981

ABSTRACT

A dry, two-dimensional version of the Colorado State University Multi-Dimensional Cloud/Mesoscale Model was used to simulate the cross-valley dynamic and thermodynamic structure in deep mountain valleys during the morning transition period when the nocturnal inversion is destroyed. This model employs a fully elastic set of primitive equations which are transformed to utilize a terrain following coordinate system. The model was forced at the lower surface by a specified sinusoidally varying potential temperature flux approximating the diurnal heating cycle. Each run was initiated with a stable layer filling the valley to ridgetop with a neutral layer above it.

Five simulations were run to examine the effects of valley width, heating distribution and heating rate on the development of the valley boundary layer. The model realistically reproduced the gross features found in actual valleys in both structure and timing. The simulated inversions were destroyed 3½-6 hours after sunrise as a result of a neutral layer growing up from the surface meeting a descending inversion top. Slope winds with speeds of 3-5 m/s developed over both sidewalls 2½-5 hours after sunrise. All cases revealed the development of strongly stable pockets of air over the sidewalls which form when cold air advected up the slope loses its buoyancy at higher elevations. These stable pockets temporarily block the slope flow and force transient cross-valley circulations to form which act to destabilize the valley boundary layer. Gravity waves rapidly redistribute heat across the valley to prevent large horizontal potential temperature gradients

from forming. As a result, even large differences in heating rates between opposing sidewalls do not result in significant cross-valley potential temperature differences. Organized cross-valley circulations and horizontally travelling eddies enhance lateral mixing in the stable layer.

Higher surface albedos resulted in a longer transition period with inversion destruction time dependent on total energy input to the valley atmosphere. The case in which a very high surface albedo over the valley floor prevented the growth of a deep neutral layer, the lapse rate through the stable layer slowly decreased as the inversion top descended. Boundary layers in wider valleys are less influenced by sidewall effects and behave much like boundary layers over flat terrain. Widening the model valley from 1 km to 2 km at the floor produced a 100 m increase in neutral layer depth after two hours.

Uses of the model results include field data interpretation and field experiment preparation. A suggested future use of the model is the examination of the effects of initial lapse rate, sidewall slope and valley orientation on boundary layer development. Other versions of the model could be employed to study nocturnal boundary layer development and along-valley effects.

ACKNOWLEDGEMENTS

TABLE OF CONTENTS

LIST OF FIGURES

1. INTRODUCTION

Mountain valley airflows have been of interest for many years. These thermally induced winds generally tend to blow up valleys from the plains and up inclined surfaces, such as hills and valley sidewalls, during the day and reverse their direction at night. They are most prevalent under conditions where synoptic scale influences are weak, particularly clear skies and weak gradient winds.

An excellent description of mountain-valley winds appears in Flohn (1969) and is briefly summarized here. At night under clear skies, radiative cooling of the earth's surface produces a temperature difference between it and the overlying layer of air. As a result, the air loses heat to the surface and cools (Geiger, 1965). Over flat terrain, a surface-based inversion forms as the cooling gradually extends deeper into the atmosphere, reaching a maximum depth at sunrise. In mountainous terrain, however, the colder, denser air slides down inclined surfaces towards regions of lower elevation, such as valleys and basins. As a consequence of the pooling of cold air in these low-lying regions, strongly stable layers often form in them extending to the height of the surrounding ridges. If unrestricted, the air will flow down the slightly inclined floors of the valleys toward the adjacent plains.

After sunrise, the surfaces slowly warm until they are warmer than the air above them. When this occurs, sensible heat is then transferred to the air, giving it buoyancy; the air begins to move up the inclined surfaces and winds reverse. Wagner (1938) observed a transition period, commencing after sunrise and lasting from three to five hours, when the winds gradually change from downslope and down-valley

to upslope and up-valley. A second transition period begins following the resumption of surface cooling in the early evening when the winds reverse back to down-valley.

Early interest in mountain valley circulations led to several studies in Alpine valleys during the 1930's and 40's, which are reviewed by Defant (1951). This research was directed toward understanding the causes of mountain wind systems and their influence on the local climate. It was these studies, particularly the work of Wagner, which brought attention to the thermodynamic-dynamic interactions in mountainous environments.

As mountainous areas became increasingly populated and industrialized, concern over the dispersion of pollutants in complex terrain heightened interest in mountain-valley wind systems (Davidson, 1961). Carroll and Baskett (1979) found evidence that up-valley winds transported pollutants over long distances from an urban plain to a remote valley. Most attempts to model pollutant dispersion in valleys have either employed overly simplified concepts, such as the ventilated box model (Fox et al., 1973), or as Start et al. (1975) noted, erroneously relied on estimates used for flat or gently rolling terrain. A major reason for the difficulties encountered in pollution modeling is the absence of a detailed understanding of the atmospheric physics which affect dispersion in mountainous areas. To gain knowledge in this field, many organizations have undertaken large research projects to identify the important processes. Principal among these groups are the U.S. Department of Energy (Dickerson and Gudikson, 1980), the U.S. Environmental Protection Agency and the Electric Power Research Institute (Holzworth, 1980) who are all concerned with the impacts on air quality resulting from future development in complex terrain.

In addition, the development of mesoscale storm complexes has been found to be influenced by mountain circulations (Wetzel, 1978). Raymond and Wilkening (1980) detailed the mountain influence on cumulus initiation through observations of dry convection over a mountain range. Orlanski (1975) separated mesoscale phenomena into different time and spatial scales and identified the processes important in each. Although many good models have been developed to deal with features on the larger scales, Pielke (1974) noted that models of the meso-γ scale (2-20 km in the horizontal dimension) are more difficult to formulate because the hydrostatic assumption may not be valid. A second major obstacle to previous model simulation studies of the developing daytime valley boundary layer was the absence of detailed observations to which model results could be compared. Whiteman (1980) helped fill this gap with his exhaustive observational studies of several deep Colorado mountain valleys. He formulated a simple cross-valley thermodynamic model to theoretically describe the inversion destruction process.

As the next step in a continuing mountain valley research program, it was determined that a dynamic model simulation study was appropriate to gain an understanding of the cross-valley physical processes which are important in valley inversion destruction. The model used for this study was a dry, two dimensional version of the Colorado State University Multi-Dimensional Cloud/Mesoscale Model (Tripoli and Cotton, 1981) which has been adapted for this investigation. A major advantage of this model is that its set of fully elastic primitive equations eliminates many of the assumptions inherent in other models. Originally developed to simulate the details of cumulus scale convection (Cotton and Tripoli, 1978; Tripoli and Cotton, 1980), the model has been extended to simulate mesoscale phenomena over irregular terrain.

   Five simulations were run to examine the effects of heating rate,
heating distribution and valley width on boundary layer development.
All were initiated identically with a stable layer filling the valley
underlying a deep neutral layer above ridgetop at sunrise; this struc-
ture is similar to that observed by Whiteman (1980). A specified sur-
face heat flux which approximated the diurnal heating cycle forced the
model at the lower boundary. One simulation consisting of a symmetri-
cally, strongly heated narrow valley was used as a reference case. An
identical configuration was used where the heat flux was halved to
determine the effects of heating rate on boundary layer development.
A third run had the same valley geometry as in the first two cases, but
the heat flux distribution was changed to simulate a valley with a high
albedo over the floor and a lower one over the sidewalls. The width
of the valley floor was doubled in the fourth simulation to ascertain
the influence of valley width on the developing atmospheric structure.
The last simulation was identical to the first, except that a more
realistic, asymmetric heating distribution was imposed. It is believed
that a greater understanding of the important local scale processes can
be gained from the simulation results.

2. BACKGROUND

2.1 Early Studies

Early on it was recognized that mountain-valley wind systems were thermally driven. Wagner (1938) provided one of the first comprehensive theories of both along-valley and cross-valley wind circulations. Using Bjerknes' circulation theorem (Holton, 1977), he concluded that thermal circulations result from the larger diurnal temperature range found in the mountains than in the free atmosphere over the plains.

During the day, the air over the mountains is heated until it is warmer than the free air at the same level, and a heat low forms. Mass descends over the plains, flows up the incline of the mountain range and valley floors then returns above ridgetop. At night, as the mountains cool the air above them, the pressure gradient gradually reverses and results in a circulation where the air descends over the mountains, flows down the incline and rises over the plains. This fundamental theory of the origin of the mountain-plain circulation has been generally confirmed by both observations and model studies.

Wagner emphasized the role of the cross-valley circulation during the transition periods when the winds reverse. He noted that although slope winds tend to reverse direction shortly after sunrise and sunset, along valley wind reversal was delayed until much later. At sunrise, valleys are filled with cold air which has pooled during the previous night. Before the daytime mountain-plain circulation can replace the down-valley winds, this cold air mass must either be warmed or replaced so that the potential temperature in the valley is near that of the air over the surrounding ridges. Once this occurs, the larger scale flow

5

can enter the valley. Wagner proposed that the air is warmed by the cross-valley circulation shown in Figure 1. Air over the sidewalls is warmed by sensible heating from the slopes until it is buoyant relative to air at the same level over the valley center. As a result, the buoyant parcels move up the slope and are replaced by cool air flowing out from the valley center at all levels. The warmed air then returns above the valley and descends into it. This type of circulation requires an upslope wind layer increasing in depth with distance up the sidewall, a feature observed by Moll (1935). At night, the cold sidewalls induce a down-slope circulation, which cools the valley air mass, thereby allowing the down-valley wind to form.

Defant (1949), in a classic paper, integrated many of the relevant mountain winds theories with one of the earliest mathematical descriptions of slope winds. He formulated a conceptual model of the complete diurnal cycle of the mountain-valley wind structure (Figure 2). This model includes many of Wagner's ideas, particularly the role of the cross-valley circulation in the evolution of the along-valley winds. Although this model is incorrect in some details, Whiteman (1980) notes that it is still useful in describing the general diurnal cycle. Through application of Prandtl's (1933) equations for stable flow down an inclined surface, Defant mathematically described the velocity distribution of the slope winds in the lowest layers above the valley sidewalls. A discussion of these calculations will be presented in a later section.

Gleeson (1953) agreed with Wagner's hydrostatic explanation for along valley wind systems, but suggested that cross-valley effects tend to balance Coriolis forces, leaving along-valley pressure gradients as
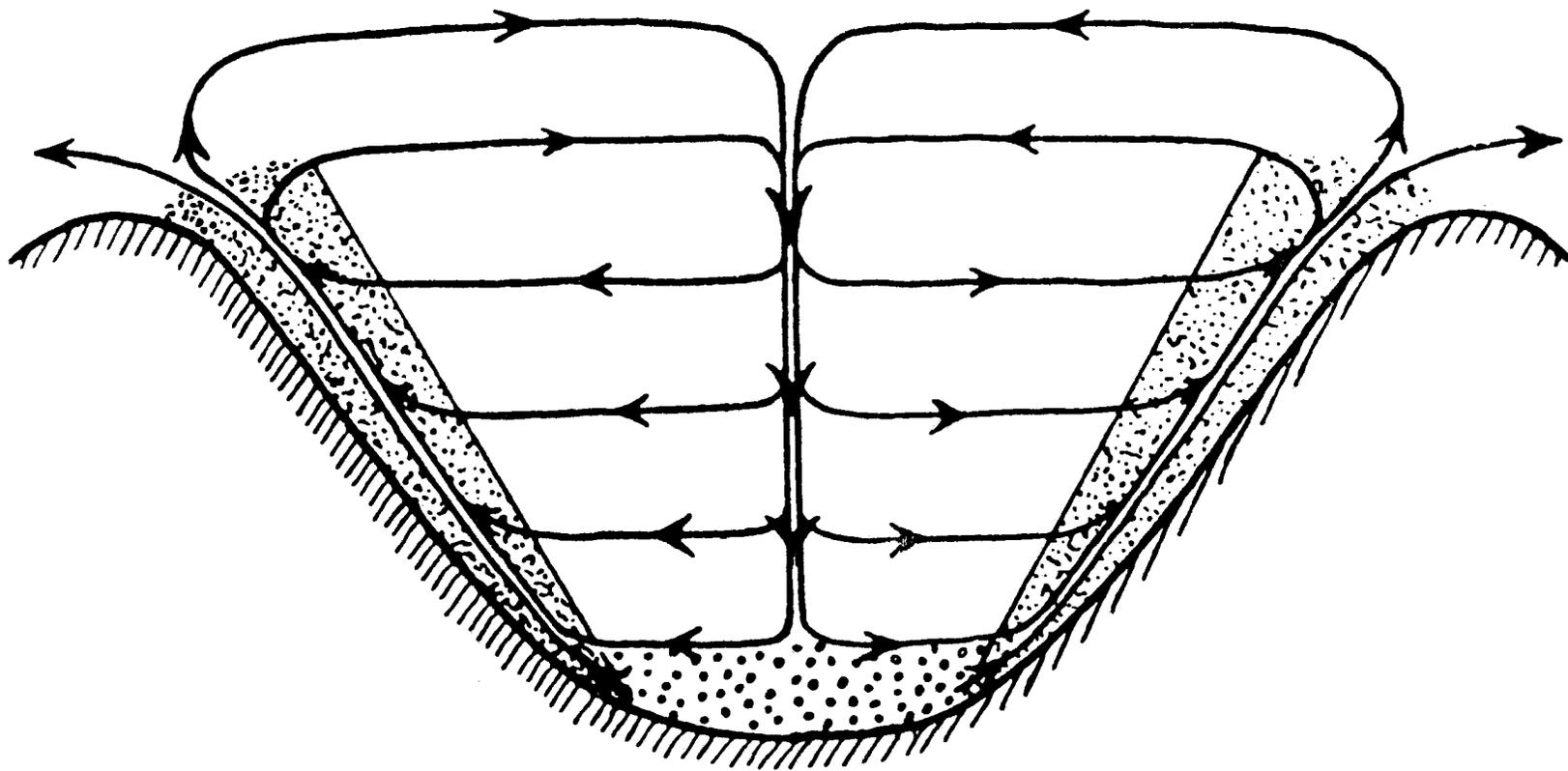
Figure 1. Wagner's (1938) cross-valley circulation model for the morning
transition period.

7

8
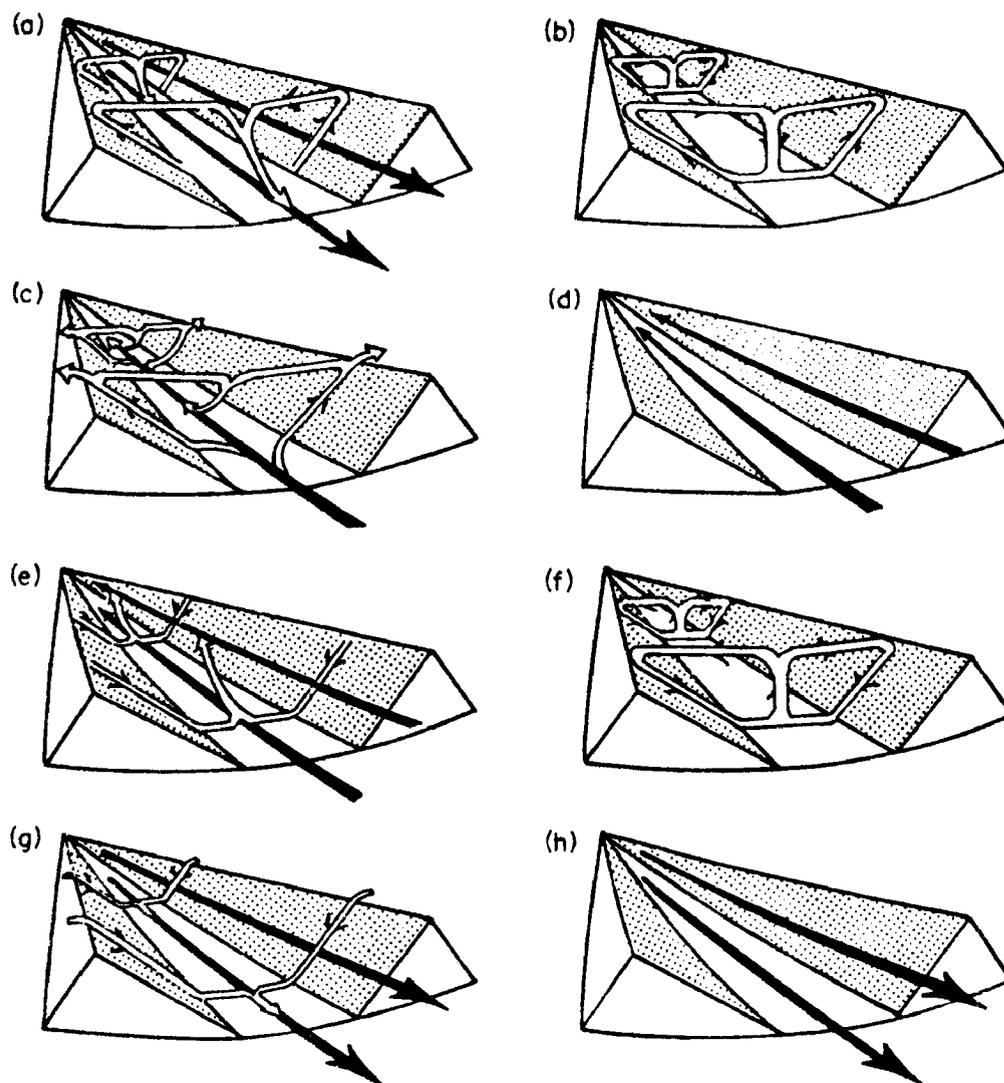
Figure 2. Schematic illustration of the normal diurnal air currents in
           a valley (after F. Defant, 1949).
(a) Sunrise; onset of upslope winds (white arrows), continuation of
     mountain wind (black arrows). Valley cold, plains warm.
(b) Forenoon (about 0900); strong slope winds, transition from moun-
     tain wind to valley wind. Valley temperature same as plains.
(c) Noon and early afternoon; diminishing slope winds, fully developed
     valley wind. Valley warmer than plains.
(d) Late afternoon; slope winds have ceased, valley wind continues.
     Valley continues warmer than plains.
(e) Evening; onset of downslope winds, diminishing valley wind. Valley
     only slightly warmer than plains.
(f) Early night; well-developed downslope winds, transition from valley
     wind to mountain wind. Valley and plains at same temperature.
(g) Middle of night; downslope winds continue, mountain wind fully
     developed. Valley colder than plains.
(h) Late night to morning; downslope winds have ceased, mountain wind
     fills valley. Valley colder than plains. From Reid (1976).

the dominant influence. Scorer (1958), on the other hand, believed that the cross-valley circulation was indeed the mechanism by which the valley air mass warmed. However, his conceptual model (Figure 3) differed dramatically with that of Wagner. Scorer proposed that the air which was warmed near the slope mixed horizontally at all levels while the stable air mass slowly descends to the valley bottom. Whiteman (1980) notes that this mechanism cannot account for Moll's (1935) observations of a wedge shaped upslope layer over the sidewall.

2.2 Observations of Boundary Layer Development in Mountain Valleys

From this early work, it is apparent that an important feature in the diurnal valley wind oscillation is the transition period when downslope and down-valley winds reverse direction. It is during this time that the interactions between the cross-valley and along-valley scales are most significant. Several researchers, among them Whiteman and McKee (1977), Davidson and Rao (1963) and Lenschow et al. (1979) noted that up-valley winds do not appear at all levels simultaneously, but rather descend into the valley from above in the first three to five hours after sunrise. Even when gradient level winds are strong enough to mask the up-valley flow, the overlying winds similarly descend into the valley from above ridgetop (Davidson and Rao, 1963). This phenomenon is consistent with Hawke's (1947) conclusion that it is difficult to replace the very stable layer in the valley at all levels simultaneously.

Davidson and Rao (1958) observed a companion phenomenon is shallow Vermont valleys where the up-valley winds appeared earlier in higher sections of the valley than in lower sections. This led Ayer (1961)
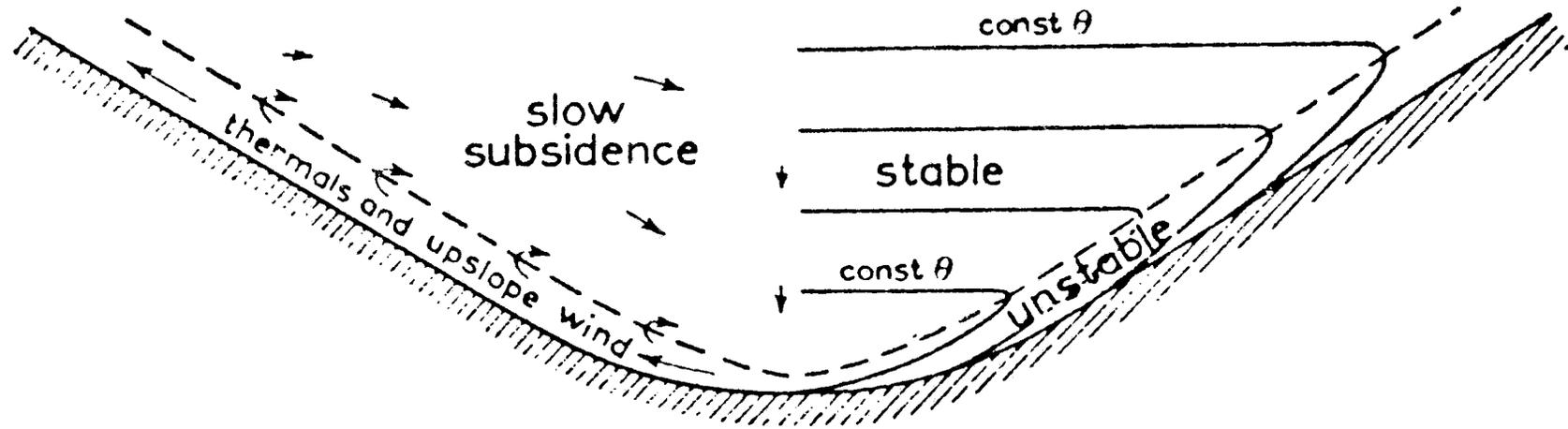
Figure 3. Scorer's (1958) cross-valley circulation model for the
morning transition period.

to conclude that the stable layer initially present through the length and depth of the valley slowly drained out onto the plain. Lenschow et al. (1979) made aircraft observations of boundary layer evolution in shallow valleys embedded in rolling terrain. From their analyses, they concluded that the top of the stable layer was slowly eroded by shear induced turbulence from winds above the valley.

Whiteman and McKee (1978), however, hypothesized that the stable layer slowly descended adiabatically as air was removed from its base. This proposed mechanism was based on observations taken in deep Colorado mountain valleys which show that the stable layer warmed through its depth while the inversion top slowly descended in the valley. They also observed the development of a convective boundary layer (CBL) under the stable air mass along the valley sidewalls and floor. This boundary layer entrains air from the base of the inversion, then warms and transports it to the neutral layer above via the slope flows (Figure 4). Banta and Cotton (1979) and Hahn (1981) observed the growth of similar convective layers under stable air masses in a broad elevated Colorado basin.

2.3 Theories of Boundary Layer Growth

Radiation inversions which form at night over flat terrain are most often destroyed by a convective layer growing up from the surface. Sensible heat is transported from the super-adiabatic surface layer to the neutral convective boundary layer (CBL) in transient buoyant regions called plumes or themals. Warner and Telford (1967) observed that plumes are 100-200 m wide and extend through the depth of the neutral layer. These thermal regions are 1-2 K warmer than their environment
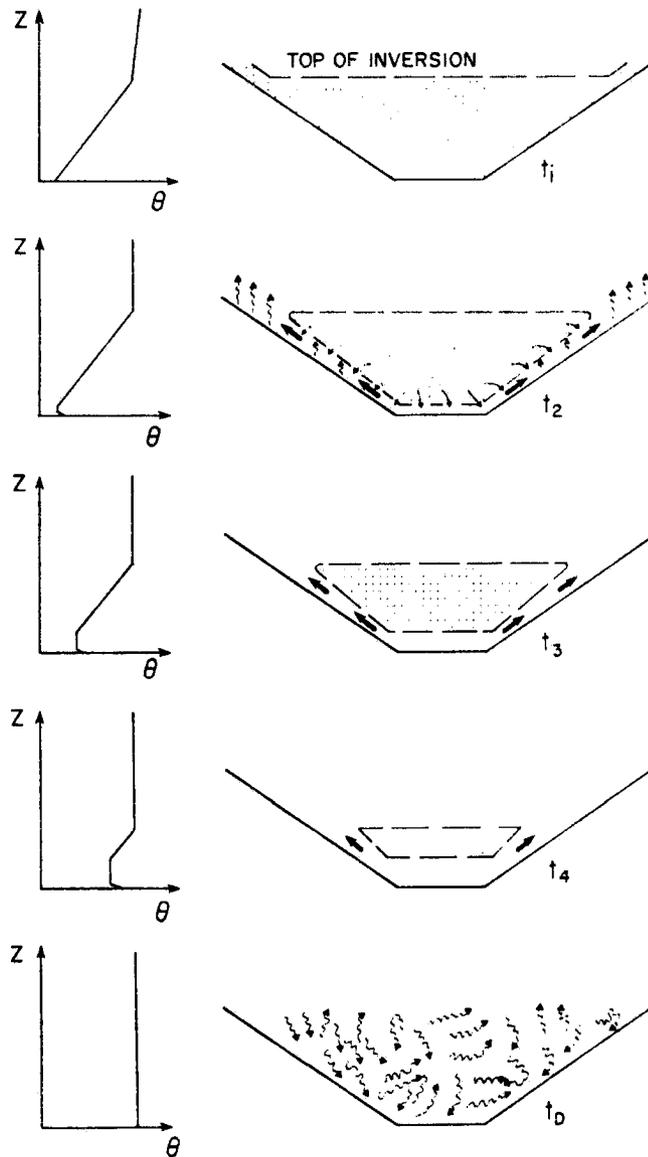
Figure 4. Whiteman's (1980) cross-valley circulation model for the morning transition period. Starting with the top figure which shows the state of the valley at sunrise, a CBL forms under the stable core (shaded area) as the morning progresses. Upslope winds carry mass from beneath the stable air to the overlying neutral layer. As a result, the inversion slowly sinks while the CBL grows until the inversion is destroyed (bottom figure).

and occupy an area of upward motion surrounded by a subsidence field. Lenschow and Stephens (1980) observed that thermals occupy 20-30% of the boundary layer, an estimate they admitted was conservative due to their strict definition of a thermal plume. Their observations show that many small thermals consolidate above the surface layer into larger plumes which remain intact through the depth of the neutral layer. Observations of plumes of different sizes in the surface layer merging into larger themals were also made by Wilczak and Tillman (1980). From their analyses, they determined that thermal plumes are quasi-steady convective elements which last longer than the time required for a parcel to travel through them.

As these thermal plumes rise through the boundary layer, they remain buoyant until they reach the stable layer above. Their positive vertical momentum causes them to penetrate a short distance into the stable region where they entrain some of the surrounding warmer air before descending back into the neutral layer. As this process is repeated by many thermals, a sharp inversion forms in this thin layer of plume penetration between the growing boundary layer and the undisturbed air above. Conceptually, this inversion is often viewed as a temperature "jump" or discontinuity between the neutral and stable layers (Figure 5).

A simple numerical model based on this concept was first developed by Ball (1960) and later refined by Lilly (1968) and Tennekes (1973). This model, sometimes called the jump model, requires initial nonzero values of boundary layer depth, the magnitude of the potential temperature jump (inversion strength) and the stability of the atmosphere above the neutral layer. A specified surface heat flux drives the model
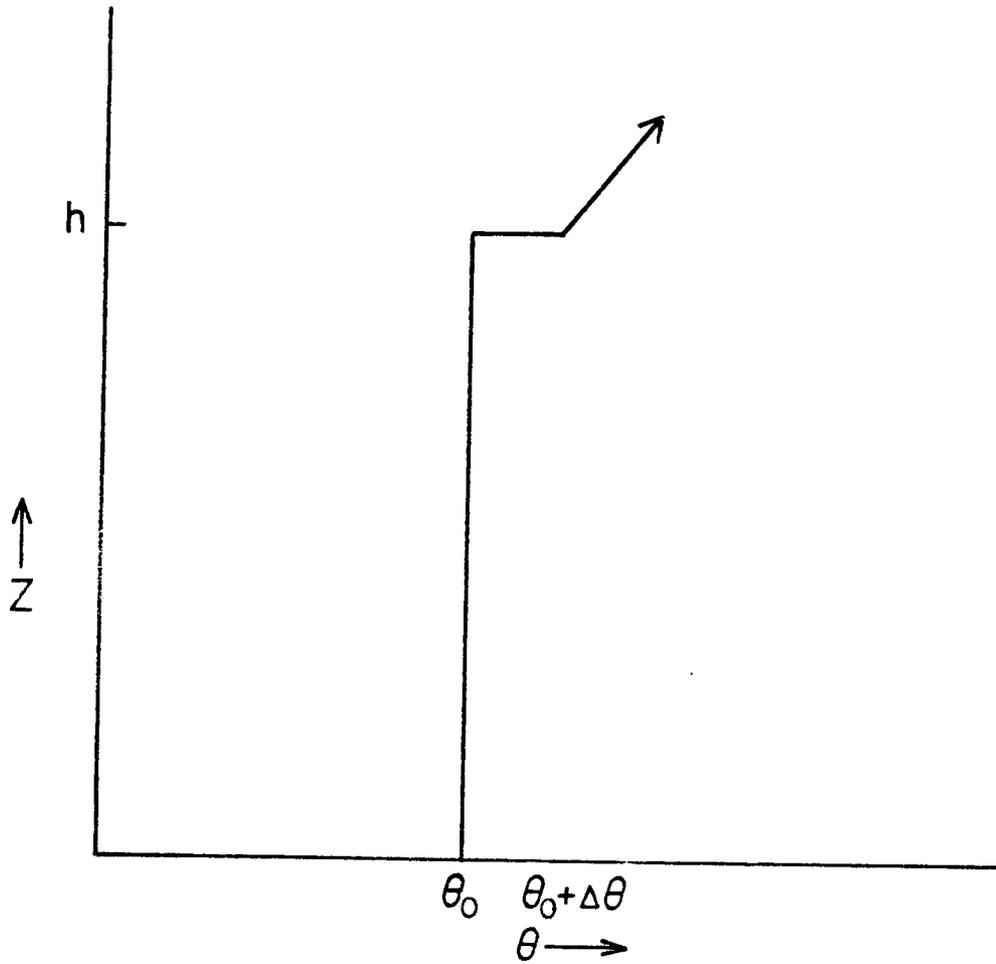
Figure 5. Jump model of boundary layer structure showing
a deep neutral layer extending to elevation,
h, which is topped by an inversion layer of
strength, $\Delta\theta$.

in time with the heat flux at the top of the boundary layer due to entrainment being a fixed function of that at the surface, generally between 10 and 20% (Stull, 1976). Calculated from the model are the depth of the neutral layer and the strength of the inversion. Experiments with this model show that the solution is nearly independent of the initial strength of the inversion after several timesteps. Stull (1973) devised a more elaborate model of boundary layer growth by mathematically describing the entrainment processes at its top. However, experiments with his model yield results very similar to those of the jump model, helping to verify the concepts on which the simpler approach is based. Fundamental to these one-dimensional models is the free convection condition described by Tennekes (1970), where it is assumed that shear production of turbulence is much less then buoyant production in the surface layer.

A more sophisticated one-dimensional model has been formulated by Wetzel (1978). He used a detailed parameterization scheme to simulate the evolution of the surface and stable layers as well as the neutral layer. Included in this model are surface radiation, heat and moisture budgets in addition to a more sophisticated method for the calculation of heat flux at the inversion level. Stull (1976) also developed a more detailed model which includes the effects of gravity waves and turbulent shear on the rate of neutral layer growth. These models are more general and are applicable to a larger number of situations than the relatively limited jump model.

Even more detailed one dimensional models of boundary layer development include the second-order turbulence closure model by Zeman and Lumley (1976). Their equations explicitly calculate the buoyant

counter-gradient transport of energy, which is impossible using eddy viscosity closure schemes. Deardorff (1974) also used a second-order closure scheme in a three-dimensional model of boundary layer growth. From his results, he was able to formulate a one-dimensional growth rate equation based on properties of the neutral and overlying stable layers.

An early attempt to simulate the two-dimensional structure of convection in the boundary layer was made by Malkus and Witt (1959). They used a filtered system of anelastic equations described by Ogura and Phillips (1962) in a vorticity model. Other researchers also used vorticity models to study convective processes. Ogura (1962) succesfully simulated laboratory experiments where a steady state convective element was observed. Lilly (1964) noted several computational problems which had been inhibiting the application of vorticity models and suggested methods to deal with them. A realistic simulation of the growth of the surface and neutral layers under an initially surface based inversion was made by Kuo and Sun (1976). They reproduced many of the observed features found in atmospheric boundary layer, particularly the joining of small thermals in the surface layer to form larger plumes. Their simulations also showed the generation and rapid damping of gravity waves over thermal domes with the accompanying entrainment of warm air from above the inversion.

2.4 Numerical Models of Upslope and Daytime Cross-Valley Air Flow

As mentioned breifly before, one of the earliest numerical investigations of slope winds was Defant's (1949) application of Prandtl's steady-state flow equations. As originally formulated by Prandtl, this model predicts the steady state velocity profile for the flow of a

stable layer down an infinite incline. The equations are developed based on a force balance between gravitational acceleration of the negatively buoyant parcels in the slope layer, and turbulent friction opposing the flow. The equations describing the generation of negative buoyancy by the loss of heat from the slope layers to the underlying surface take into account both conduction and turbulent mixing. The flow is maintained by a constant potential temperature deviation from hydrostatic balance at the surface. Defant calculated the downslope wind profile above one of the sidewalls for a location in the Inn Valley in Austria and compared it to observations (Figure 6). The results show that the model accurately reproduces the observed profile in the lowest 40 m. Above this level, however, the model breaks down as the assumption of confinement of parcels to a level is no longer valid.

Interestingly, Defant also applied the Prandtl equations to upslope flow as well. The fact that he was able to reproduce the velocity profile in the lower levels reveals a characteristic of the upslope layers. For the stable, downslope case, the negatively buoyant air is confined to the surface layers by gravity. In upslope situations, the positively buoyant air would tend to rise away from the surface layers, violating the basic model assumption of confinement of parcels in layers. Since the information shown in Figure 7 shows that the model calculations are reasonably correct in the lowest 30 m, there is the implication of a restraining effect which holds the upslope air near the surface. One possible explanation is that a strongly stable layer above the slope flow layer inhibits penetration of the buoyant parcels through its base, similar to the structure suggested by Whiteman and McKee (1980). Defant computed the time required to warm the valley air mass

18
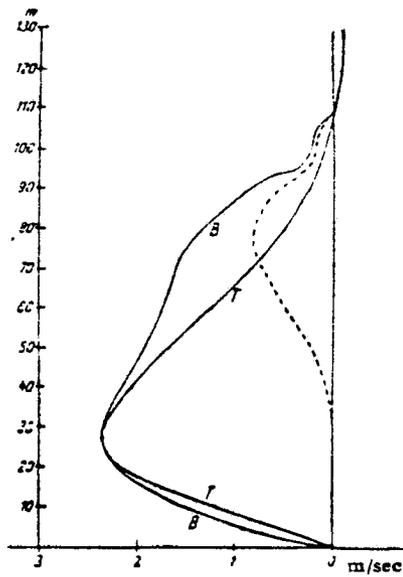
Figure 6. Defant's (1949) comparison of theoretical and
observed downslope wind profile. B = observed
values, T = theoretical values, dashed line =
difference between theoretical and observed.
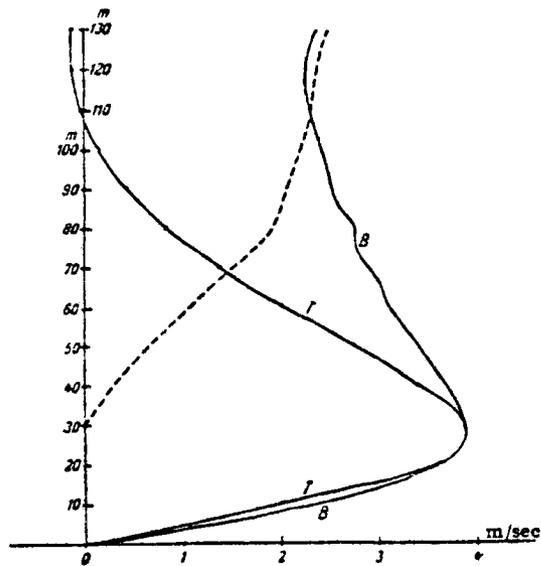
Figure 7. Defant's (1949) comparison of theoretical and
observed upslope wind profiles. B = observed
values, T = theoretical values, dashed line =
difference between theoretical and observed.

through this upslope wind system and found it to be consistent with the observed transition period of three to five hours.

Analytical models of cross-valley circulations have been developed by Gleeson (1951) and Tang (1979). Unfortunately, Gleeson's model revealed only qualitative information. A nondimensional term which served as an independent variable was formed by grouping together several terms which could not be quantified. However, his results show that cross-valley winds increase with both slope angle and the magnitude of the heating difference between the opposite sidewalls. Tang used a Boussinesq system of equations to determine the effects of a steady state wind blowing across the valley above ridgetop on circulation in the valley. His calculations reveal the existence of a separated flow region on the slope where the prevailing wind would tend to counter the slope wind (the lee slope for upslope winds, the windward slope for downslope winds). This feature allows the local slope winds to continue despite the opposing influence of the overlying flow.

Thyer (1966) and Orville (1964) used vorticity models to simulate the development of upslope winds generated by surface heating. Thyer's model became computationally unstable after only two minutes of simulated time. His computations do show the development of an upslope circulation with winds of 0.5-1 m/s and a weak return circulation over the valley center. Orville used a more computationally stable system of finite difference equations and was able to obtain simulations lasting over an hour. His results show the development of a circulation cell originally centered over the slope-plain junction which slowly moves up the slope. Analysis of his simulation for a stably stratified environment reveal that the upslope winds are confined to the region

adjacent to the slope. A weak return flow is also evident with a subsidence field over a broad area of the plain.

Dirks (1969) used a two-dimensional vorticity model to investigate the mesoscale convective effects of the Rocky Mountains and sloping plains to the east. In a three-dimensional study of dry convection for the same region, Hughes (1978) used the hydrostatic, primitive equation model formulated by Pielke and Mahrer (1975). His simulations failed to produce upslope flows in the presence of strong gradient winds on convectively active days, a result contrary to observations. This was probably due to the coarse vertical model resolution and the overly diffusive nature of the model equations mixing westerly momentum to the surface. Gal-Chen and Sommerville (1975a, b) used a system of anelastic equations in a transformed coordinate system to simulate the development of convective cells over a hill. They were able to reproduce many features of upslope circulations, including the development of a convective boundary layer under a stable atmosphere.

3. EXPERIMENTAL DESIGN

Whiteman (1980) identified many factors which determine the length of time required for valley inversions to break. Among these are energy input, valley geometry and stability of the inversion layer. For this initial study, only the effects of two were examined. The experimental program was designed to determine the effects of heating distribution and valley width, factors which cannot be examined adequately with Whiteman's thermodynamic approach. Before the simulation study is detailed, a description of the dry, two-dimensional version of the CSU Milti-Dimensional Cloud/Mesoscale Model (Tripoli and Cotton, 1981) is presented.

3.1 Coordinate Transform

To allow the specification of irregular topography, a terrain following coordinate system developed by Gal-Chen and Sommerville (1975a) and extended by Clark (1976) is employed. Known as a "sigma z" system it results from the transformations

$$x^* = x \ ,$$

$$z^* = \frac{z - z_s(x)}{H - z_s(x)} \, H \ , \tag{1}$$

where x and z are the Cartesian independent spatial variables, x^* and z^* are the transformed independent spatial variables, z_s is the height of the surface, and H is the elevation of the horizontal top of the model domain. From Clark, the spatial derivative of any quantity A can be written as

$$\frac{\partial A}{\partial x_i} = \frac{1}{a}\left[\frac{\partial ab^{ij}A}{\partial x_j^*}\right]$$

$$a(x^*) = 1 - z_s(x^*)/H = \frac{\partial z}{\partial z^*} \qquad (2)$$

where the transformation tensor, b^{ij} is defined by

$$b^{ij} = \begin{bmatrix} 1 & 0 & \frac{1}{a}\frac{\partial z_s}{\partial x}\left(\frac{z^*}{H}-1\right) \\ 0 & 0 & 0 \\ 0 & 0 & \frac{1}{a} \end{bmatrix} . \qquad (3)$$

It should be noted that the three-dimensional form of tensor quantities is used to maintain the conventional notation. However, it is understood all y derivatives as well as v velocity components are set to zero in the two-dimensional simulations described here. From these equations it can be shown that the cartesian and transformed velocities are related by

$$u^* = u_1 ,$$

$$w^* = u_3 + u_1 ab^{13} . \qquad (4)$$

3.2 Theoretical Development of Model Equations

The set of model equations was formulated to describe perturbations about a dry, hydrostatic base state. Finite difference forms of the momentum, continuity and thermodynamic energy equations were used to predict velocity, density and potential temperature at points on a staggered grid system. Pressure and temperature are then diagnosed from the predicted quantities.

Using the notation of Cotton and Tripoli (1978) and others, any variable A can be decomposed as

$$A = \overline{A} + A'' , \tag{5a}$$

where the overbar represents an average value resolvable on the time and space scales of the model and the double prime denotes an unresolvable turbulent fluctuation about this average. The mean value can be further decomposed as

$$\overline{A} = A_0(z) + \overline{A}' , \tag{5b}$$

where A_0 is the temporally and horizontally invariant base state and $\overline{A}'$ is the average deviation from this state. Because it is conserved in adiabatic processes, potential temperature is used as the thermodynamic variable and is defined by Poisson's equation,

$$\theta = T\left(\frac{P_{oo}}{P}\right)^{R/c_p} . \tag{6}$$

Here, θ is the potential temperature, T is temperature and P is pressure. The constant P_{oo} is a reference pressure, taken to be 1000 mb, and R and c_p are the gas constant and constant pressure specific heat of dry air, respectively. Substitution of (6) into the ideal gas equation yields

$$P\left(\frac{P_{oo}}{P}\right)^{R/c_p} = \rho R\theta . \tag{7}$$

The base state is assumed to obey both (6) and the hydrostatic relation and is therefore defined by

$$\theta_0 = T_0\left(\frac{P_{oo}}{P_0}\right)^{R/c_p} , \tag{8}$$

and

$$dP_0/dz = -\rho_0 g , \tag{9}$$

where P_o, ρ_o, θ_o and T_o are the base state pressure, density, potential temperature and temperature. If it is assumed that the deviations from the base state are small for these quantities, (7), (8) and (9) can be combined and linearized to yield the following equations relating pressure and temperature deviations to the predicted values for potential temperature and density:

$$\frac{1}{\gamma} \frac{\overline{P}'}{P_o} = \frac{\overline{\rho}'}{\rho_o} + \frac{\overline{\theta}'}{\theta_o} \, , \tag{10}$$

$$\frac{\overline{T}'}{T} = \frac{\overline{\theta}'}{\theta} + R/c_p \frac{\overline{P}'}{P} \, . \tag{11}$$

The constant γ is the ratio of the constant pressure and constant volume specific heats of dry air.

The momentum equation in the tansformed domain is

$$\frac{\partial(\rho_o \overline{u}_i)}{\partial t} + \frac{1}{a} \frac{\partial(ab^{ij} \overline{p}')}{\partial x_j^*} + \overline{\rho}'g \, \delta_{i3} =$$

$$- \frac{1}{a} \left[\frac{\partial(ab^{jk}\rho_o \overline{u_i u_j})}{\partial x_k^*} - \overline{u}_i \frac{\partial(ab^{jk}\rho_o \overline{u}_j)}{\partial x_k^*} \right] - \frac{1}{a} \frac{\partial(ab^{jk}\rho_o \overline{u_i'' u_j''})}{\partial x_k^*} \tag{12}$$

where δ_{i3} is the Kroneker delta function and g is the gravitational acceleration. The terms on the first line comprise the acoustically active variables which are capable of propagating disturbances at sonic velocity. On the second line are the non-acoustic advection and turbulence terms which are active on the longer gravity wave time scale. The Coriolos terms have been neglected because they are unimportant on the model's spatial scale. The fully elastic continuity equation predicting density deviations is given by

$$\frac{\partial \overline{\rho}'_a}{\partial t} + \frac{1}{a} \frac{\partial}{\partial x_j^*} (ab^{ij}\rho_o \overline{u}_i) = 0 \, , \tag{13}$$

where the non-linear divergence term has been replaced by the linearized verson. Tripoli and Cotton (1981) justify this replacement with both a scaling argument and experimental results.

The thermodynamic variable in the model, ice-liquid water potential temperature $(\theta_{i\ell})$, is conserved in all adiabatic motions and phase changes of water substance. However, since all water is eliminated from the model in these simulations, $\theta_{i\ell}$ reduces to potential temperature. Therefore, the predictive form of the thermodynamic energy equation used here is

$$\frac{\partial \overline{\theta}_i}{\partial t} = -\frac{1}{\rho_0 a} \left[\frac{\partial ab^{jk}}{\partial x_k^*} \rho_0 \overline{u_j \theta_i} - \overline{\theta}_i \frac{\partial (ab^{jk} \rho_0 \overline{u}_j)}{\partial x_k^*} \right]$$
$$- \frac{1}{a} \left[\frac{\partial ab^{jk} \overline{\theta_i'' u_j''}}{\partial x_k^*} \right] \quad , \tag{14}$$

where the right hand side of the first line represents the contribution of advection to the local change in potential temperature and the second line represents the turbulent contribution.

The turbulent flux terms $\overline{u_i'' u_j''}$ and $\overline{\theta_i'' u_j''}$ are parameterized using an eddy-viscosity closure scheme described by

$$-\overline{u_i'' u_j''} = \frac{K_M}{a} \left[\frac{\partial (ab^{j\ell} \overline{u}_i)}{\partial x_\ell^*} + \frac{\partial (ab^{i\ell} \overline{u}_j)}{\partial x_\ell^*} \right] \quad , \tag{15}$$

$$-\overline{\theta'' u_j''} = \frac{K_H}{a} \frac{\partial (ab^{j\ell} \overline{\theta}_i)}{\partial x_\ell^*} \quad , \tag{16}$$

where K_H and K_M are the eddy exchange coefficients for heat and momentum and are related to each other by

$$K_H / K_M = 3 \quad . \tag{17}$$

This value is the probable upper limit for atmospheric processes, but is still a realistic ratio (Gal-Chen and Sommerville, 1975a). The eddy exchange coefficients are computed from

$$K_m = \frac{(0.25)^2}{\sqrt{2}} \Delta^2 |D|^2 \left(1 - \frac{K_H}{K_M} R_i\right) , \qquad (18)$$

where Δ is the mixing length and 0.25 is an arbitrary coefficient found to suppress numerical noise. The magnitude of the deformation tensor, $|D|$, and the Richardson number, R_i, are defined by

$$|D| = \left[\sum_j \sum_k \left(\frac{\partial \overline{u}_j}{\partial x_k} + \frac{\partial \overline{u}_k}{\partial x_k}\right)^2\right]^{\frac{1}{2}} , \qquad (19)$$

$$R_i = g/\theta \; \frac{1}{|D|^2} \cdot \partial \overline{\theta}_i / \partial z \; . \qquad (20)$$

The correction term $K_H/K_M R_i$ is a buoyancy adjustment factor (Cotton, 1975) to account for enhancement or suppression of turbulence due to local stability. In neutral or unstable layers, both the horizontal and vertical mixing lengths are simply the spacings between grid points. However in stable layers, where the eddy-viscosity scheme is overly diffusive, the vertical mixing length is arbitrarily reduced to 25 m.

3.3 Model Domain

The model domain is shown in Figure 8. With the boundary conditions used in this model, it is necessary to have an interior domain boundary and a second exterior mesoscale boundary. The total width of the domain, the sidewall slope and length, and the location of the mesoscale boundaries were identical for all of the simulations. For all but one experiment, the valley width, w, was 1 km and the length of the ridge, ℓ, was
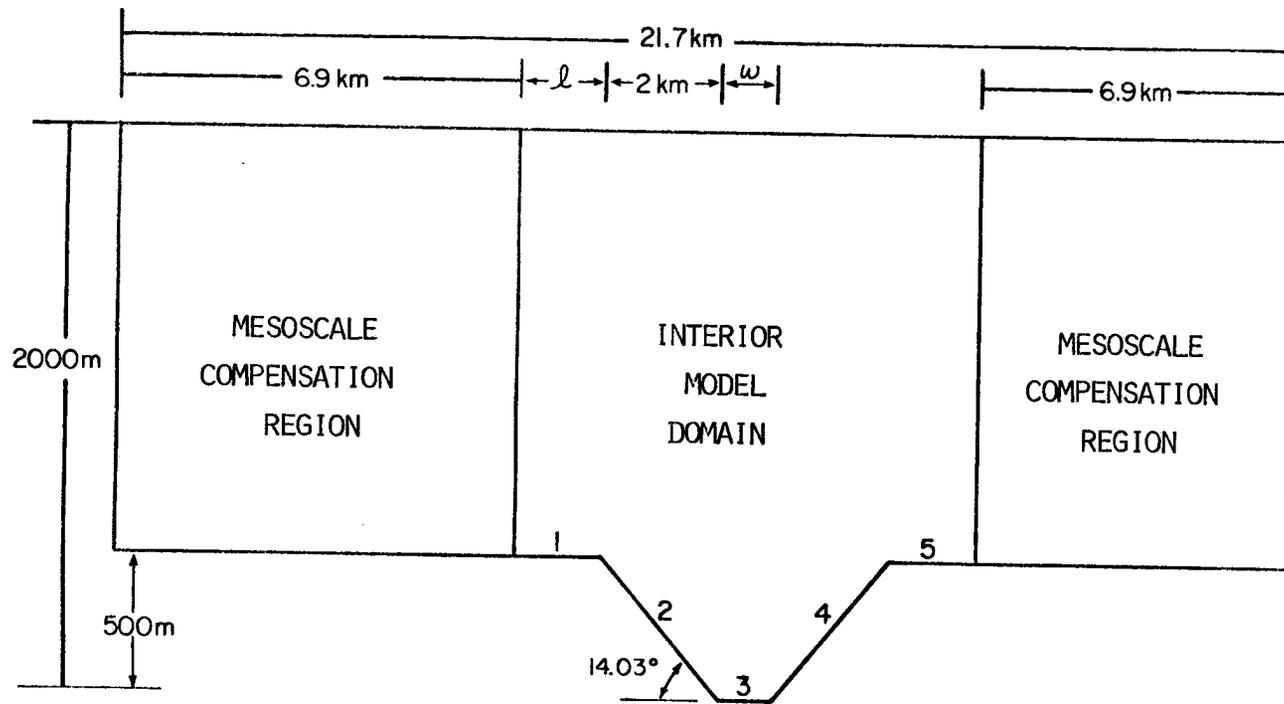
Figure 8. Model domain (not to scale).

1.95 km. For the one exception, w was 2 km and ℓ was 1.45 km. Prelim-
inary experiments revealed that the solution was unaffected by the
shorter ridge. The five surfaces are numbered for future identification.

The interior domain was divided into 80 equidistant grid columns
100 meters apart. Vertical spacing was uneven due to both the transform
and telescoping grid above the first 11 points. The $z_s = 0$ level was
coincident with the valley floor. A grid spacing above the floor of
50 m was used to an elevation of 500 m, above which was a logarithmi-
cally expanding grid with twelve additional levels extending to 2000 m.
Vertical grid spacing for points above elevated terrain was calculated
using (1) to obtain a rectangular transformed grid.

3.4 Finite Differences

The model equations were numerically integrated on a staggered mesh
described by Cotton and Tripoli (1978). This type of grid centers
scalars in each grid box with velocities defined normal to the sides.
When used with standard second order spatial finite differencing, this
system conserves quadratic properties and suppresses numerical diffusion.

A time differencing scheme described by Klemp and Wilhemsen (1978)
is used to separately integrate the acoustic and non-acoustic terms in
the predictive equations. The acoustically active terms were stepped
forward on a smaller time step using a semi-implicit scheme. After a
specified number of acoustic steps, the non-acoustic terms are stepped
forward once using a leap-frog scheme to complete the integration. An
Asselin filter is employed to prevent solution separation. To meet
linear stability criteria for these simulations, the acoustic variables
were integrated 40 times during each long time step of 2 s.

3.5 Boundary Conditions

The top boundary condition was simply a wall which allowed neither mass nor energy to propagate through it. The method for determination of quantities at the lateral boundaries coupled the Orlanski (1976) radiation boundary condition with a mesoscale adjustment procedure formulated by Tripoli (1981). In this arrangement, variables at the domain boundary adjust to a mesoscale influence, thereby inhibiting runaway circulations. The mesoscale boundaries in Figure 8 allow no mass or energy to propagate through them and the large mesoscale region helps stabilize the interior domain.

As originally formulated by Orlanski, variables at the boundary are calculated from

$$\partial \phi / \partial t = -C_\phi \, \partial \phi / \partial x \, , \qquad (21)$$

where ϕ is any variable and C_ϕ is the phase speed of a propagating wave. For the outflow condition, C_ϕ is calculated from values of ϕ at neighboring grid points while the phase speed is set to zero for inflow conditions. The mesoscale adjustment allows the temperature and pressure in the mesoscale region to influence the quantities at the domain boundary. The scalar quantities are defined for each level at a grid point midway between the mesoscale and domain boundaries. It is assumed that there is no gradient outside of this mesoscale point. Computations of quantities at the mesoscale and first domain scalar and w points are then carried out identically to the other model points. For the u velocity component equation, (21) is modified to account for the mesoscale pressure influence to yield the expression for normal velocity at the domain boundaries,

$$\frac{\partial u}{\partial t} = -C_u \frac{\partial u}{\partial x} \pm \frac{1}{\rho_0} \left(\frac{<P> - P_m}{D} \right) .$$

In this equation, $<P>$ is the average pressure on the level in the model domain, P_m is the pressure in the mesoscale region and D is the distance between the domain center and the mesoscale grid point. This extra term damps artificial accelerations at the boundaries as mass buildup in the mesoscale region feeds back into the pressure adjustment.

The surface layer parameterization is adapted from the formulation by Louis (1979). Surface friction velocity is computed for the bottom grid boxes based on the u velocity component and a specified surface temperature flux. The surface temperature flux for each of the five model surfaces was described by

$$\overline{w'\theta'}_s = s_i \ \overline{w'\theta'}_{max} \sin (\pi t/T) , \qquad (23)$$

where the subscript s denotes surface layer properties. In all runs, the period, T, was set to twelve hours to approximate the diurnal solar cycle. The horizontal distribution and magnitude of the amplitude, $\overline{w'\theta'}_{max}$, was constant for each run but was changed between simulations to determine its influence on the boundary layer development. The heating factor, s_i, is a constant coefficient defined for the ith surface. By using different values for these constants, the relative heating distribution can be specified along the lower boundary.

The initial structure of the model domain was identical for all simulations. A sounding with a potential temperature lapse rate (dθ/dz) of 0.025 K/m in the valley with a neutral layer above was input to model. A slightly stable layer was imposed in the upper levels of the domain to create a more realistic model atmosphere. The specified sounding

values were then fit to a cubic spline to yield a horizontally homogeneous base state shown in Figure 9. All initial winds were set to zero.

3.6 Description of Experiments

Characteristics of the five separate simulations run to examine the effects of heating and valley width appear in Table 1. The baseline run (Case 1) modeled a 1 km wide, symmetrical heated valley with $\overline{w'\theta'}_{max}$ = 0.25 K m/s.. This simulation was chosen as a reference because it is typical of conditions in many valleys for which there is adequate observational data. The amplitude of the potential temperature flux was inferred from observational data (Sundararajan and Macklin, 1976), for clear, dry conditions. The heating factor for the sidewalls, s_2 and s_4, is simply the cosine of the slope angle. These restrictions reduce the simulation to a somewhat unrealistic situation where an east-west Colorado mountain valley is modeled as though it was located at the equator on the day of the equinox. However, it was felt that a symmetric simulation was necessary to better determine the physical processes controlling inversion destruction.

Case 2 was identical to Case 1 except that the amplitude of the heating function was halved. Case 3 was an attmept to model a winter situation in which the albedo of the snow covered valley floor is higher than that of the forested ridges and sidewalls. For this simulation, the heating over the elevated and sloping surfaces was 60% of Case 1 and the temperature flux form the valley floor was reduced to 20% of the reference case. With this configuration, the total energy input to the model from the valley surfaces were approximately equal for Cases 2 and 3.
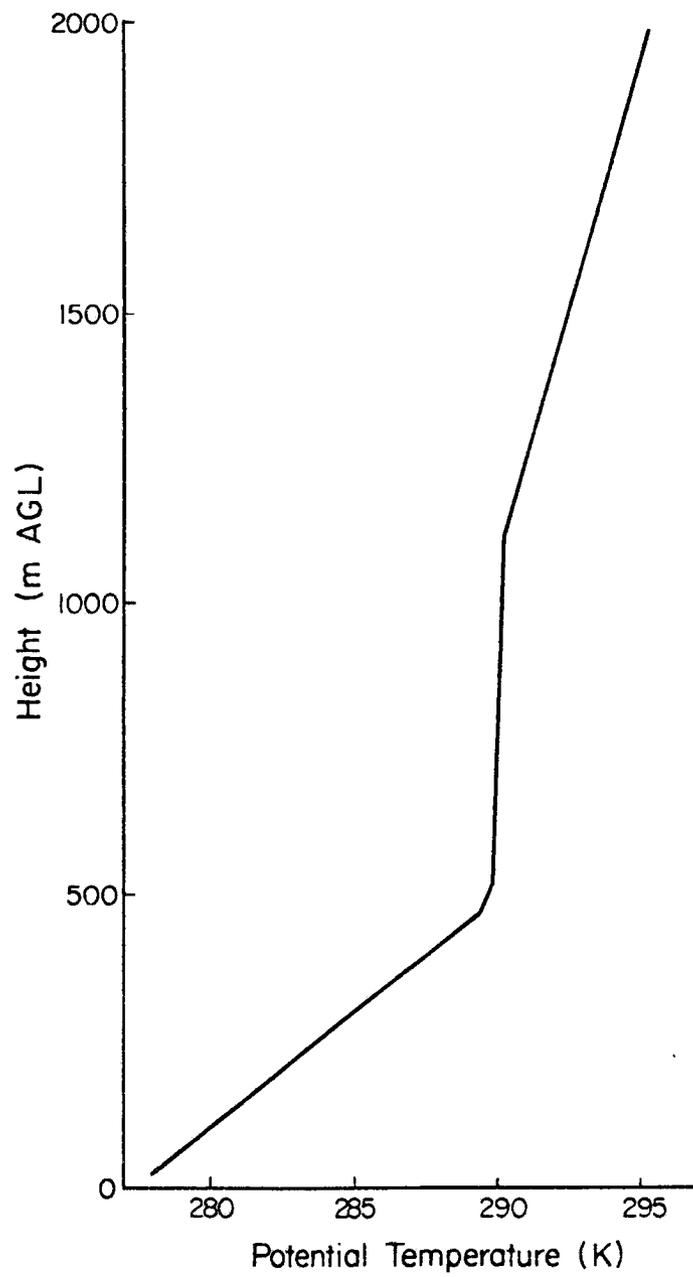
Figure 9. Initial model potential temperature
           profile.

TABLE 1. Description of Model Parameters

	Case 1	Case 2	Case 3	Case 4	Case 5
Valley width (w)	1 km	1 km	1 km	2 km	1 km
Ridge length (ℓ)	1.45 km	1.45 km	1.45 km	0.95 km	1.45 km
Amplitude of Potential Temperature Flux ($\overline{w''\theta''}_{max}$)	0.250 K ms^{-1}	0.125 K ms^{-1}	0.150 K ms^{-1}	0.250 K ms^{-1}	0.250 K ms^{-1}
Heating factors:					
S_1	1.0	1.0	1.0	1.0	1.0
S_2	0.97	0.97	0.97	0.97	1.17
S_3	1.0	1.0	0.33	1.0	1.0
S_4	0.97	0.97	0.97	0.97	0.77
S_5	1.0	1.0	1.0	1.0	1.0

Cases 4 and 5 examined some of the influences of valley geometry on inversion destruction. In Case 4, the valley was widened to 2 km and each ridge reduced by 0.5 km in length, while the heating factors were identical to Case 1. A more realistic heating distribution was imposed on the valley in Case 5. Based on calculations for direct solar radiation on inclined surfaces (Revfeim, 1976), the heating factors for the five surfaces were adjusted to model an east-west valley lying at 40° N latitude. The amplitude of the temperature flux was set to 0.25 K m/s on the horizontal surfaces and heating factors for the sidewalls were computed based on the assumption that the temperature flux is proportional to the distribution of direct solar radiation. In this way, the total heat input is identical to the reference case, but the distribution is altered.

4. RESULTS AND ANALYSIS

Model output included instantaneous fields of wind, temperature and pressure at intervals of ten minutes simulated time. Also, ten minute averages of vertical velocity and potential temperature over the valley center at each level were computed. These were calculated by taking the time average of the mean values for the center five grid points at each level for each time step. In addition, every minute, instantaneous values for all model variables were written on a permanent file for later analysis. For the wide valley case (Case 4), the data were saved on file only once every 2.5 minutes of model time and the ten minute averages over the valley center were not computed. Since this was the first simulation actually run on the computer, it was not apparent that the instantaneous fileds would be inadequate until the results were obtained. However, the instantaneous potential temperature fields were less prone to short term fluctuations than the wind fields and were, therefore, more suitable for analysis.

The contour-vector plots show five minute average values computed from the instantaneous fields saved on file. For Cases 1, 2, 3 and 5 these are six point averages of instantaneous fields saved every minute. The Case 4 plots show three point averages of fields saved every 2.5 minutes. To increase the resolution of the graphs, only the lowest fourteen levels were plotted to observe the physical features below the inversion and in the lower part of the neutral layer. In all of these figures, the vertical coordinate has been exaggerated five times with respect to the horizontal for greater clarity. The length of the wind vectors are not exaggerated, however.

4.1 Case 1 Results

In this simulation the amplitude of the potential temperature flux was set to 0.25 K m/s with a symmetric distribution imposed. The development of the valley boundary layer from its initial state until the stable layer is removed is shown in Figures 10 (a-j). Since the valley is symmetric about the axis (broken vertical line) only the south half is shown. The initial state (also the base state) is shown in Figure 10a. A constant lapse rate ($\partial\theta/\partial z$) of 0.025 K/m extends to the ridge top. A less stable transition layer between the stable valley core and the neutral layer was formed by the cubic spline initialization and is apparent by the distance between the 289 K and 290 K isentropes. The plot is somewhat deceptive, however, as the base state temperature at the 528 m level is 289.94 and marks the elevation at which the sharp gradient ends. Therefore, the 290 K isentrope is used as a convenient marker for the inversion top.

The first feature which is observed to develop is the weak eddy circulation at the ridge-sidewall junction after 40 minutes (Figure 10b). The peak up-drafts are 0.7 m/s located over the ridge 400 m from the corner. A shallow upslope with a maximum speed of 1.0 m/s feeds the circulation from the upper extent of the sidewall. The 290 K isentrope can be seen dropping as the ridge warms slightly. Perturbations in the potential temperature field over the lower sidewall can be seen as the surface layer warms.

Forty minutes later, the circulation over the ridge has intensified as the heating there begins to form a thermal low pressure region (Figure 10c). The peak winds are now 2.6 m/s over the ridge and the upslope flow feeding the circulation extends down to the 375 m elevation level,

but is still weak (0.5 - 1.0 m/s). Development of the convective bound-
ary layer (CBL) over the lower sidewalls and floor is clearly evident
by this time. An eddy over the floor-sidewall corner can be seen ini-
tiating an upslope wind. These lower levels have warmed to over 280 K
from their initial values between 278-279 K. Surface heating has
created disturbances which propagate through the stable air in the form
of gravity waves. An interesting feature can be observed over the side-
wall between the 125 and 175 m elevation levels. The top of CBL is
capped by a very stable region which can be identified by the packing
of isentropes. Above this level, a much less stable region has formed
over the sidewall resulting from a horizontal convergence of mass flow-
ing outward from the valley center. The 290 K isentrope has descended
almost to ridgetop to more clearly mark the inversion top.

Figure 10d shows the state of the valley atmosphere after 100 min-
utes. The eddy over the lower corner has become more organized as the
heating strengthened. This circulation has warmed the CBL, but is con-
fined to the lowest 175 m as the strongly stable layer over the sidewall
has prevented the upslope from penetrating through this level. A second
enhanced stability region is apparent over the sidewall between the 225
and 275 m elevation levels. As before, the overlying air is less stable
as air from the valley center converges over the slope. The mass flow-
ing outward from the valley center between 375 and 425 m levels forms an
elevated region of increased stability over the valley center. There is
no upslope wind below this elevation; the air can be seen turning and
converging over the valley center, and a layer with a much weaker lapse
rate forms under the strongly stable region. Weak subsidence over the
valley feeding the upper level divergence is clearly evident by this

time. The upslope thickness has increased at the sidewall summit and the accompanying cold advection has caused the inversion top to have a concave upward shape.

Different stabilities in regions over the sidewall have created two distinct circulations separated by the strongly stable layer in the valley center. The lower one is somewhat masked by the circulations of the growing CBL, but is shown by the lower, board dark arrow. Air moves up the heated sidewall in the slope flow until it encounters the strongly stable layer and loses its buoyancy. It then turns and flows toward the valley center. The other broad arrow shows the upper circulation where mass diverges from the valley center and feeds the upslope layer over the upper levels of the sidewall.

Just ten minutes later (Figure 10e) the upslope has penetrated the stable regions and the lapse rate over the sidewall is much more uniform. For the first time, the upslope flow is continuous over the entire length of the sidewall with speeds ranging from 0.1 to 1.0 m/s. Cross-valley winds can be seen beginning to mix out the regions of uneven stability over the valley center. The CBL has grown to almost 200 m and the lower portion of the boundary layer has warmed as a result of the circulation in the bottom layers of the valley. A subsidence rate of 0.05 - 0.1 m/s in the lower portion of the valley has lowered the 284 K isentrope over 50 m. The maximum wind speeds over the ridge are still near 2.7 m/s.

After 130 minutes the inversion layer has a more uniform shape as a result of the cross-valley flows. As can be seen in Figure 10f, the inversion top, still at ridgetop, is more horizontal. The stable core between the CBL and ridgetop now has a nearly constant lapse rate, but is considerably less stable than the original state of the valley at

sunrise. The upslope winds now range between 0.5 and 1.5 m/s. The cross-valley circulations have nearly diminished, except in the very upper levels of the inversion. The potential temperature in the CBL is approximately 284 K and the layer is over 200 m deep. Over the ridge, a strong eddy circulation has developed and created an intense updraft with vertical velocities in excess of 1.0 m/s.

Figure 10g shows the valley atmosphere after 150 minutes of model time. The lapse rate through the stable layer and the speed of the upslope wind remained nearly constant. The ten minute averages reveal a general subsidence of 0.03 m/s through all levels in the stable core. The vector plot, however, shows organized areas of descending air and not a uniform motion. As the air enters the CBL, it is swept into the upslope flow. The upslope layer now shows no sign of increasing thickness with elevation and the isentropes have a nearly horizontal shape. The stability of the layer has been reduced to 0.013 K/m, roughly half the original lapse rate.

After 170 minutes (Figure 10h), the valley atmosphere has reached a state similar to that hypothesized by Whiteman (1980), in which the stable layer slowly descends and feeds the upslope flow. The 290 K isentrope has dropped 50 m over the valley center. Organized areas of descent rather than uniform sinking are again apparent, but in different locations. It appears that these motions are transient circulations that develop for several minutes in preferred areas then diminish. Over longer time frames, they result in a near constant subsidence rate for the stable layer as a whole. The upslope wind strength has increased to 1.5 - 2.0 m/s. Cold advection in the slope layer has again created a concave upward shape in the isentropes.

Twenty minutes later (Figure 10i), the upslope wind speed has become more uniform over the length of the sidewall and averages close to 1.5 m/s. The heat low over the ridge can be seen accelerating air laterally from above the inversion to a maximum wind speed of 3.3 m/s. Subsidence has lowered the 290 K isentrope an additional 50 m and the now rapidly growing CBL is 350 m deep over the valley center. After 210 minutes, the inversion is nearly broken (Figure 10j) and the organized daytime circulation is developing. The upslope winds have strengthened even more to 2.0 - 3.0 m/s and are fed by a 0.5 m/s downdraft over the valley center. The CBL approaches the inversion top at 375 m elevation.

The ten minute averages of potential temperature over the valley center showing the evolution of the thermal structure are shown in Figure 11. These profiles show average values for the ten minute period ending at the labeled time. Starting with the sunrise profile on the far left, the development of the thermodynamic structure resulting from the valley dynamics can be traced as the boundary layer is heated.

CBL formation can be observed after just 60 minutes of model time as eddy circulations confined to the lowest layers mix the heat coming from the valley floor and lower sidewalls. The effects of the formation of the strongly stable "pockets" of air over the sidewalls which block the slope flow appear after 120 minutes of model time. Between 275 m and 375 m, convergence of mass which results as air encounters the stable regions over the slopes and turns towards the valley center has caused the layer to destabilize significantly. Above 375 m, diverging air which feeds the upper slope flows is replaced by warmer air from above and a more stable region results.
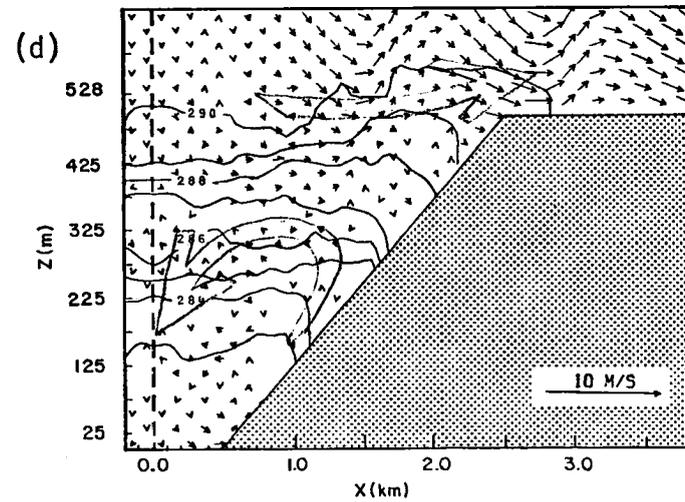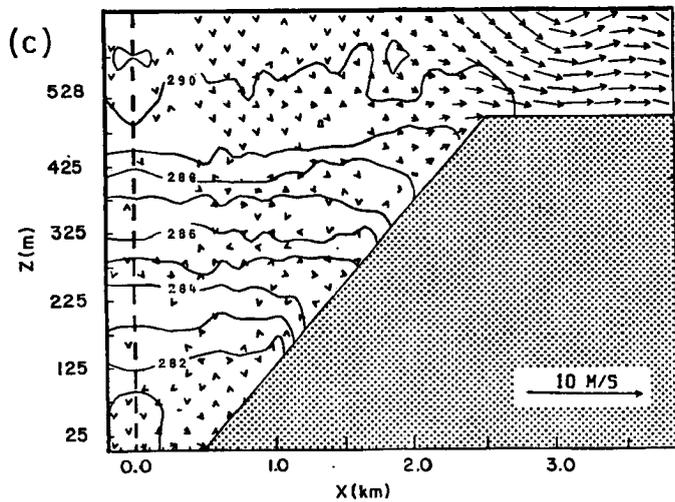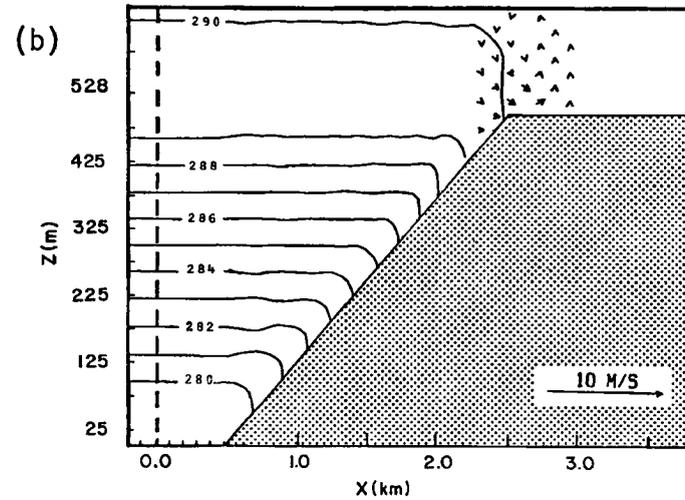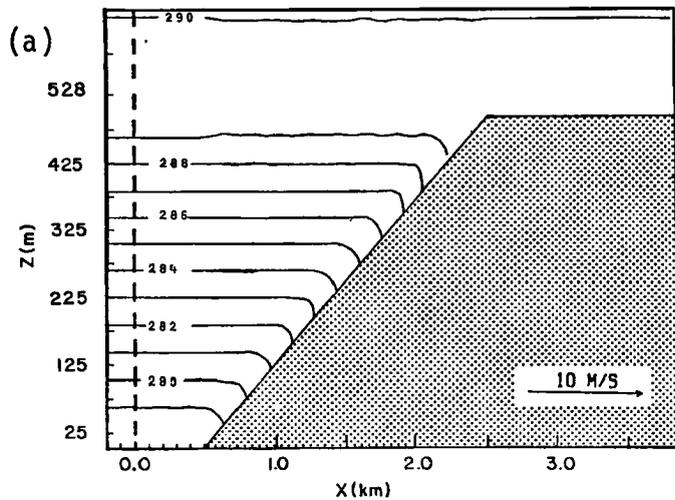
Figure 10a-d. Five minute average wind and potential temperature fields after (a) 0 min., (b) 40 min., (c) 80 min., and (d) 100 min. for Case 1.
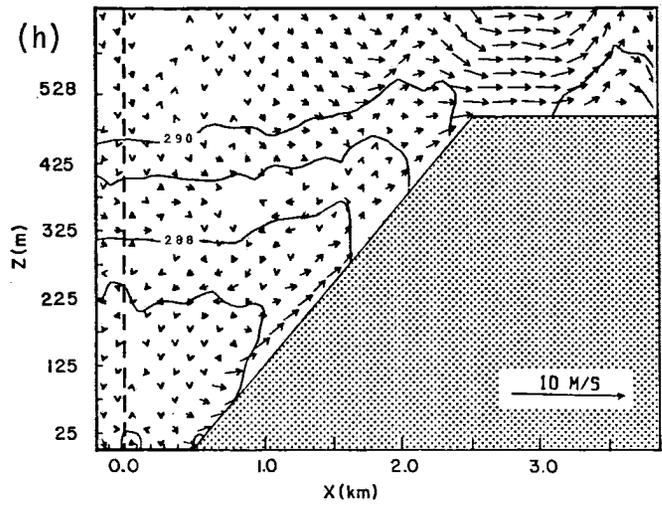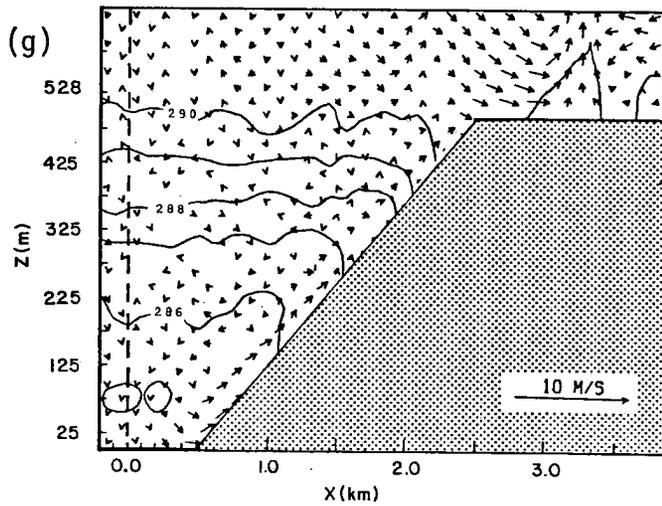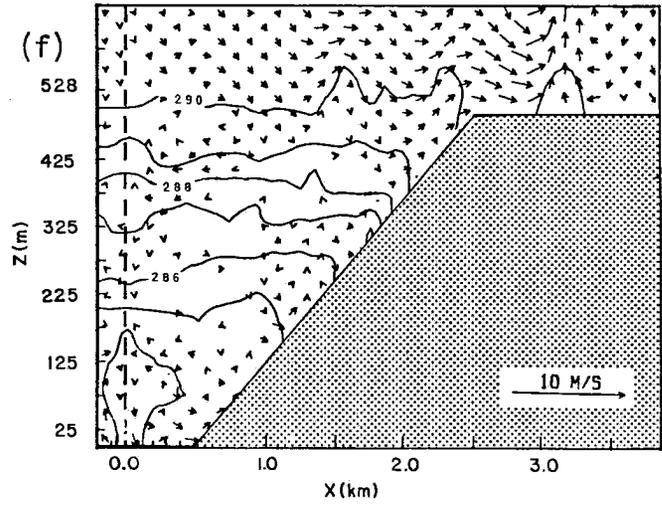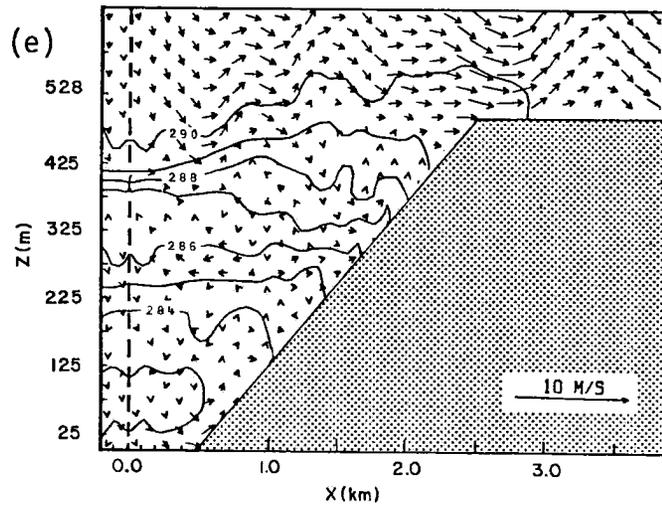
Figure 10e-h. Five minute average wind and potential temperature fields after (e) 110 min., (f) 130 min., (g) 150 min., and (h) 170 min. for Case 1.
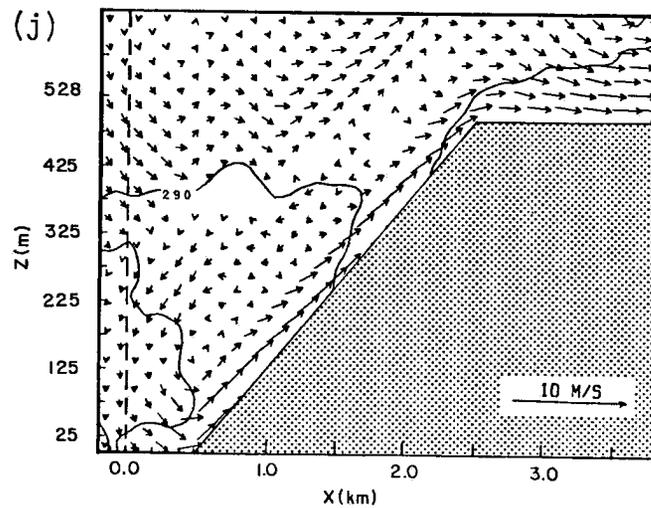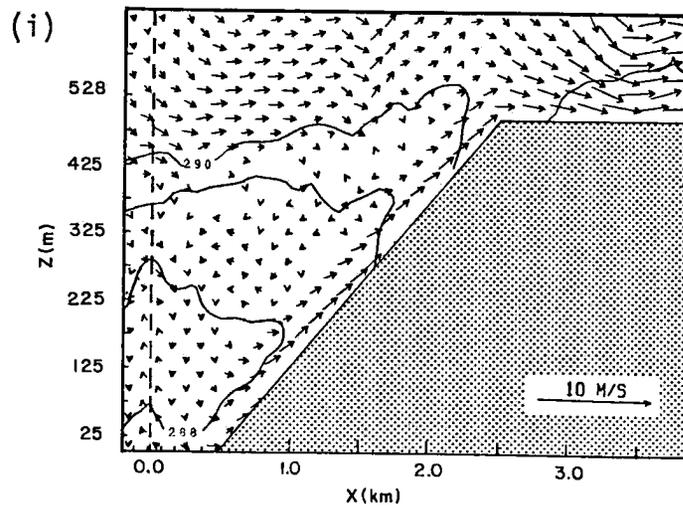
Figure 10i-j. Five minute average wind and potential temperature fields after (i) 190 min. and (j) 210 min. for Case 1.
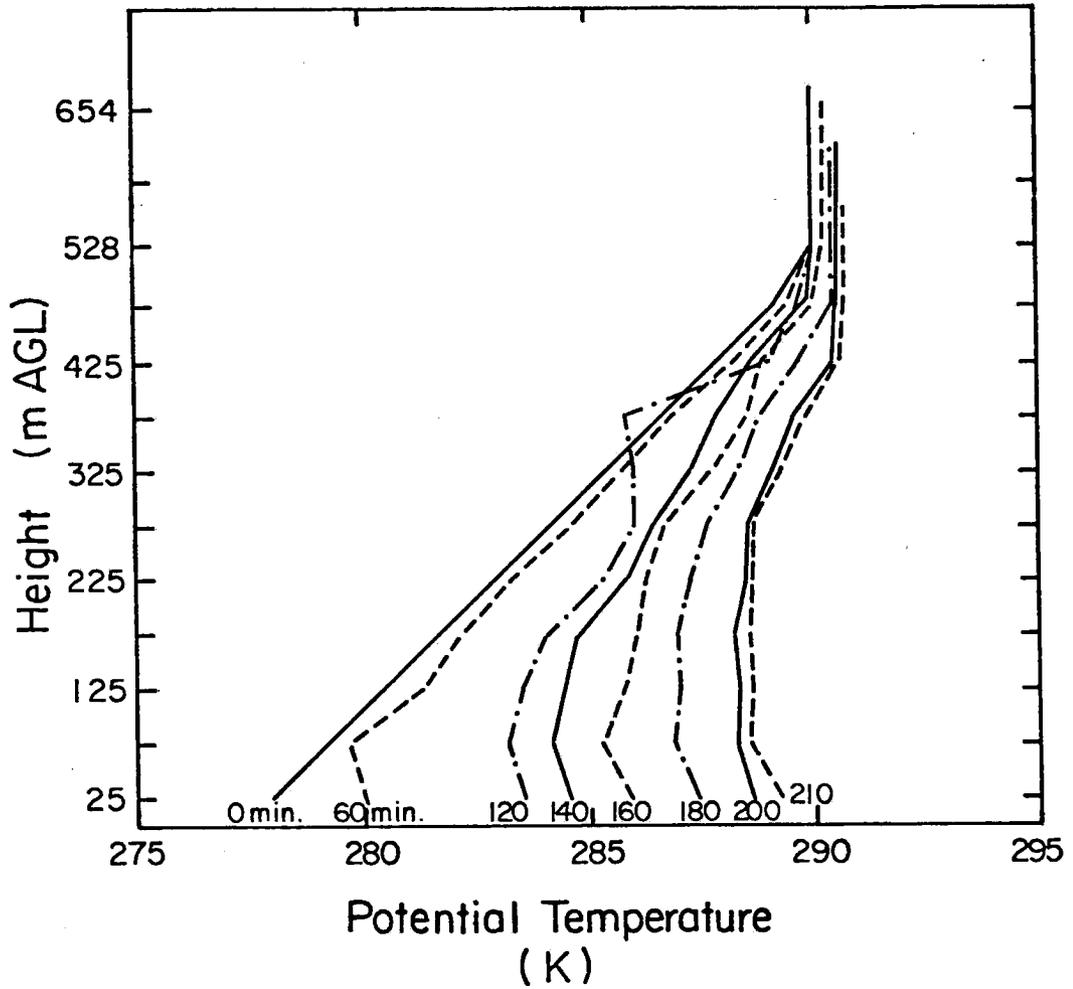
Figure 11. Ten minute average potential temperature profiles over the valley center for Case 1. Time in minutes shown below profiles.

Just 20 minutes later, the air travelling up the lower slopes acquires enough buoyancy to penetrate the stable pockets and form a continuous flow. As a result, the regions of differing stability are rapidly mixed out to produce the profile shown. By this time, the stable layer's lapse rate has been reduced from 0.025 to 0.013 K/m. The remaining profiles reveal the dual effects of the sinking stable core and growing CBL. The stable layer warms through its depth while the neutral layer grows. After 210 minutes, the layer is nearly adiabatic and the inversion is broken.

4.2. Case 2 Results

For this simulation, the amplitude of the surface temperature flux was reduced to 0.125 K m/s, 50% of the Case 1 value. As expected, the development of the boundary layer proceeded more slowly than in the reference case, but more details of the physics were apparent from the analysis. The initial state of the valley atmosphere was the same as that shown in Figure 10a. As in the first case, the first signs of the effects of the surface heating are the development of circulations over the ridge and the floor sidewall junction. After 60 minutes (Figure 12a), the CBL has warmed to 280 K and the 290 K isentrope is starting to descend over the valley. The circulation in the CBL is just beginning to form, while the one over the ridge is more organized.

Figure 12b shows many details of the interactions between the dynamic and thermodynamic processes after 90 minutes. Two pockets of increased stability are present over the sidewall, one between 125 and 225 m elevation and a second between 325 and 400 m. At the same elevations over the valley center, the layers have destabilized slightly due

to a horizontal mass convergence. Above these layers are regions where this characteristic is reversed. The areas between 225 and 325 m and between 400 and 500 m have more stable regions over the valley center and less stable ones over the sidewall. There are indications of an outflow from the valley center forcing a horizontal convergence over the sidewall.

The state of the boundary layer after 120 minutes is shown in Figure 12c. The outflow of air above 400 m is still evident as it feeds the upslope wind over the upper sidewall. While winds in the upslope layer are less than 1.0 m/s at all levels, the peak winds over the ridge have increased to over 1.2 m/s. Air in the levels immediately above the ridgetop elevation can be seen accelerating toward the ridge as the heat low intensifies. The 290 K contour has lowered to ridgetop and clearly marks the inversion top at this time. A mean subsidence over the valley center averaging 0.06 m/s replaces the air lost to the cross-valley circulation. The CBL has grown to over 150 m in depth and its influence can be seen by the penetration of winds through the strongly stable region over the sidewall. As a result, the lapse rate there is more uniform than before and mixing is eliminating the horizontal gradient at this level.

After 140 minutes (Figure 12d) another pocket of very stable air has formed over the valley sidewall between 225 and 325 m. As a result, an isolated circulation has formed in the lower part of the valley with subsidence over the center, an upslope flow between 1.0 and 1.3 m/s over the lower sidewall and a return flow towards the valley center between 0.1 and 0.2 m/s. The 50 m descent of the 284 K isentrope and the formation of a horizontal temperature gradient due to advection

confirms the presence of the circulation. The region of enhanced stability over the upper sidewall has been penetrated by the upslope flow beneath it and the lapse rate there is more uniform. Horizontal mixing in the upper levels is acting to also smooth the lapse rate over the valley center and diminish the horizontal temperature gradient between 325 and 475 m. Cold advection in the upper inversion levels has formed a concave upward shape to the stable core.

Just 10 minutes later (Figure 12e), this enhanced stability region over the sidewall has forced a cross-valley flow to form a convergence zone over the valley center. This circulation has again yielded a near neutral layer surmounted by a much more stable region. After 160 minutes, the upslope wind has mixed out the differences in lapse rate over the sidewall (Figure 12f). An organized cross-valley circulation between 275 m and 475 m acts to destabilize the strongly stable zone over the valley center and strengthen the stability in the less stable layer below it. The previous wind patterns in these regions have reversed. Outflow of air from the layer between 275 and 375 m and convergence over the valley center between 375 and 475 m is observed. The CBL has grown to almost 200 m in depth and has warmed to nearly 284 K.

Figure 12g shows the valley atmosphere after 180 minutes of model time. The CBL is over 200 m deep and the 290 K isentrope has descended farther into the valley. The lapse rate through the stable layer is a nearly constant 0.017 K/m, significantly less stable than the initial valley atmosphere. The upslope wind is still not continuous and is only evident at the sidewall corners. Heating over the ridge has intensified the eddy circulation there to form a very broad convective cell with peak updrafts of 2.1 m/s. The ten minute average data reveals weak subsidence over the valley center in the lowest 325 m.

Twenty minutes later (Figure 12h), the upslope wind is nearly continuous over the length of the sidewall. Cross-valley winds are acting to eliminate horizontal temperature gradients and organized areas of descent are starting to develop. The CBL has warmed to over 285 K but has only grown to 225 m by this time. Averages computed over the valley center indicate the presence of a mean subsidence field, a feature observed by the descent of the isentropes. Advection of cold air in the slope flows is contributing to the development of a horizontal temperature gradient in the upper levels, again giving rise to a cup-shaped inversion top. After 20 minutes (Figure 12i), the CBL has grown to over 275 m and the slope flow is well established below this level. The stable core can be seen to lie between 275 and 475 m over the valley center as the 290 K isentrope has descended significantly. The heat low over the ridge has further developed and can be seen accelerating mass toward the lateral boundary. Most cross-valley circulations in the stable air have diminished and a mean subsidence at all levels over the valley center of approximately 0.01 m/s is evident from the ten minute average data.

The descent of the stable core is still obvious after 240 minutes of model time (Figure 12j). The 288 K isentrope has dropped to the 325 m level and the entrainment of air from the stable layer base is evident by the appearance of the 287 K isentrope in the CBL. The upslope winds range between 0.4 and 0.8 m/s over the length of the sidewall and the rate of descent averages 0.1 m/s. Ten minutes later (Figure 12k), the 288 K isentrope has descended to the 275 m level and marks the top of the CBL. The upslope winds have increased in strength to greater than 1.0 m/s over the entire length of the sidewall. Strong

cold advection in the upper part of the inversion has exaggerated the concave shape of the 290 K isentrope. Organized downdrafts feed the upslope layer in the CBL and have acted to lower the 290 K isentrope to the 450 m level over the valley center.

The upslope continues to strengthen and the stable core sink as the simulation continues. After 270 minutes (Figure 12ℓ), the peak upslope winds are over 2.0 m/s and the 290 K level has descended to 425 m elevation. The ten minute average data reveals that the CBL is still 275 m deep with a slightly stable region above it. By 290 minutes into the run (Figure 12m), the 289 K isentrope marks the top of the CBL and the organized daytime circulation over the valley center is clearly evident. Descending air feeds the upslope wind in the CBL and is then transported through the upslope layer to ridgetop. The CBL and inversion top meet at the 350 m level after 310 minutes of model time (Figure 12n) and the inversion is almost destroyed. The organized daytime circulation feeding the upslope winds and accelerating mass toward the heat low over the ridge are now dominant. The upslope wind now averages 2.0 m/s over the length of the sidewall and increases in depth only near the ridge-sidewall junction.

Similar to Figure 11, Figure 13 shows the evolution over the valley center as the development of the boundary layer progresses. Although the timing of the development of the observed features was different, the structure of the boundary layer evolution was similar to that in Case 1. Stable pockets once again form over the sidewalls as air travelling up the slope loses its buoyancy in the stable air then turns and converges over the valley center. As a result, the uneven thermal stratification evident after 140 minutes appears. The unstable layer
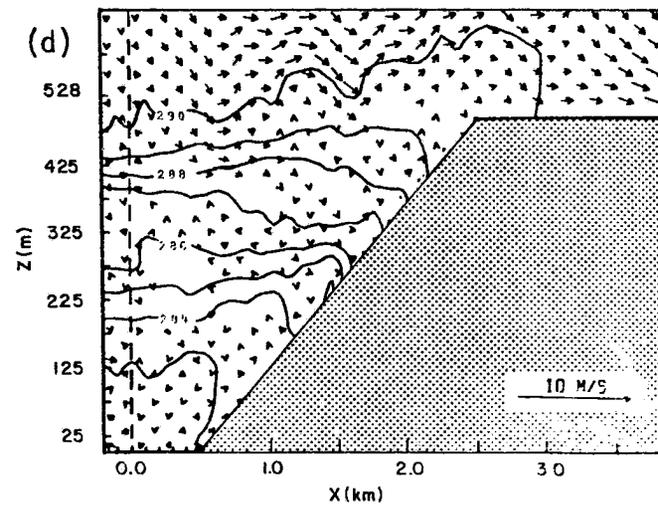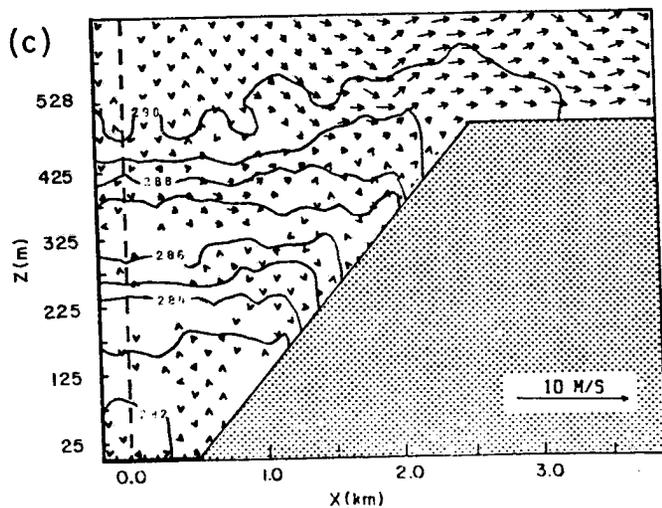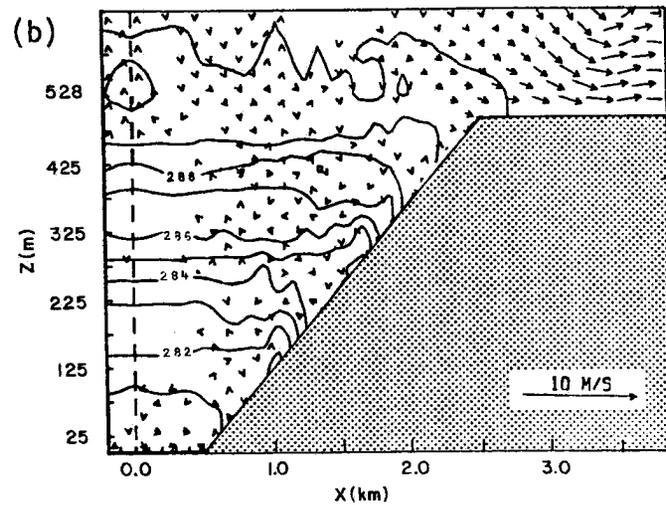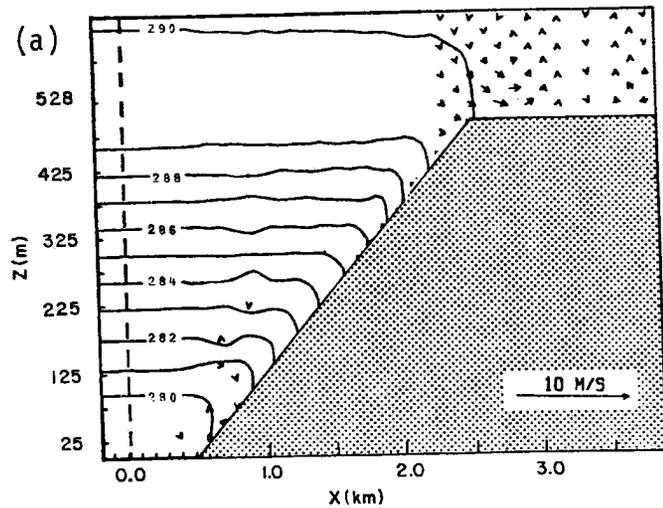
Figure 12a-d.   Five minute average wind and potential temperature fields after (a) 60 min.,
(b) 90 min., (c) 120 min., and (d) 140 min. for Case 2.
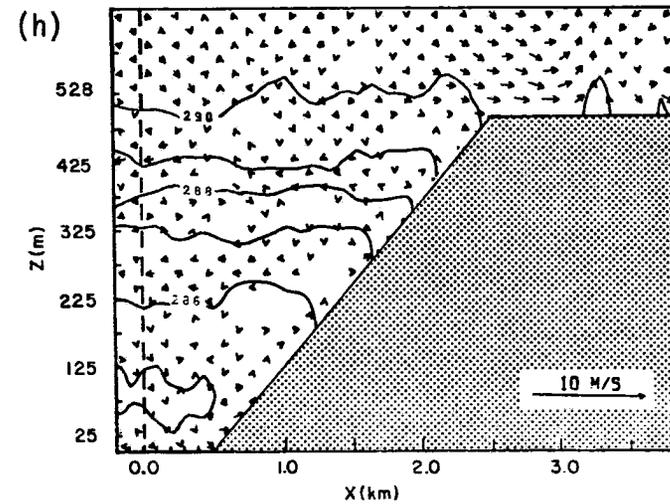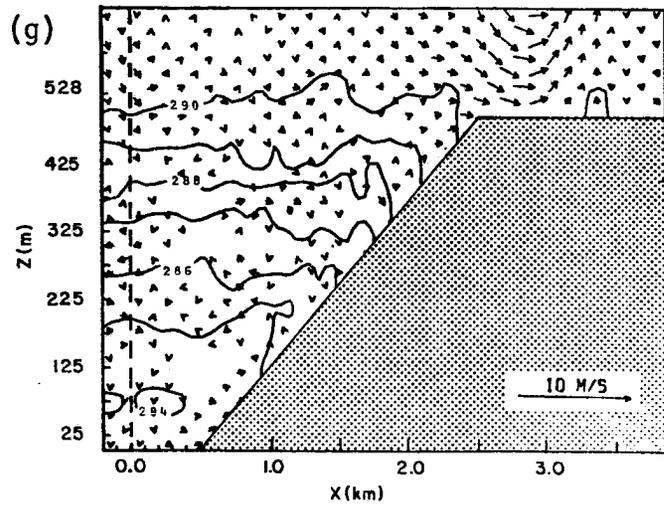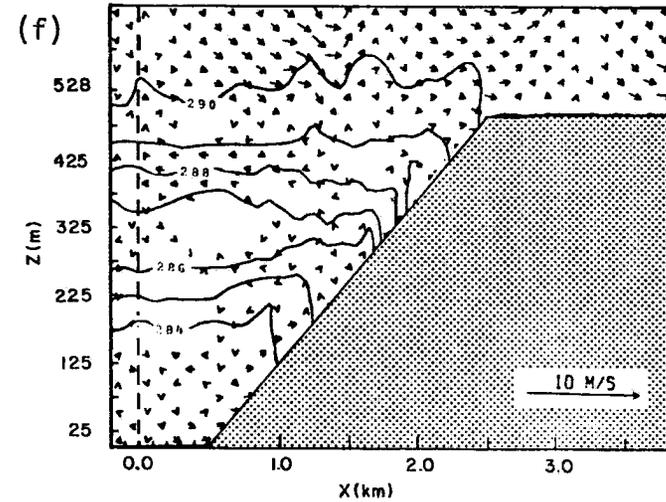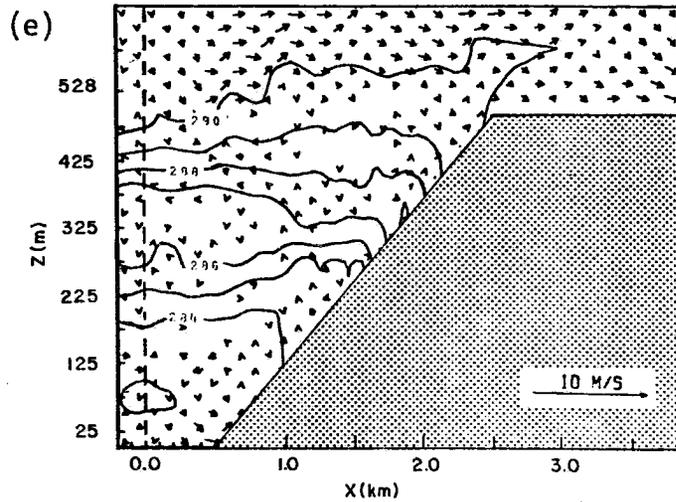
Figure 12e-h.   Five minute average wind and potential temperature fields after (e) 150 min., (f) 160 min., (g) 180 min., and (h) 200 min. for Case 2.
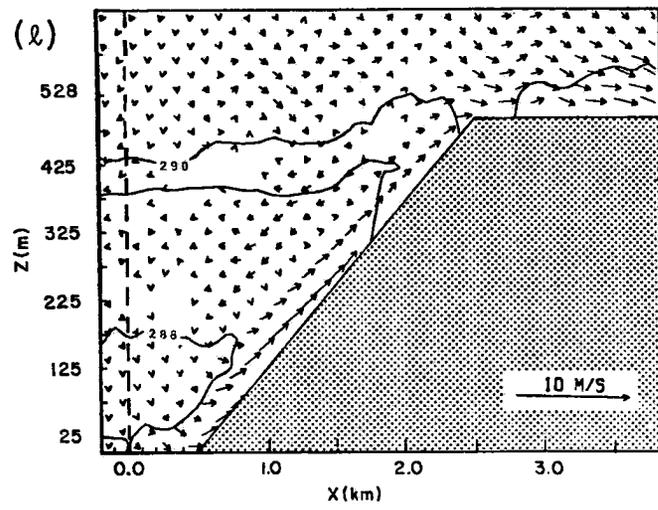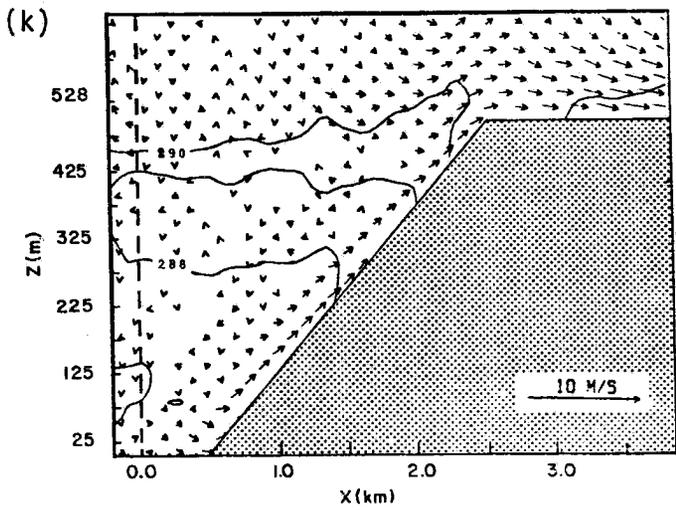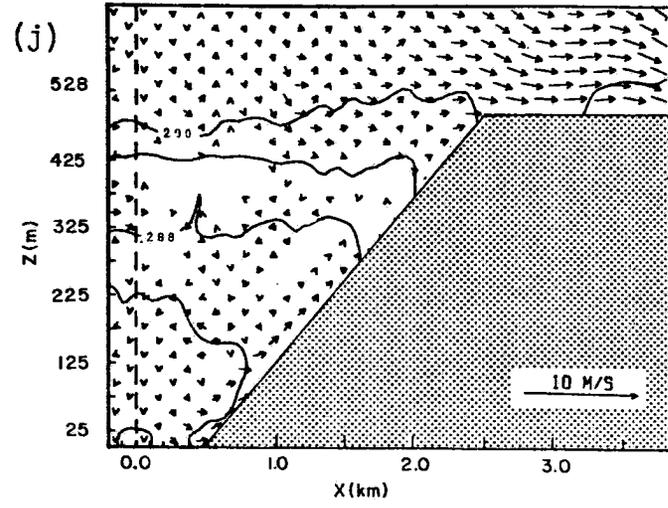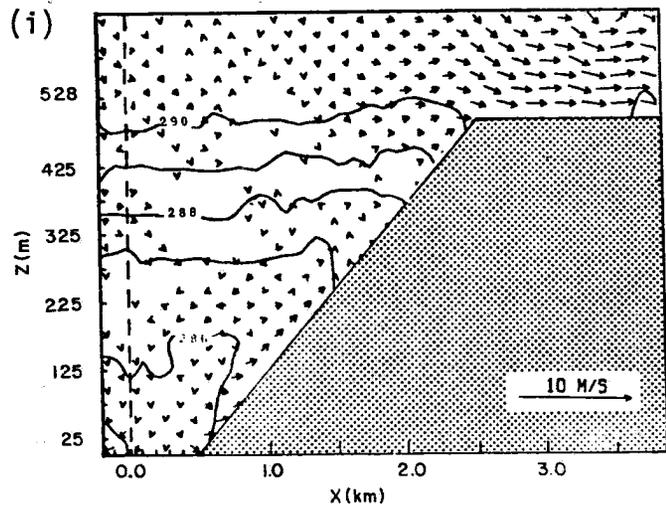
Figure 12i-ℓ. Five minute average wind and potential temperature fields after (i) 220 min., (j) 240 min., (k) 250 min., and (ℓ) 270 min. for Case 2.
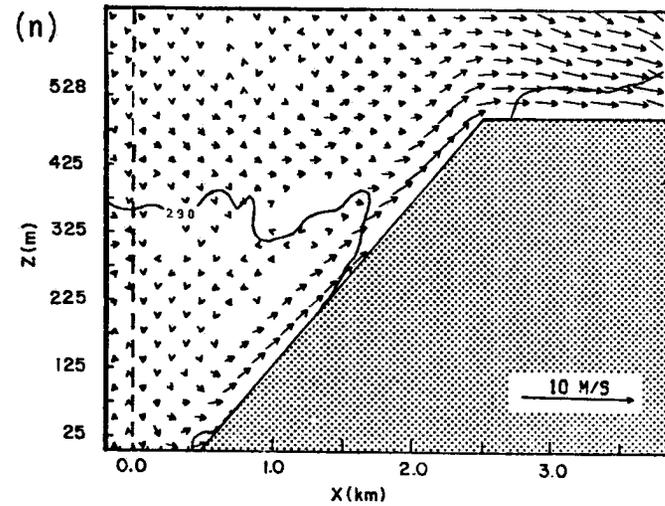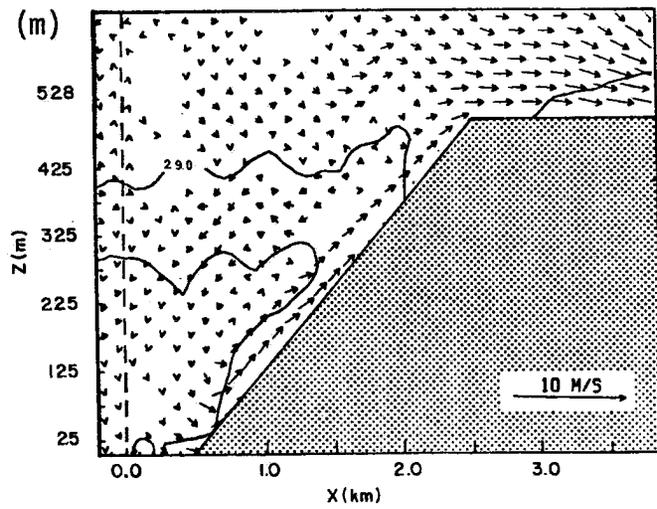
Figure 12m-n. Five minute average wind and potential temperature fields after (m) 290 min. and (n) 310 min. for Case 2.

53
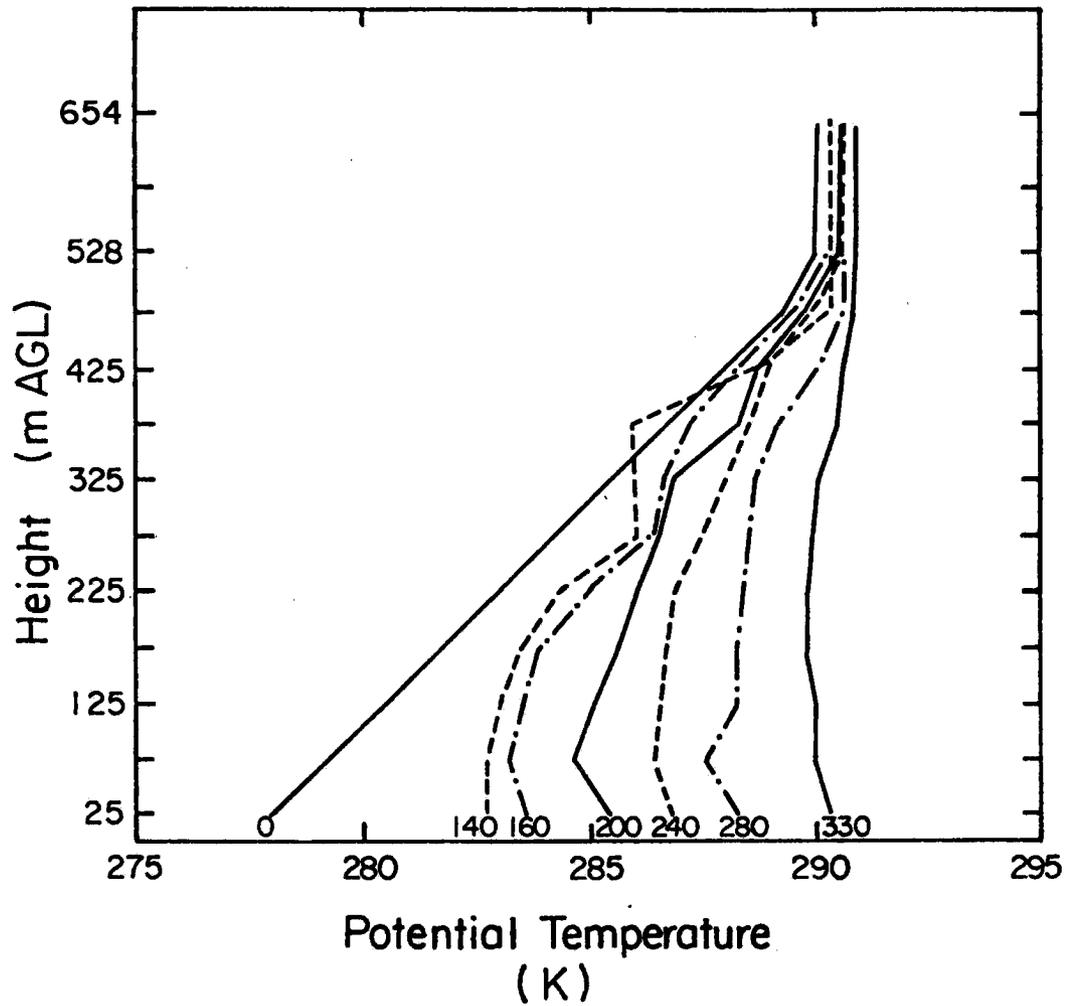
Figure 13. Ten minute average potential temperature profiles over the valley center for Case 2. Time in minutes shown below profile.

between 275 and 375 m is a consequence of the cross-valley convergence over the valley center while the stability of the overlying region is increased as a result of a cross-valley divergence necessary to feed the upper slope flow.

After the upslope has penetrated the stable regions over the side-wall, the regions of different stabilities rapidly mix out to produce the profile observed after 160 minutes. Once the continuous upslope layer is firmly established after 200 minutes, the CBL grows while the stable core sinks to destroy the inversion after 330 minutes.

4.3 Case 3 Results

For this simulation, the heating distribution was altered to provide more surface heating along the slopes, but less over the valley floor. The amplitude of the potential temperature flux function was set to 0.15 K m/s with the heating factors s_1, s_2, s_4 and s_5 remaining the same as in the previous runs. The floor heating factor, s_3, was changed to 0.333 so that very little energy was input from the valley floor. This simulation was an attempt to model a snow covered valley where the albedo on the floor is higher than the forested sidewalls. Total potential temperature flux from the sidewalls and floor was only 3% less than in Case 2, therefore, the total energy input to the valley was approximately equal for both cases.

As before, the initial state of the atmosphere at sunrise is identical to that shown in Figure 10a. After 60 minutes have elapsed, the development of the convective cell over the ridge has begun, but there is no noticeable change in the structure of the lower valley (Figure 14a). The winds over the ridge have already reached speeds greater than

1.5 m/s, although there is no detectable upslope flow. The 290 K isentrope is starting to descend as the ridge warms slightly. Ninety minutes into the run (Figure 14b), disturbances initiated by heating over the sidewalls can be observed propagating into the stable core. An upslope flow has developed over the upper sidewall with speeds between 0.1 and 1.0 m/s. There is no indication of the formation of a CBL as even the lowest layers of the model atmosphere are stably stratified. Over the ridge, the circulation has intensified to produce wind speeds of 2.5 m/s. The 290 K isentrope has descended to near ridgetop level over the sidewall, but still is high in the undisturbed air over the valley floor. As in the previous simulations, areas of increased and decreased stability over the sidewalls have been produced by the small circulation cells.

Two very stable pockets have formed over the sidewall at 150 and 375 m elevation after 110 minutes (Figure 14c) as a result of the loss of buoyancy of air moving up the slope. Once again, the effects of these regions on the thermodynamic structure of the stable layer are evident in the uneven thermal stratification over the valley center. Mass moving up the slope in response to surface heating encounters these stable pockets and flows toward to the valley center where it converges and decreases the lapse rate in the layer. To feed the slope flow above the stable pockets, air flows outward from the valley center toward the sidewall. An increased lapse rate in this layer is observed as the diverging mass is replaced by warmer air from above. By this time, the 290 K isentrope has descended to ridgetop level and serves as the useful marker for the top of the stable air.

As the surface heating continues to intensify, the air warms sufficiently to penetrate the stable pockets of air over the slope. This results in the development of a slope wind over a greater portion of the sidewall, as can be seen in Figure 14d. As the lapse rate over the sidewall becomes more uniform, gravity waves propagate outward and smooth the profile over the valley center as well. Additionally, large eddies enhance horizontal mixing in the stable core. One of these large eddies can be seen in the center of the valley between 275 and 425 m. The stable core is significantly less stable at this point than it was originally. Although the inversion top has moved little, the 284 K isentrope has descended nearly 50 m in the lower half of the valley. The first signs of CBL development over the valley floor are detected as an eddy forms above the floor sidewall corner.

The state of the valley atmosphere 160 minutes after model sunrise appears in Figure 14e. A weak upslope wind can be seen over the length of the sidewall, except for a small area above the middle section. The cross-valley circulations have diminished significantly as the lapse rate slowly becomes more uniform through the stable core. Circulations in the CBL have become more organized with air from the valley center feeding the slope flow at the sidewall base. The top of the stable core is still located near ridgetop. Over the ridge, the convective cell is developing into a heat low and has created an updraft with vertical velocities exceeding 2 m/s.

By 180 minutes into the simulation (Figure 14f), the slope flow has become continuous. The limited amount of heat added at the valley floor has severely restricted the growth of the CBL. Evidence of inversion descent is apparent, but the ten minute averages show only very weak

subsidence. The base of the stable core, marked by the 284 K isentrope, has been lowered from an original elevation of 270 m to 125 m and the top of the inversion has fallen below 475 m. Similar to the previous simulation, no uniform subsidence is evident, but rather regions of organized downdrafts can be seen flowing through the stable air. The upslope flow exceeds 1.0 m/s in many locations, especially over the upper sidewall. The low pressure area over the ridge has produced a more horizontal acceleration toward the lateral boundary in place of the cell type circulation there previously.

After 200 minutes, cross-valley circulations in the form of large eddies appear again in the stable layer in response to the stronger heating over the sidewall (Figure 14g). The growth of the CBL is still limited as the principal source of heat to drive it comes from the lower sidewall. Cold advection over the upper sidewall produces the familiar cup-shaped inversion top. Strong cold advection from the CBL has acted to form a region of increased stability over the lower sidewall between 225 and 275 m. Although the stable pocket is much weaker than those formed early in the simulation, its effect on the boundary layer is similar. Some of the air in the slope flow penetrates the pocket, but a portion of it turns and converges over the valley center with a resultant decrease in the stability of the layer.

By 220 minutes into the simulation (Figure 14h), the horizontal temperature gradients have again mixed out and a near uniform, but weaker, lapse rate through the stable air is produced. The organized downdraft regions have moved to different locations, an indication that they are transient phenomena which act, on the average, to provide a uniform subsidence field in the stable air. Mass is accelerated to over 4.0 m/s

as it flows toward the lateral boundary by the low over the ridge. The depth of the CBL is still less than 150 m as the warmer air above continues to slowly descend into it. Wind speeds in the slope flow are still low and have even decreased over the upper sidewall where they were previously the strongest.

The stable core continues to destabilize in response to cross-valley circulations which enhance horizontal mixing. After 240 minutes of model time (Figure 14j), the slope winds are still below 1.0 m/s over much of the sidewall and the lapse rate through the stable core has been reduced to 0.010 K/m. Twenty minutes later (Figure 14j), the first signs of the steady daytime circulation can be seen as mass descends into the valley center at the higher elevations. The warming of the neutral layer is detected by the appearance of the 291 K isentrope over the ridge.

The remnants of the original inversion after 280 minutes can be seen lying between 175 and 425 m in Figure 14k. The upslope wind is well developed by this time with winds in excess of 1.0 m/s over the length of the sidewall. Subsidence rates over the valley center range between 0.02 and 0.04 m/s as the stable core slowly sinks. By 300 minutes into the simulation (Figure 14ℓ), the original inversion top has fallen to 375 m. The large scale circulation cell is very apparent with air descending over the valley center to feed the slope flow. The air above the inversion has stabilized slightly due to the advection of warm air from the ridge to the valley center.

Figure 14m shows the boundary layer 320 minutes after model sunrise. The appearance of the 291 K isentrope over the valley center is indicative of the advective warming in the neutral layer. The 290 K level

has descended to the 300 m level with the upslope flow continuing to draw air from the shallow CBL. The upslope layer increases in depth near the sidewall summit in response to the dynamic influence of the heat low over the ridge. Wind speeds over the sidewall have increased to over 2.5 m/s after 340 minutes (Figure 14n) of model time as the last remaining layer of stable air descends into the valley. Twenty minutes later, the daytime circulation has replaced the transition flows in the valley (Figure 14o).

Figure 15 depicts the evolution of the thermal structure over the valley center based on the ten minute average data. This simulation differed greatly from the two previous runs in that the entire stable layer slowly destabilized as a result of cross-valley redistribution of heat. The 120 minute profile distinctly shows the development of the layers of increased and decreased stability resulting from the cross-valley circulations induced by the formation of stable pockets over the sidewalls. These regions slowly mix out and redevelop to give the appearance of a slowly destabilizing layer. Also evident in this run are the slow descent of the inversion top, the gradual warming of the overlying neutral layer and the lack of CBL development. The steady daytime circulation replaces the cross-valley flows after 360 minutes and the inversion is destroyed.

4.4 Case 4 Results

For this model simulation, the valley floor was widened to 2 km and each ridge was reduced to 0.95 km in an attempt to determine the effects of valley width on boundary layer development. Both the amplitude of the surface potential temperature flux and the heating factors were
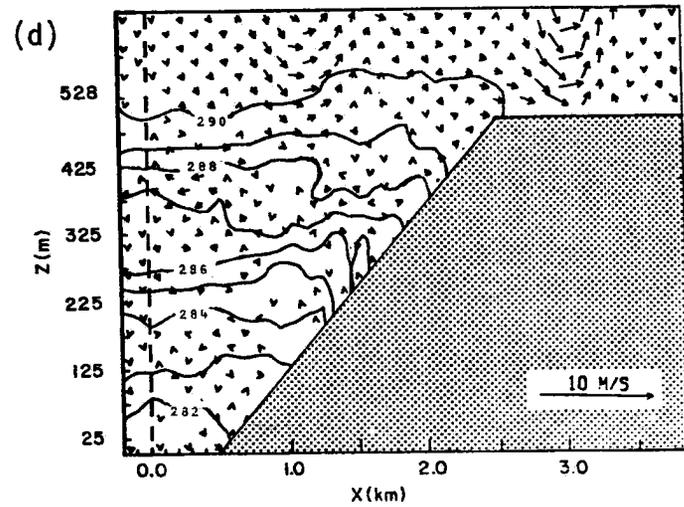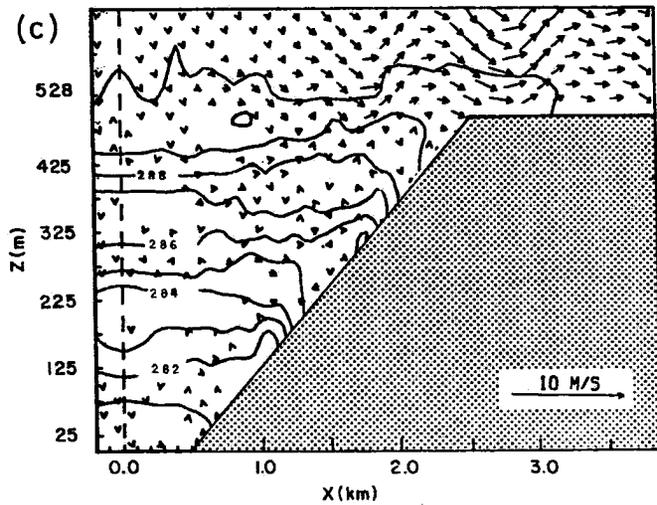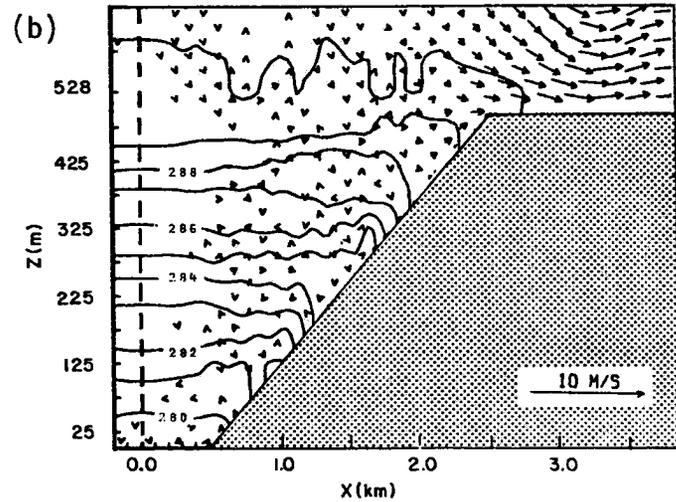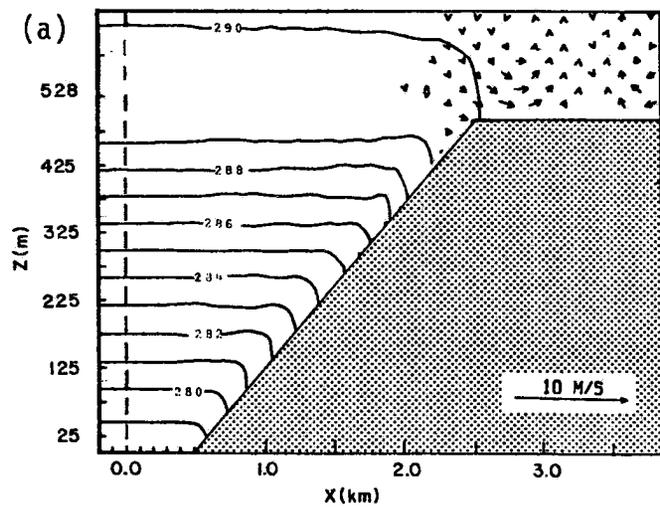
Figure 14a-d.   Five minute average wind and potential temperature fields after (a) 60 min., (b) 90 min., (c) 110 min., and (d) 140 min. for Case 3.
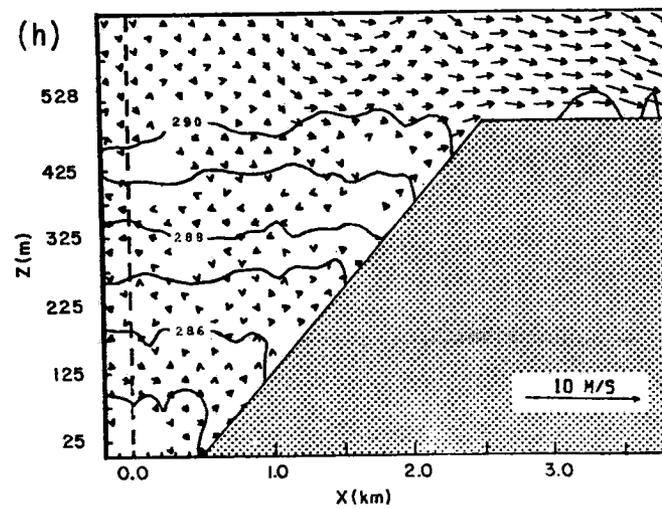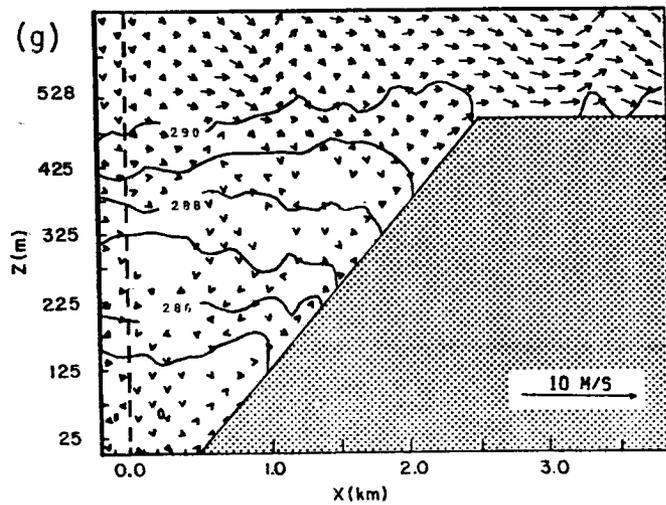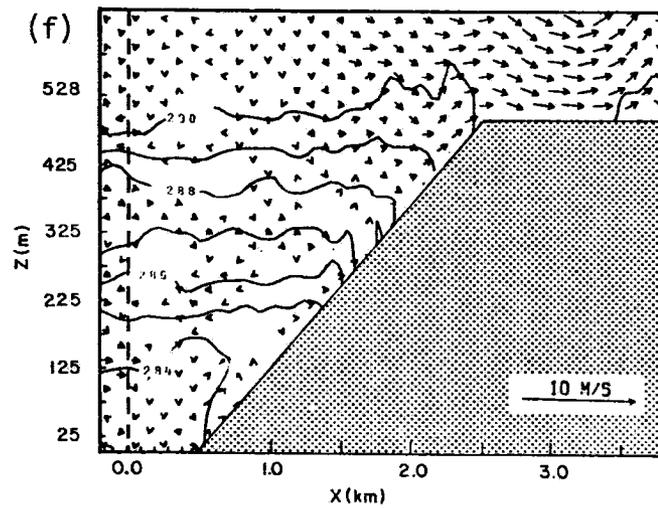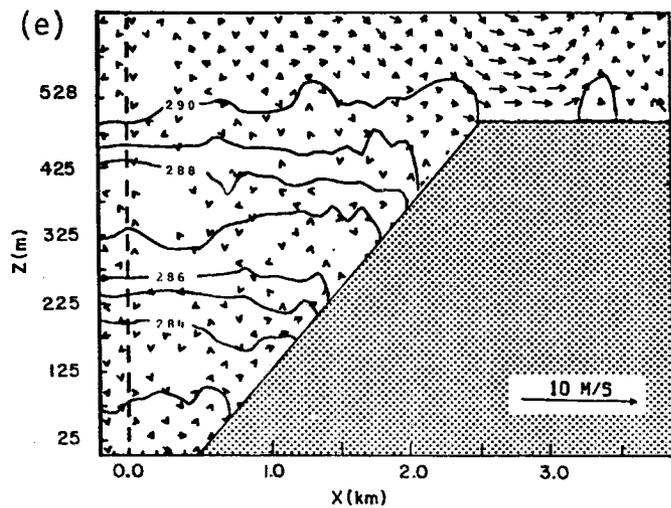
Figure 14e-h.   Five minute average wind and potential temperature fields after (e) 160 min., (f) 180 min., (g) 200 min., and (h) 220 min. for Case 3.
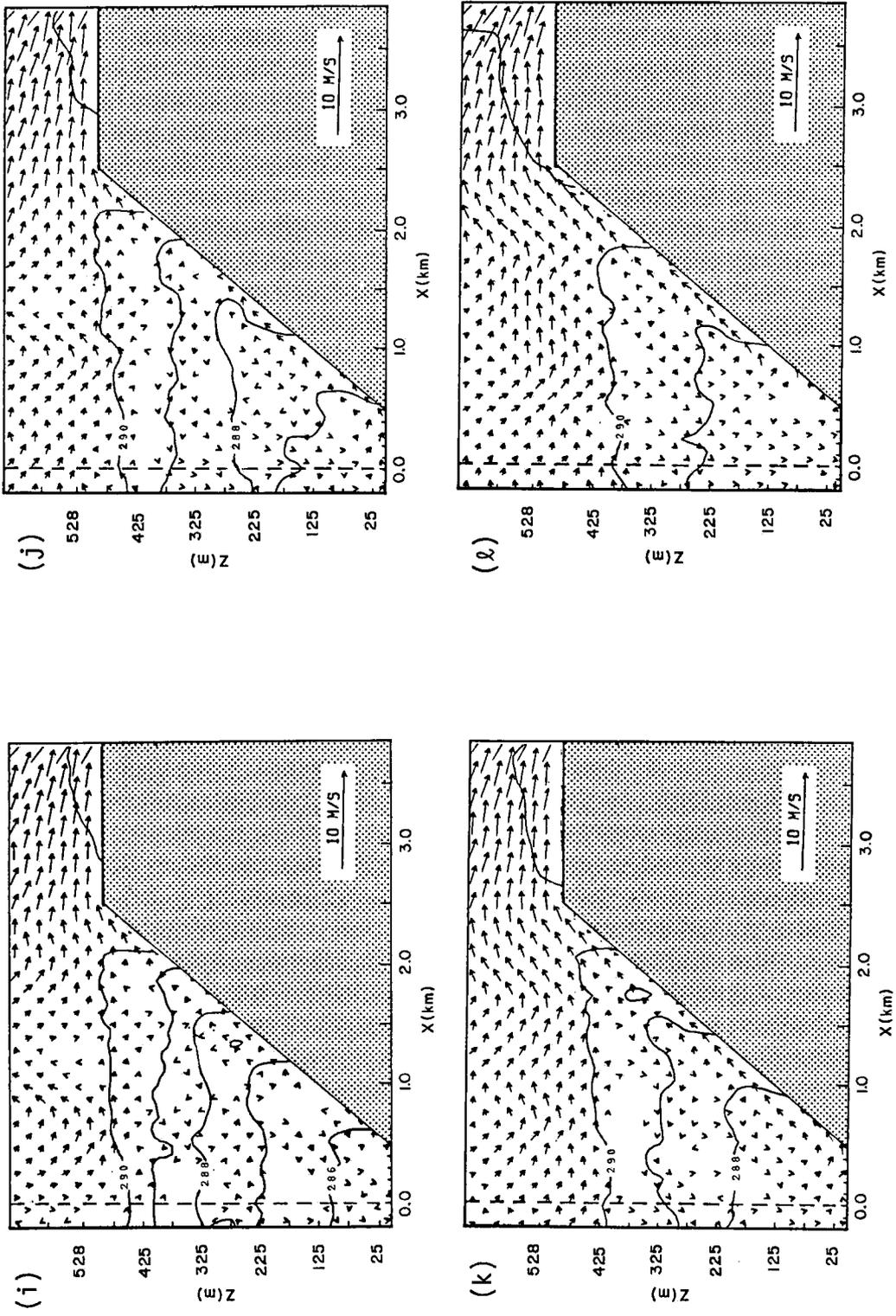
Figure 14i-ℓ. Five minute average wind and potential temperature fields after (i) 240 min., (j) 260 min., (k) 280 min., and (ℓ) 300 min. for Case 3.
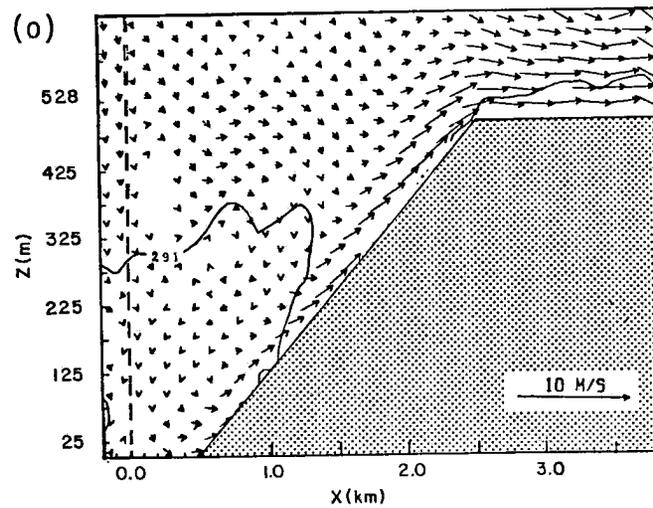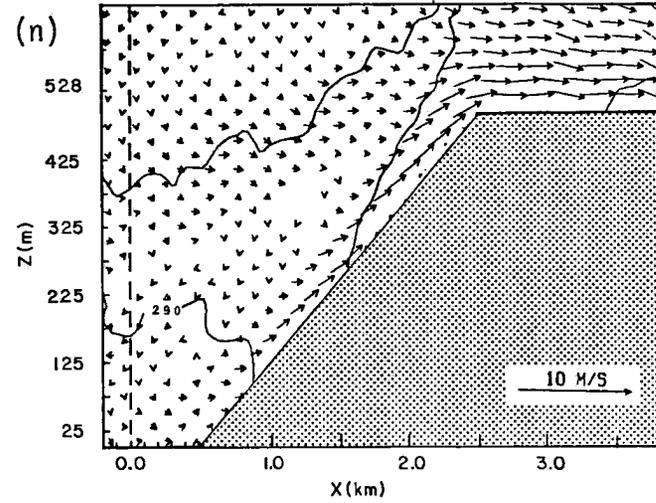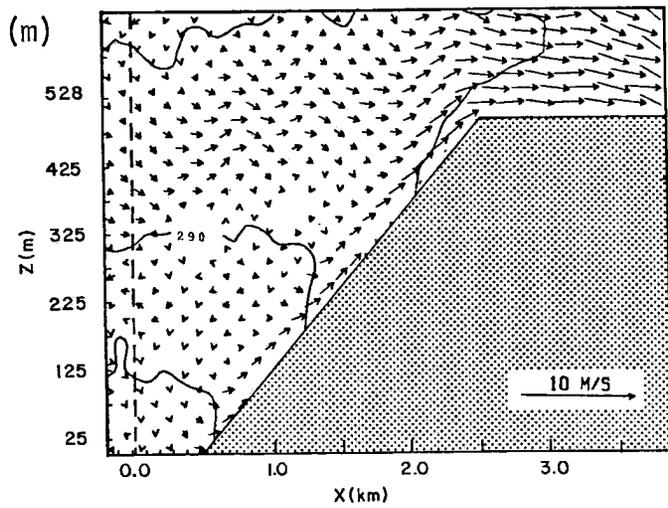
Figure 14m-o. Five minute average wind and potential temperature fields after (m) 320 min.,
(n) 340 min., and (o) 360 min. for Case 3.
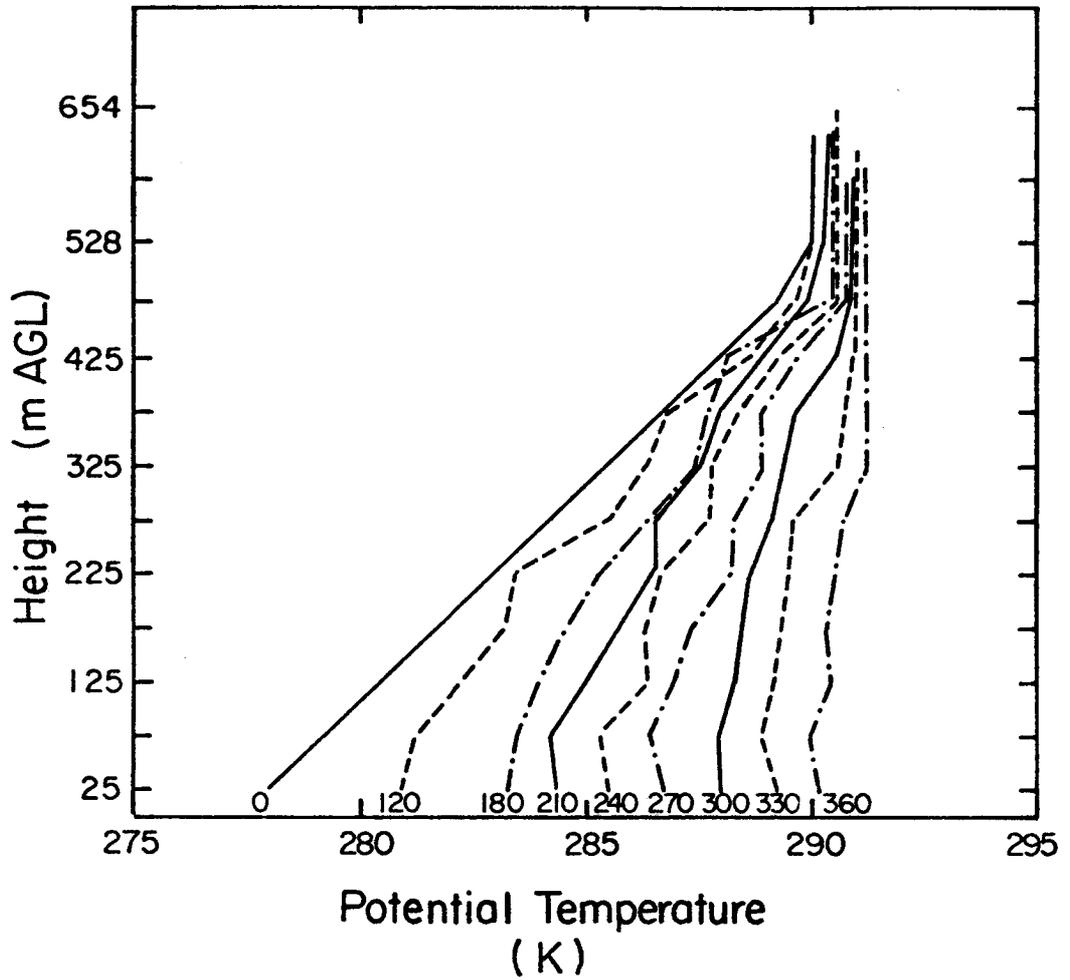
Figure 15. Ten minute average potential temperature profiles over the valley center for Case 3. Time in minutes shown below profile.

identical to the Case 1 simulation as was the initial state of the atmo-
sphere. As before, the first feature to appear in response to the sur-
face heating is a weak convective cell in the neutral air over the
ridge. Shortly thereafter, an eddy forms at the base of the sidewall,
the first indication of CBL formation. By 60 minutes into the simula-
tion (Figure 16a), the developing heat low over the ridge is already
accelerating air toward the lateral boundary. The eddy over the lower
sidewall is causing gravity wave disturbances in the stable layers
above it.

After 100 minutes (Figure 16b), the eddy at the sidewall base has
grown into a 150 m deep CBL circulation. Wind speeds over the ridge
have increased to over 1.0 m/s through a 100 m deep layer. An area of
increased stability, similar to those evident in previous runs, is
beginning to form at the 275 m level. The upslope air can be seen turn-
ing and flowing toward the valley center as it loses its buoyancy in the
stable pocket. Twenty minutes later (Figure 16c), the effect of these
circulations on the thermodynamic structure is apparent. A stable layer
caps the growing CBL above 200 m while the converging mass over the val-
ley center at 325 m has destabilized that region. The 284 K isentrope
has descended about 75 m since model sunrise as a result of subsidence
in the lower half of the valley. Heating over the upper sidewall has
produced a weak upslope flow (< 0.5 m/s) toward the ridge. Outflow from
the valley center between 375 and 425 m has resulted in the formation of
a very stable layer as the diverging mass is replaced by warmer air from
above.

As the simulation continues and the heating rate increases, the
mass in the slope flow warms sufficiently to maintain its buoyancy in

the stable pockets over the sidewall. The upslope layer becomes contin-
uous and after 140 minutes (Figure 16d), the wind speeds exceed 1.5 m/s
over the base and summit, but are weaker over the middle section. The
outward flow of mass toward the lateral boundary continues with wind
speeds near 2.5 m/s over the ridge. Cold advection has produced the
familiar cup-shape appearance to the inversion top. Although the
strongly stable layer between 375 and 475 m is still evident over the
valley center, cross-valley circulations in the form of gravity waves
are acting to eliminate horizontal temperature gradients. Organized
downdrafts can be seen pushing the base of the stable layer into the
CBL, which has warmed to over 284 K.

Figure 16e shows the extent of boundary layer development after
160 minutes of model time. The CBL is growing very rapidly in response
to the increased surface heating. Over the valley center, its depth has
increased to over 225 m and the upslope winds at the sidewall base have
attained speeds approaching 2.0 m/s. By this time, cross-valley circu-
lations have smoothed the lapse rate through the stable core until it is
a near constant 0.015 K/m. Subsidence over the valley center extending
through the depth of the stable layer is causing warmer air to descend
into the valley. Although average subsidence rates were not calculated
for this run, instantaneous values of vertical velocities at both 150
and 160 minutes reveal downdrafts exceeding 0.1 m/s through a deep layer
over the valley center. Air from the domain center above the inversion
moves toward the heat low over the ridge. Just 10 minutes later (Figure
16f), the CBL has grown an additional 50 m and is approaching 300 m in
depth. Large eddy circulations can be seen entraining air from the base
of the stable layer. Cold advection continues to give the top of the
stable core its concave upward shape.

As subsidence continues to slowly lower the inversion top, the CBL is growing rapidly to meet it. After 180 minutes (Figure 16g) a shallow but stronger inversion caps the CBL as the entrainment of air from the stable core becomes more vigorous. The upslope winds have also intensified with speeds ranging from 0.7 m/s at the 375 m level to 3.0 m/s at the sidewall base. The top of the stable layer has descended only slightly, but is located below ridgetop. Winds over the ridge have grown stronger and exceed 3.0 m/s through a 200 m deep layer. Ten minutes later (Figure 16h), the descent of the stable core is more obvious with the 290 K isotherm located at the 450 m level. The CBL has warmed to over 287 K and contains thermal circulations very similar to convective cells found in mixed layers over flat terrain.

The inversion top begins to descend more rapidly as the slope flow continues to develop and intensify. The 290 K isentrope has dropped an additional 50 m by 210 minutes (Figure 16i) and has nearly merged into the CBL. Upslope winds are more uniform at this time with speeds averaging 2.0 m/s over the length of the sidewall. The upslope layer shows no indications of increasing depth with elevation. Organized downdrafts in the upper levels above the sidewall base can be seen feeding the upslope, while a separate convective cell circulates over the valley floor. After 230 minutes (Figure 16j), the CBL meets the inversion top at the 350 m level and the small eddies in the lower levels are replaced by the larger daytime circulation. A subsidence field of 0.1 - 0.2 m/s over the valley floor feeds the upslope winds at the sidewall base. The slope winds have not increased in speed, but have increased to 100 m in depth over the entire sidewall length.
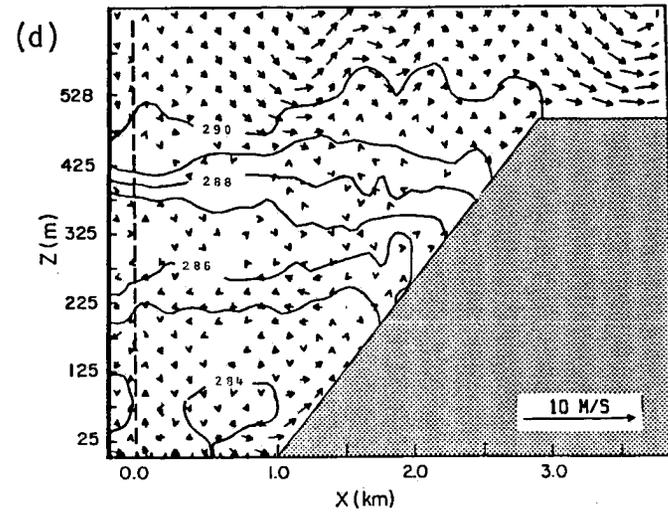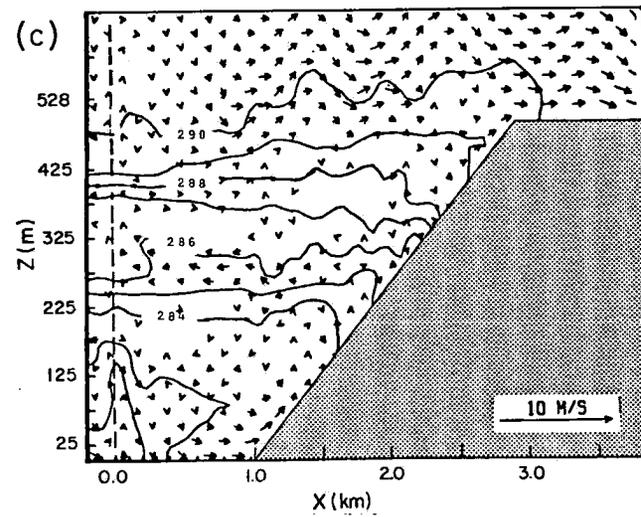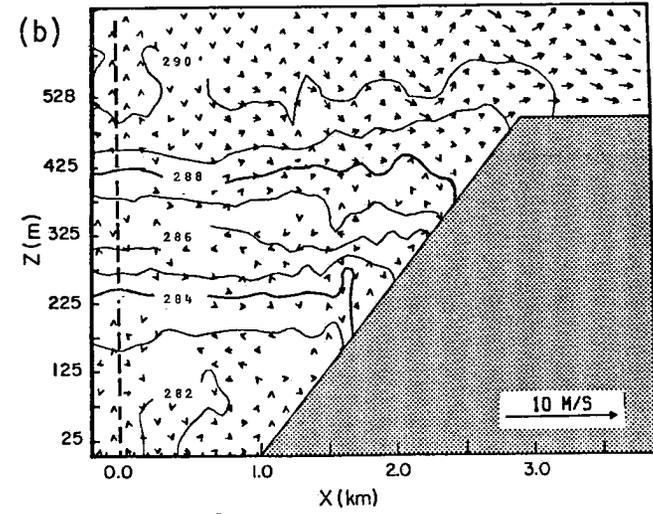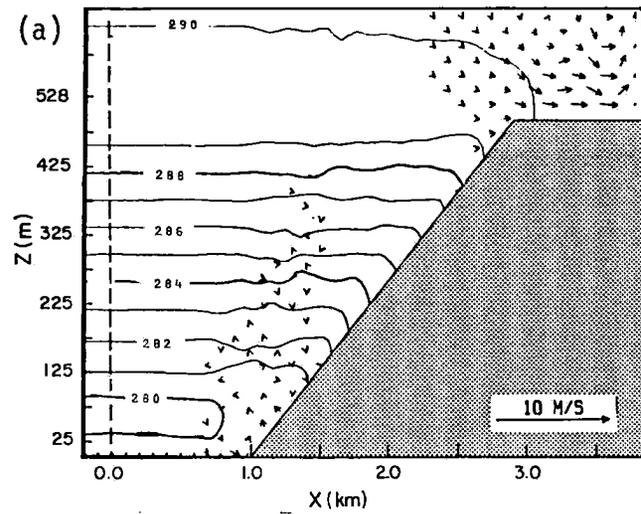
Figure 16a-d. Five minute average wind and potential temperature fields after (a) 60 min., (b) 100 min., (c) 120 min., and (d) 140 min. for Case 4.
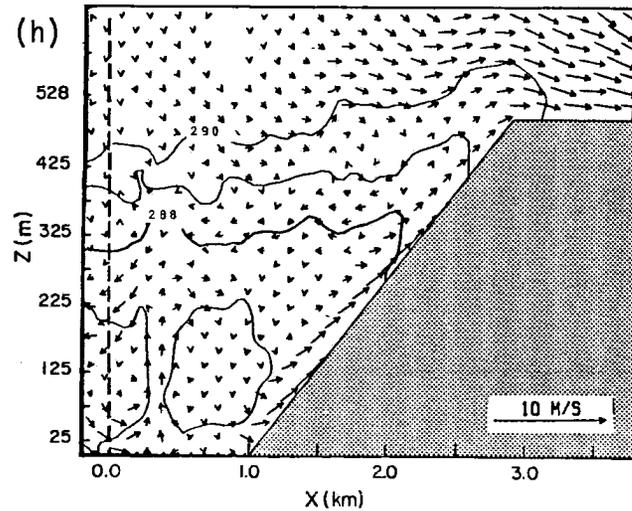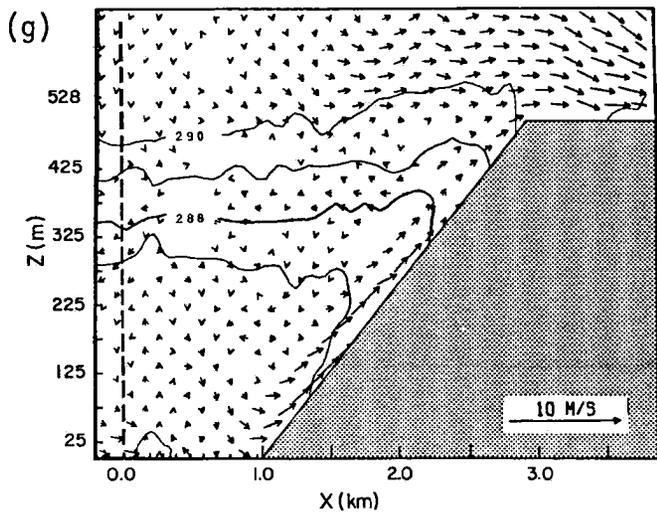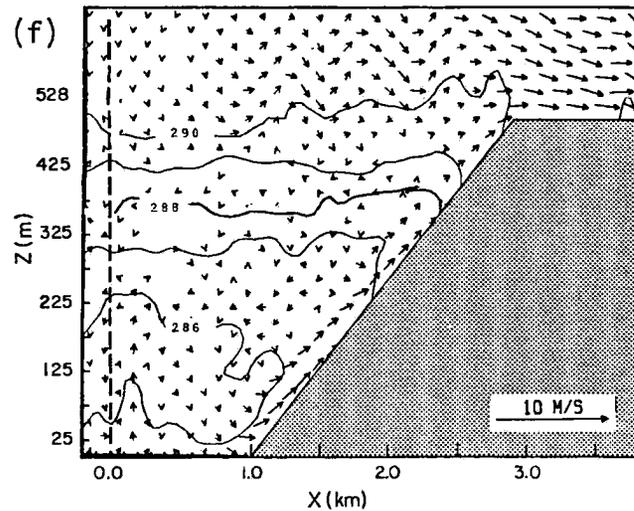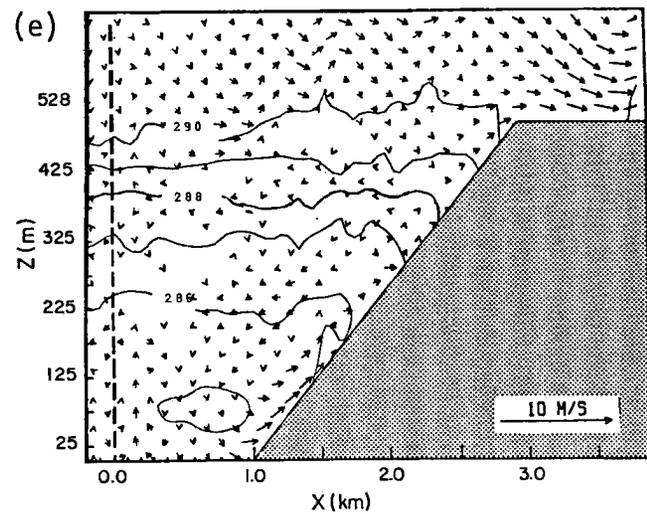
Figure 16e-h.   Five minute average wind and potential temperature fields after (e) 160 min., (f) 170 min., (g) 180 min., and (h) 190 min. for Case 4.
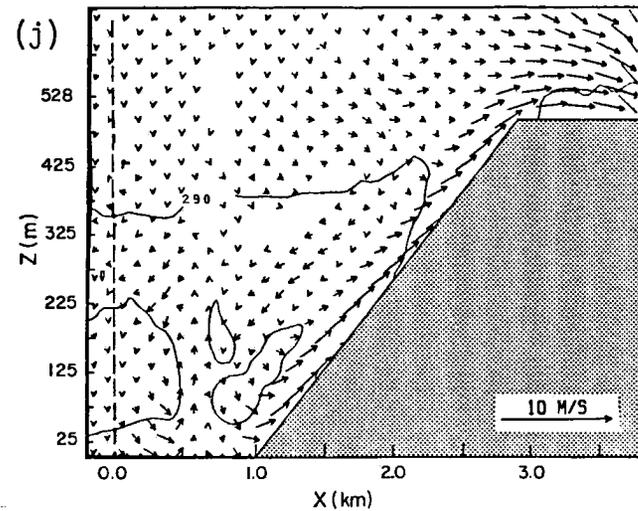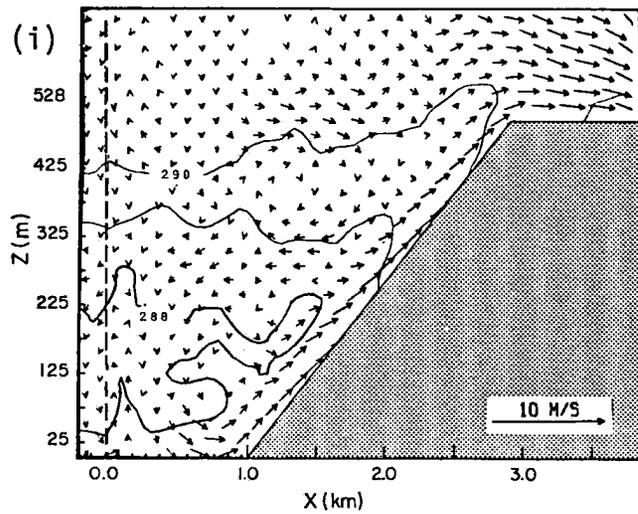
Figure 16i-j. Five minute average wind and potential temperature fields after (i) 210 min. and (j) 230 min. for Case 4.

Shown in Figure 17 are the instantaneous potential temperature profiles over the valley center at the labeled times. These profiles appear to closely represent the average structure of a ten minute period, as no significant deviations were found from five point averages computed from data saved on the analysis tape. The thermal structure after 100 minutes shows the first signs of the influence of the closed circulations. Capping the 125 m deep CBL is a shallow strongly stable layer which lies under an unstable region. These two layers will quickly mix out and become part of the growing CBL.

The next profile clearly shows the effects of the circulations after 120 minutes of model time. The CBL circulation is capped by a very stable layer, much like ones found above growing mixed layers over homogeneous terrain. Between 275 and 375 m, an unstable region resulting from the cross-valley convergence is evident under a more stable layer formed as the outflow of air at the higher levels continues. The remaining profiles show the gradual destabilization of the stable layer due to cross-valley mixing, the descent of the inversion top and growth of the CBL until the steady daytime circulation fills the valley between 200 and 240 minutes.

4.5 Case 5 Results

For this simulation, a more realistic heating distribution was imposed so that an east-west oriented valley lying at 40° N was modeled. The amplitude of the surface potential temperature flux remained at 0.250 K m/s as did the heating factors for the horizontal surfaces s_1, s_3 and s_5. However, the sidewall heating factors s_2 and s_4 were changed to 1.17 and 0.77 respectively based on the relative distribution of

73
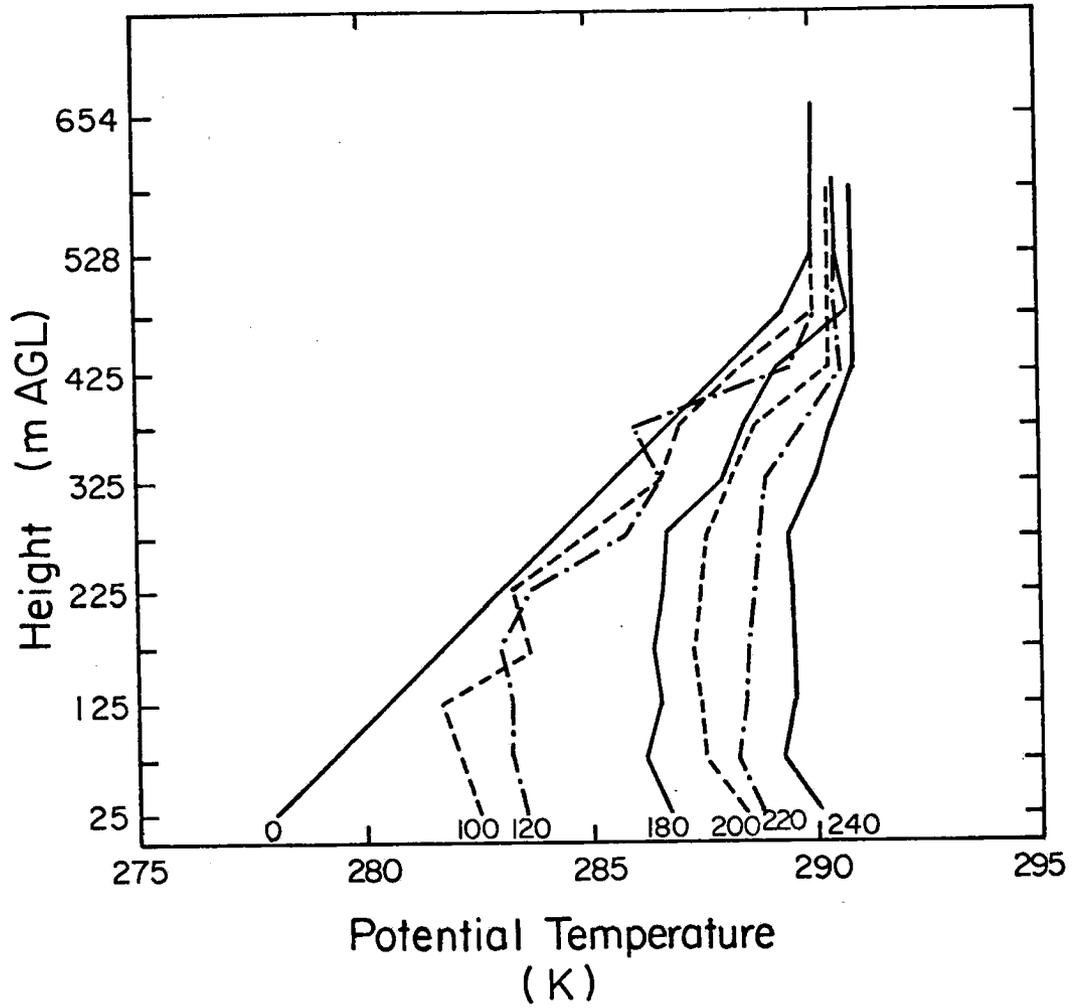
Figure 17. Instantaneous potential temperature profiles over the valley center for Case 4. Time in minutes shown below profile.

direct solar flux on the day of the equinox (Revfeim, 1976). Sixty minutes after model sunrise (Figure 18a), the development of convective cells over the ridges and the CBL circulation is apparent. Wind speeds over the ridge exceed 1.5 m/s and the potential temperature at the CBL has reached 280 K. Only slight deviations from symmetric conditions can be detected at this point.

After 80 minutes have elapsed (Figure 18b), the thermodynamic structure of the valley atmosphere remains nearly symmetric. Loss of buoyancy has caused air moving up the sidewalls in the slope flows to form the familiar "stable pockets" over both sidewalls between 125 and 225 m. In these regions of increased stability, the mass in the slope flows turns and converges over the valley center. Slope winds over both sidewalls near the summits feed the developing heat lows over the ridges. Subsidence above the valley replaces the mass loss to these slope flows in the elevated divergence region over the valley center. Two eddies have formed over the corners of the valley floor with a larger one circulating over the more strongly heated slope. As the simulation continues, another stable pocket pair forms over the upper sidewalls at 350 m. By 100 minutes into the simulation (Figure 18c), the thermodynamic structure over the valley center has been altered in a similar manner to that in the reference simulation. The enhanced stability regions over the sidewalls force cross-valley convergence and destabilization of these layers over the valley center. Above these regions, divergence increases the stability in the overlying air as mass moves outward to feed the slope flows. Winds speeds over the upper sidewalls have reached 1.0 m/s by this time and the upslope extends down to 425 m. Slope flows in the CBL reach the capping stable layer with velocities averaging 0.5 m/s.

Although the gross features appear to be symmetric, one important difference between the two valley sides is observed. The regions of enhanced stability cutting off the slope winds are more stable over the north-facing wall than over the opposite slope. It appears that more intense heating over the south-facing wall has partially overcome the advective cooling.

Two separate circulations, similar to those formed in the reference simulation, develop as a result of the varying stability over the sidewalls. Below 325 m, converging mass in the valley center forces a middle level subsidence. The growing CBL entrains mass from the base of the stable layer and feeds the slope winds. Above the lower circulation a cross-valley outflow feeds the upslope winds over the upper sidewall, and descending warmer air replaces the diverging mass. After 120 minutes, the increased heating rate gives the upslope air enough buoyancy to penetrate the stable pockets over the sidewall and the separate circulations break down (Figure 18d). However, the distortions in the potential temperature profile over the valley center remain. While the 284 K isentrope is over 50 m lower than was initially, the inversion top has descended only slightly. Only slight asymmetries are evident in the fine structure of the valley atmosphere and still no large cross-valley differences can be observed. Although the heating rates over the south-facing wall are over 50% greater than over the opposite slope, the cross-valley potential temperature difference is less than 1 K. Slope velocities differ by less than 0.1 m/s and range between 1.0 m/s near the summits to 0.2 m/s over the center sections.

After 140 minutes have elapsed, the horizontal temperature gradients have diminished and the lapse rate through the stable layer is nearly

constant (Figure 18e). Cross-valley circulations have also decreased as the slope flows intensified. The heat low has produced an updraft region with speeds exceeding 1.0 m/s over the ridge as it draws air from above the valley. Slope winds flow from the sidewall base through the 200 m deep CBL and stable layer to the sidewall summit. Counter winds can be seen flowing immediately above the slope layers on both sidewalls. Twenty minutes later, the cumulative effect of these descending motions has been to lower the inversion top slightly (Figure 18f). Similar to the other runs, the locations of the organized downdrafts appear to change with time and the result is a time averaged subsidence of the stable core. The CBL has grown an additional 50 m by this time and has warmed to nearly 286 K. The ridge circulations have been transformed from convective cells into lateral accelerations toward the boundaries with wind speeds exceeding 2.0 m/s. Average subsidence rates over the valley center vary between 0.02 and 0.08 m/s as the stable layer begins its period of rapid descent.

The inversion top is located at the 425 m level 180 minutes after sunrise (Figure 18g) and is descending 0.06 m/s. Winds speeds in the slope flow average 2.0 m/s over the lower sidewall but decrease as the air moves toward the summit. At this point, early signs of the steady daytime circulation appear as a uniform subsidence in the neutral layer above the valley. For the first time, large asymmetries are apparent as cold advection resulting from the stronger slope winds over the south-facing slope have distorted the shape of the stable core. Figure 18h shows more effects of the differential heating 200 minutes after sunrise. The lower section of the south-facing slope is warmer than the opposite sidewall and generates a stronger slope flow. Over the upper sidewall,

however, advective cooling keeps the temperatures nearly equal on both sides of the valley. By this time, the top of the stable layer has descended to 375 m while the CBL has grown to 300 m. The heat lows over the ridges continue to accelerate mass toward boundaries with peak velocities near 4.0 m/s.

The steady daytime circulation begins to dominate the valley dynamics as the original inversion is nearly destroyed 220 minutes after the start of the simulation (Figure 18i). Wind speeds greater than 2.0 m/s extend over the length of both sidewalls. A near uniform subsidence over the valley center at all levels is obvious as the mass loss to the slope winds is replaced. Air in the valley center has warmed to nearly 290 K with the layers above the upper sidewalls and ridges reaching 291 K as the surface heating continues to grow stronger.

Figure 19 shows the average thermal structure over the valley center as the simulation progresses. There are only minor differences between the development in this simulation and the Case 1 structure. The closed circulations perturb the potential temperature field in the stable layer and result in the structure shown in the 100 minute profile. Of particular interest is the strongly stable layer between 375 and 425 m which has formed in response to the cross-valley divergence at this level. The low level convergence region over the valley center results in a 100 m deep unstable layer forming after 120 minutes which erodes the base of the stable layer. As in Case 1, the development of continuous slope flows marks the onset of cross-valley mixing and gravity wave propagation which together act to slowly smooth out the lapse rate through the stable layer. The stable layer then warms uniformly as it descends into the valley. After 220 minutes, the CBL approaches the top of the stable air and the inversion is destroyed.
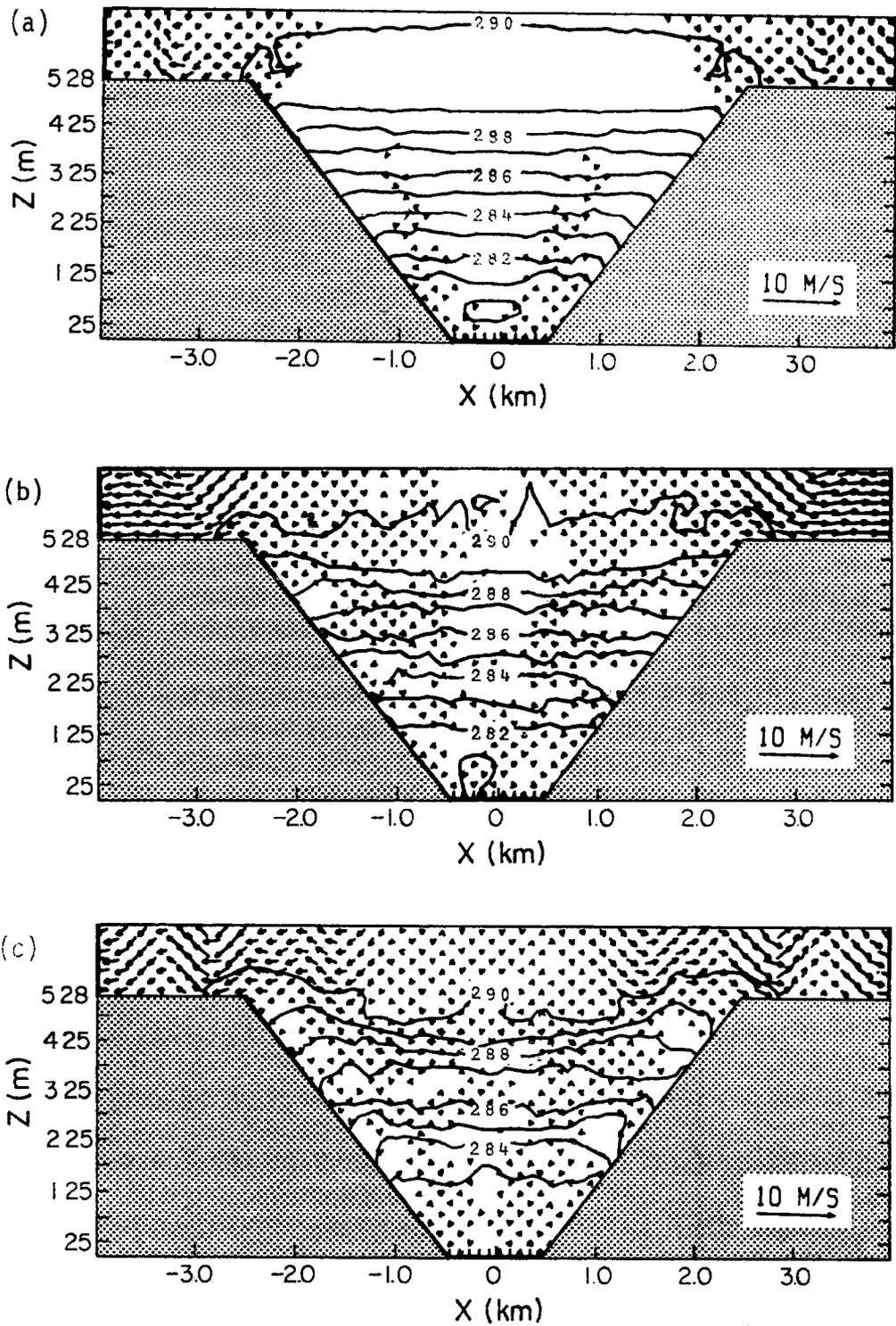
Figure 18a-c. Five minute average wind and potential temperature fields after (a) 60 min., (b) 80 min., and (c) 100 min. for Case 5.
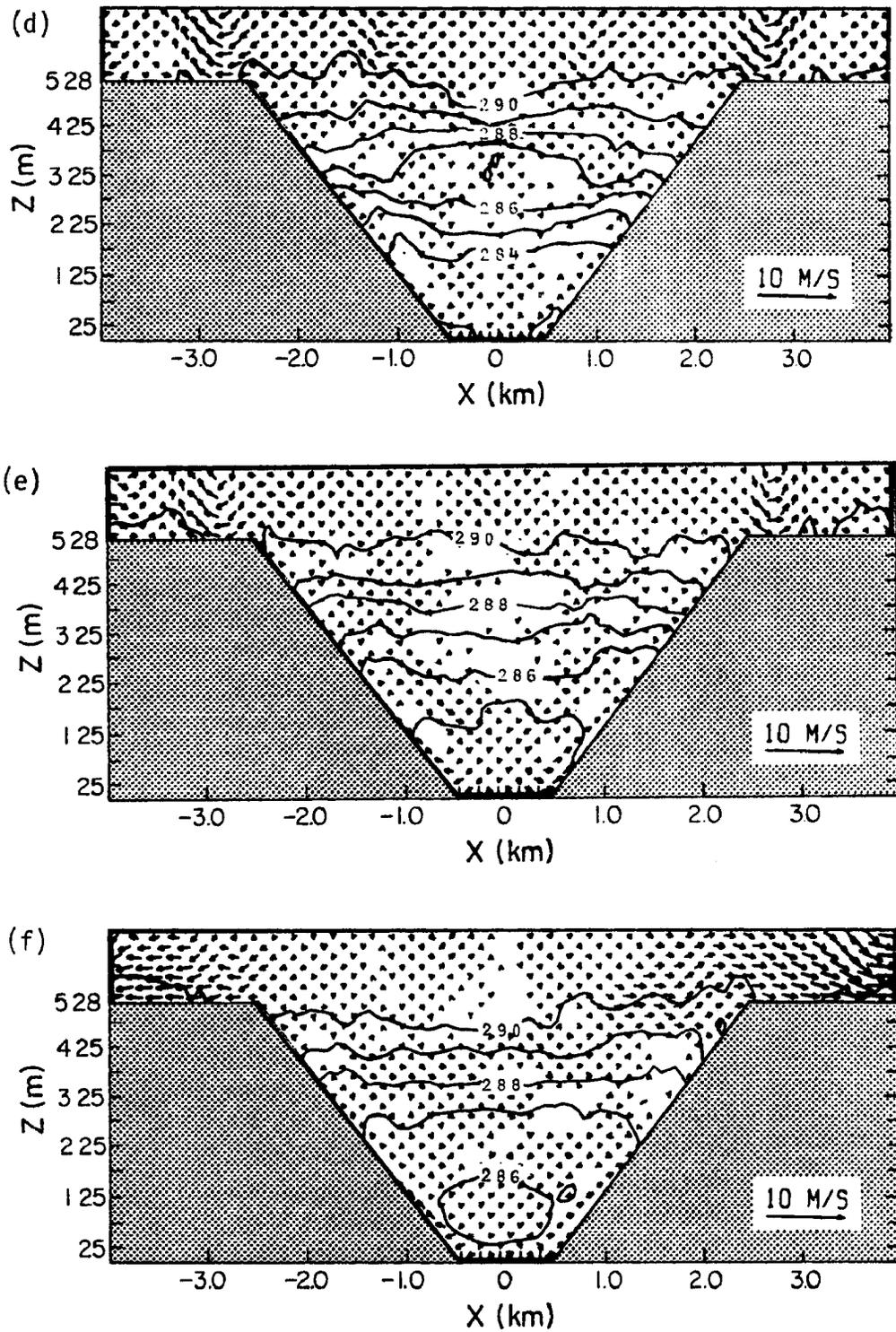
Figure 18d-f. Five minute average wind and potential tempera-
ture fields after (d) 120 min., (e) 140 min., and
(f) 160 min. for Case 5.
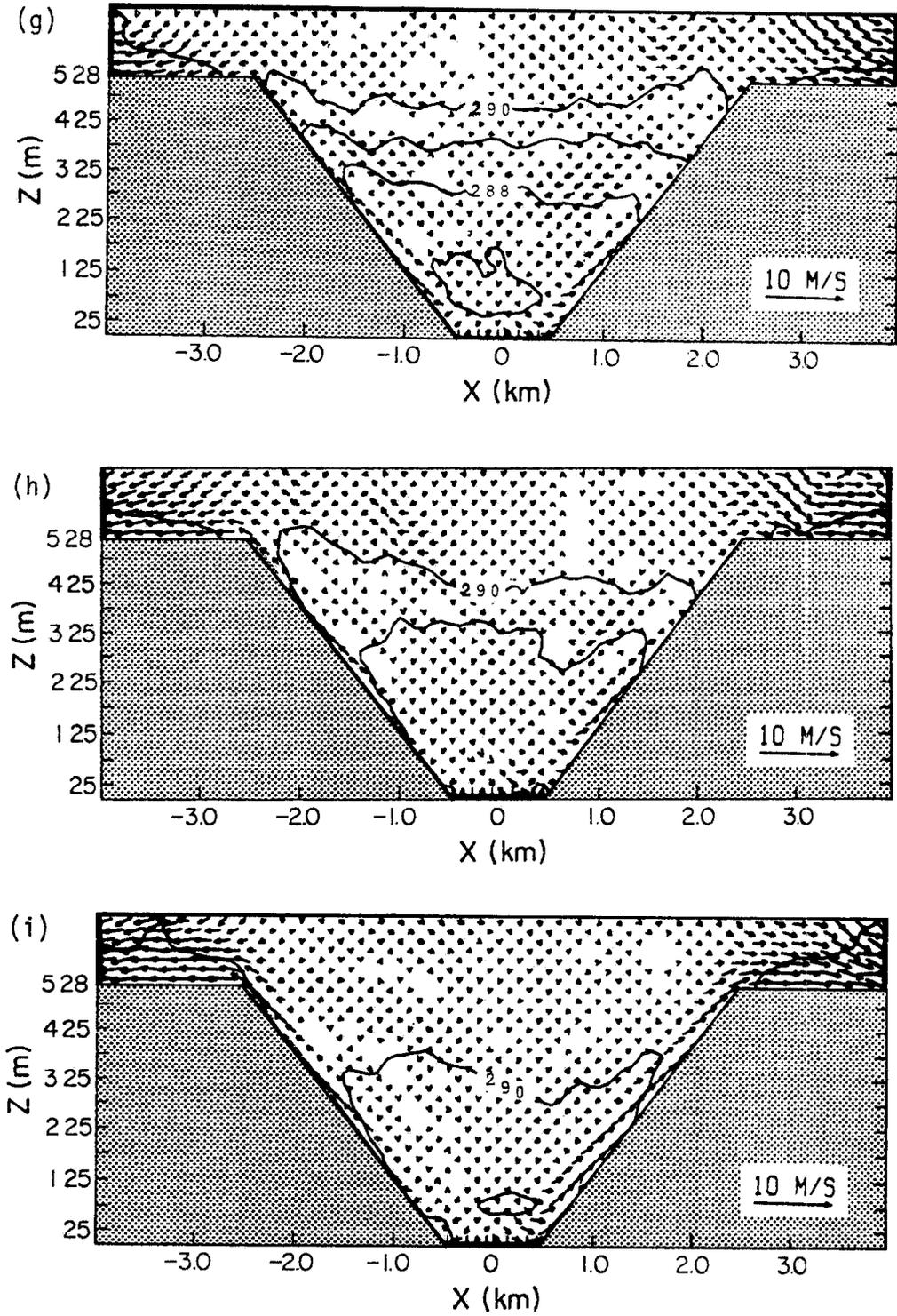
Figure 18g-i. Five minute average wind and potential temperature fields after (g) 180 min., (h) 200 min., and (i) 220 min. for Case 5.
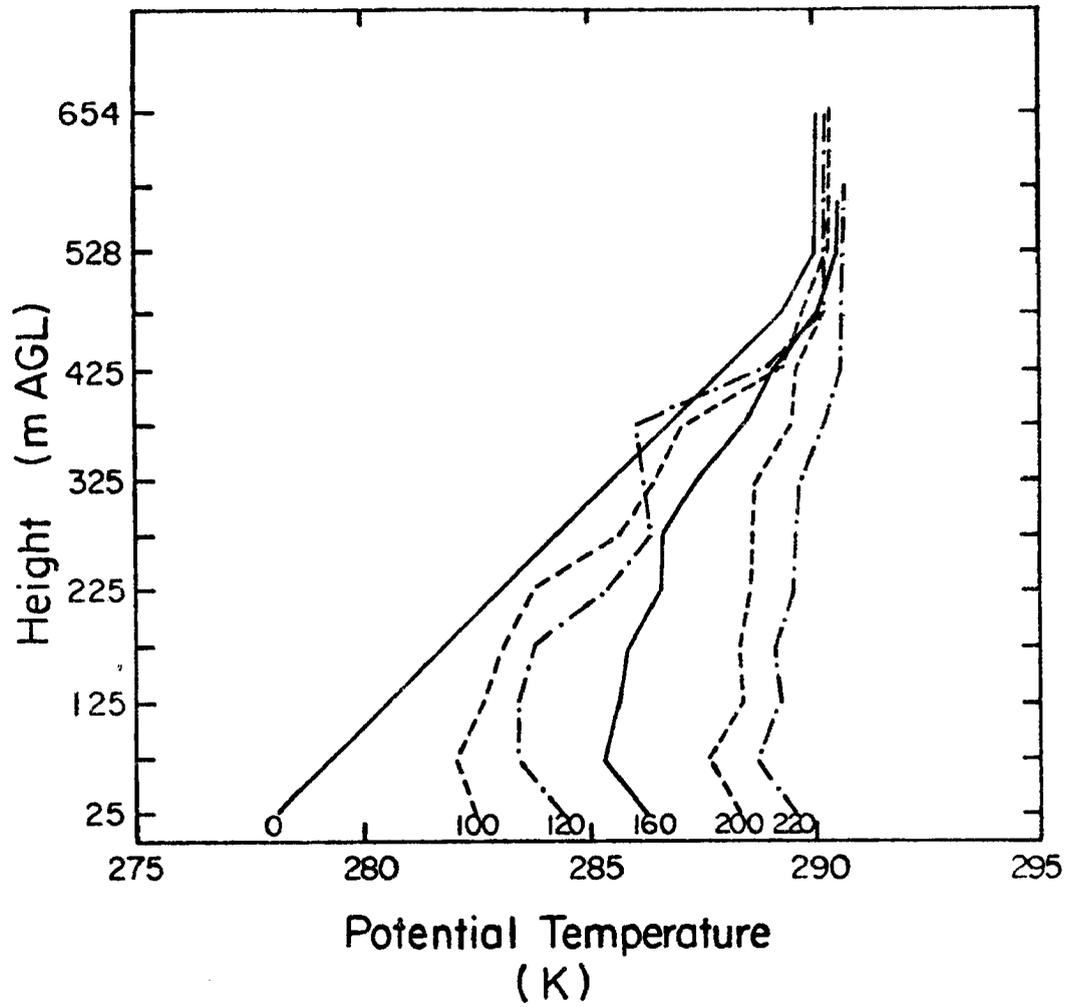
Figure 19. Ten minute average potential temperature
profiles over the valley center for Case 5.
Time in minutes shown below profiles.

4.6 Comparison of Model Results with Observations

Since this study was a theoretical evaluation of factors influenc-
ing valley boundary layer evolution, no attempt was made to simulate
the development in a particular valley. Nonetheless, two of the valleys
studied by Whiteman (1980) have characteristics similar to the model
valley used in the simulations. The Eagle River valley near Edwards,
Colorado, is 700 m deep at the observational site with sidewall angles
of 21° and 10°. This valley runs east-west and is 1.45 km wide at the
floor. The Yampa River valley directly east of Steamboat Springs,
Colorado, is 450 m deep and 2.58 km wide at the valley floor. At the
study site the valley is oriented north-south and the sidewalls meet
the floor at angles of 16° and 9°. The data collected in the program
were profiles of wind, temperature, wet-bulb temperature and pressure
taken over the middle of the valley using a tethered balloon sounding
system described by Morris et al. (1975).

Comparison of wind data was difficult because the winds in the
real valleys were dominated by the along valley flow, which, of course,
was not studied in the cross-valley simulations. The mean cross-valley
pressure gradients giving rise to the two-dimensional circulations are
very weak and are obscured in the high frequency disturbances initiated
by the transient gravity waves. For example, the maximum winds gener-
ated in the model simulations were approximately 4 m/s which built up
over a 500 m ridge during three hours simulated time. To achieve this
speed in one hour requires a pressure difference of only 5.6×10^{-3} mb
over the length of the ridge. On the other hand, transient gravity
wave gradients approach 1×10^{-4} mb/m. This fact is not totally un-
expected considering the nature of the orgins of the cross-valley

circulations. The forcing surface temperature flux is changing continuously but slowly and, therefore, acts on a time frame much longer than the time required for the atmosphere to compensate, characteristically the Brunt-Väisällä frequency. Since the winds were of thermal origin, examination of thermodynamic structures provided the best comparisons which could be made between the model and observational results.

Figure 20a shows data collected in the Eagle valley during the morning transition period on 12 October 1978 when the initial lapse rate and depth of the stable layer were similar to the model conditions. Sunrise was listed at 0717 LT and the initial sounding was recorded 0718 to 0728 LT. The next profile shows the state of the boundary layer approximately 70 minutes later. The stable layer appears to have warmed slightly and the shallow layer at the surface, which was originally much more stable than the rest of the valley air mass, has attained a lapse rate near that of the overlying air.

The next sounding was initiated approximately 120 minutes after the first and shows details revealed in the model simulations. A stable layer surmounts the 100 m deep CBL. Above this capping stable region lies a 100 m deep neutral layer, possibly formed by cross-valley convergence. Above this level is another enhanced stability region similar to the elevated divergence layers formed in the model simulations. The last profile was taken nearly 180 minutes after the first and shows the boundary layer in the last stages of transition as the daytime circulation begins to dominate the valley. The super-adiabatic CBL lies under a shallow, weakly stable layer which contains the remnants of the initial valley inversion.
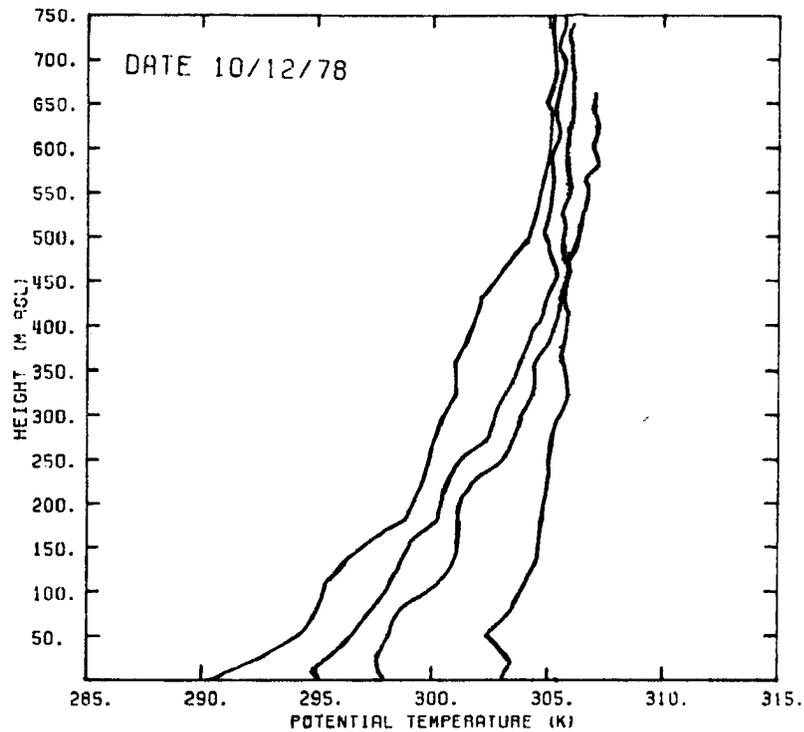
Figure 20a: Observations of potential temperature profiles in Eagle
River Valley at sunrise, sunrise + 70 min., sunrise +
120 min., and sunrise + 180 min.
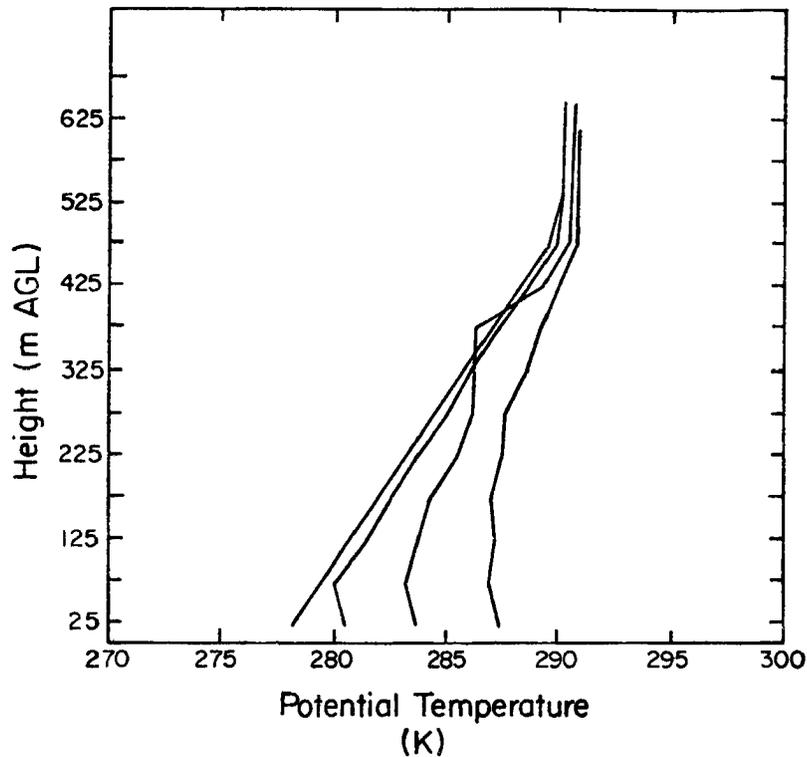
Figure 20b: Ten minute average potential temperature profiles from
Case 1 simulation for same times shown in Figure 20a.

Model soundings of the ten minute average potential temperature profiles over the valley center for the Case 1 simulation are shown in Figure 20b for comparison. The times of these profiles were chosen to match the observation times as closely as possible. Although this was not the case study, the similarity between the model results and the data is remarkable. The details of the model results were described previously and will not be repeated here.

Figure 21a shows the boundary layer development in the Yampa Valley on the morning of 9 August 1978. The pre-sunrise profile shows a more stable lower layer above the surface underlying a deeper layer with a weaker and more constant lapse rate. Like the Eagle valley case, this data set was chosen because the initial conditions closely resembled the model valley. In this observational study, the CBL grew rapidly and only limited descent of the inversion top occurred. Due to the initially strongly stable layer at the surface, the development proceeds slowly until 120 minutes after sunrise when the CBL begins to form (second profile). The next sounding shows the state of the valley 195 minutes after sunrise where the boundary layer has grown to nearly 275 m and the stable layer above has warmed slightly. The final sounding was taken about 250 minutes after sunrise when the inversion is nearly destroyed. For comparison, Figure 21b shows the instantaneous profiles of potential temperature for the wide valley (Case 4) simulation at approximately the same times the observations were made. Again, there are striking similarities in the details at the thermodynamic structure as the boundary layers develop. The CBL grows rapidly and to a large depth in the wide valley simulation, which correlates well with the observations.
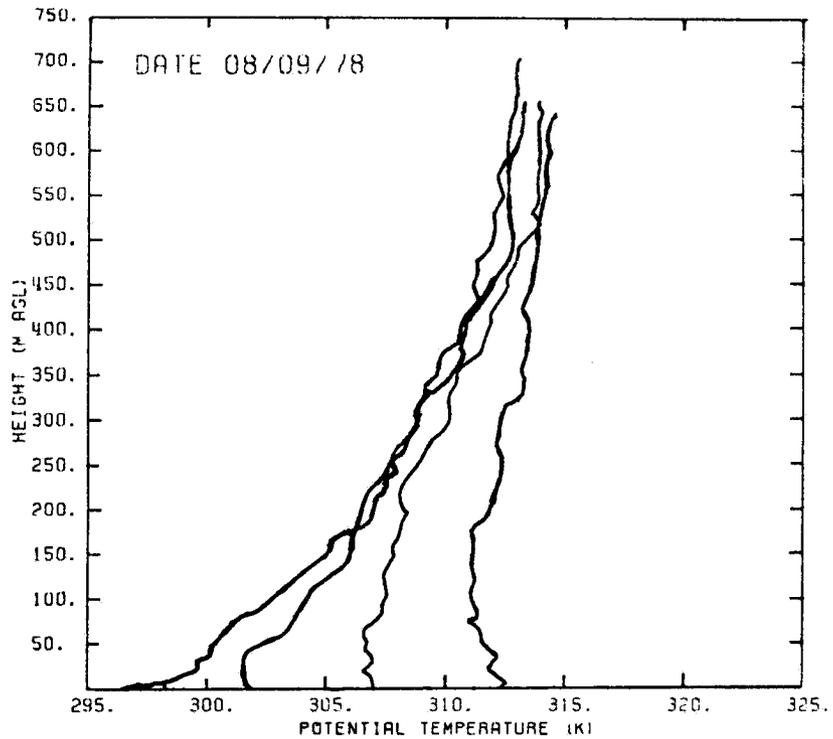
Figure 21a: Observations of potential temperature profiles in Yampa River Valley at sunrise, sunrise + 120 min., sunrise + 195 min., and sunrise + 250 min.
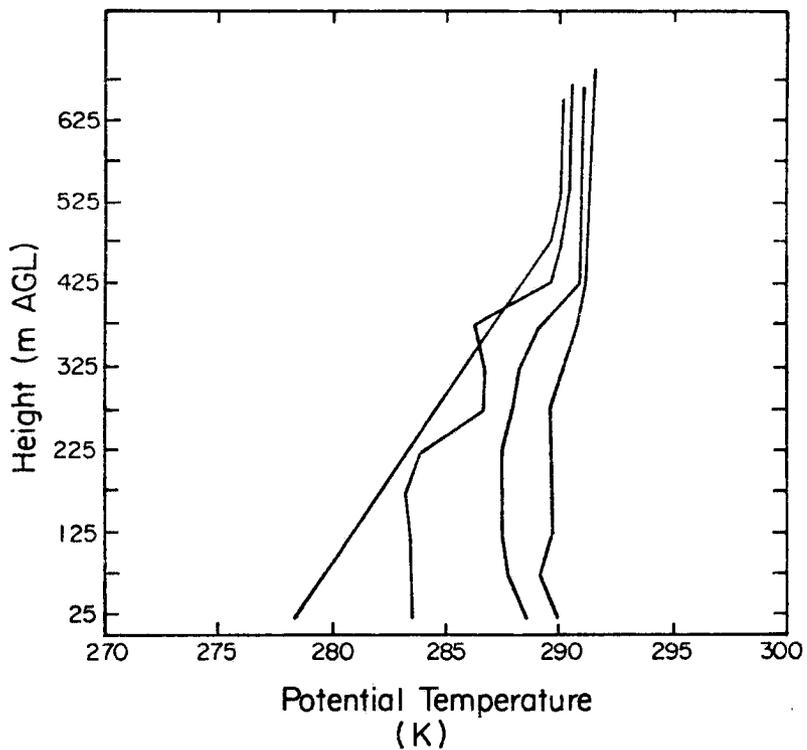
Figure 21b: Ten minute average potential temperature profiles from Case 4 simulation for sunrise, sunrise + 120 min., sunrise + 200 min., and sunrise + 240 min.

4.7 Analysis of Results

The influence of transient circulations lasting 30-60 minutes is important in the evolution of the thermodynamic structure in all of the model simulations. These circulations result from the formation of strongly stable pockets of air blocking the upslope flow in the early stages of boundary layer development. It appears that as the air adjacent to the slope is heated, it acquires buoyancy and starts to move up the sidewall. However, the parcels in the slope flows do not heat sufficiently to maintain their buoyancy as they move into the warmer layers. As a result, mass "piles up" at one elevation and forms the strongly stable pocket of air observed in the simulations. Air moving up the sidewalls in the slope flows encounters the stable pocket and rapidly loses its buoyancy as well. Eventually, as this process continues, the flow turns and converges in the valley center from both sdiewalls. Above the stable pockets, air flowing outward from the valley center replaces mass loss to the slope winds. The outflow from the middle of the valley is, in turn, compensated by the subsidence of warmer air from above. Uneven thermal stratification results from these dynamic processes with a near neutral layer underlying strongly stable region in the valley center and the reverse situation appearing over the sidewall.

The number, strength and time of formations of these stable pockets determine their effect on boundary layer development. In the reference case (Case 1), two separate circulations formed which caused the lower part of the valley to destabilize significantly while the upper part remained nearly unaffected. On the other hand, the entire stable core slowly destabilized in response to the development of many

smaller and weaker stable pockets as the Case 3 simulation proceeded. The other model runs showed effects similar to these two examples. Later in the morning, when the heating rate is greater, the parcels acquire enough buoyancy to penetrate the stable pockets and a continuous slope flow develops. At this point, gravity waves originating over the sidewalls propagate horizontally through the stable layer and smooth the lapse rate. The end result is a deep layer between the CBL and the overlying neutral layer which is significantly less stable than it was originally.

These transient circulations would be difficult to identify in an observational study that was not designed specifically to detect them. They exist on time and space scales which are too small for most instrumentation to resolve or produce effects which could easily be misinterpreted. For example, Whiteman (1980) assumed that the irregularly shaped potential temperature profiles he observed resulted from the instrument penetrating a thermal plume.

A second obstacle which may have caused researchers to be misled is the historical belief that a continuous slope flow formed over the length of the sidewall shortly after sunrise. The valley circulation theories mentioned in Chapter 2 are based on this assumption. Wagner's (1938) circulation required that mass diverging simultaneously at all levels be carried by the slope flows to the overlying neutral layer. As middle valley divergence proceeds, the stable core becomes increasingly more stable and the heating rate along the sidewall must increase rapidly to maintian the slope flow. This is unlikely in view of the slowly changing nature of any heating function dependent on the solar cycle. On the other hand, Scorer's (1958) conceptualization has mass

converging in the valley center at all levels as some air in the slope flows mixes horizontally. In this case, the stable core would slowly destabilize and allow the parcels heated over the sidewalls to retain their buoyancy through a deeper layer. However, it is a loss of buoyancy which causes the parcels to turn and flow into the valley center, thus producing an inherent problem in this theory. In order to compensate for this increase in buoyancy, either the heating rate must decrease, which is improbable, or the slope flow must accelerate rapidly to reduce contact time, a feature which is not observed. Whiteman's (1980) hypothesis concludes that there are no significant cross-valley circulations. All of the mass in the slope flows in his model originates in the CBL and is warmed to the neutral layer temperature as it travels up the sidewall. This process would be difficult to establish in the early morning hours when the heating rates are low and the temperature differences are large.

To a limited degree all of these processes are seen in the model simulations, with their development dependent on time and elevation. Early in the simulations, outflows from the valley center appear in layers above cross-valley convergence regions. Later in the morning, the valley atmosphere behaves much like Whiteman's conceptual model, where continuous slope flows transport mass from the CBL to the neutral layer above the valley.

Insight into the mechanisms controlling inversion destruction can be gained from comparisons between model runs. As expected, the strength of the surface heating has a great impact on the timing of inversion destruction. However, the details of the structure of the evolving valley atmosphere are not substantially affected. Although the amplitude of

the surface potential temperature flux was only half of the Case 1 value, the development of the Case 2 atmosphere paralleled the reference simulation except for a time lag. The elevation of the stable pocket development as well as the maximum depth and temperature of the CBL were nearly equal. Due to the sinusoidal nature of the heating function, the same amount of energy is transferred to the valley atmosphere in the six hours required to break the Case 2 inversion as is transferred in the Case 1 simulation in four hours.

The effects of relative heating distribution between the floor and sidewalls can be found by examining the differences between the Case 2 and Case 3 simulations. The total energy input to the valley was nearly the same for both runs and the initial inversion was destroyed in about the same time period. However, the details of the boundary layer development were dramatically different. In Case 2, where the floor is heated as strongly as the sidewalls, the lapse rate becomes more uniform after the continuous upslope wind is established 200 minutes after sunrise. After this time, cross-valley circulations diminish and the lapse rate remains constant until the inversion is destroyed. In the Case 3 simulations, where the reduced heating over the floor prevents a deep CBL from becoming established, stable pockets still form despite the presence of a continuous slope flow. As a result, part of the slope flow mass converged in the valley center at the elevations of the stable pockets. As many of these pockets formed and were later destroyed, the stable core slowly destabilized until the inversion was broken. This type of circulation is not surprising considering the large potential temperature difference between the CBL and neutral layer. The parcels cannot warm fast enough to maintain their buoyancy

in the slope flows and the dynamics are similar to those seen during the early stages of the other simulations. The slow destabilization continues until late in the transition period when the steady daytime circulation begins to dominate the dynamics.

The results of the wide valley (Case 4) simulation reveal the effects of valley width on boundary layer evolution. This valley displayed deeper CBL development than any of the narrow valley simulations. A sharp inversion formed as the CBL grew and entrained air from the base of the stable layer, much like mixed layer growth over flat terrain. This result is consistent with Whiteman's (1980) observations which showed that inversions in strongly heated wider valleys were broken in much the same way as nocturnal radiation inversions over the plains. This finding implies that the influence of slope processes on boundary layer evolution diminishes with distance from the sidewall. Observations taken during the early morning transition period in a broad, elevated basin show no evidence of inversion descent (Banta and Cotton, 1981), and further support this conclusion.

Perhaps the most surprising result of this study was the lack of any significant difference in boundary layer structure between the Case 1 and Case 5 simulations. It was thought that the imposition of the middle latitude heating distribution would affect the evolution of the valley atmosphere. However the development of the thermodynamic structure over the valley center was nearly identical for the two runs, despite the dramatic differences in the distribution of potential temperature flux from the sidewalls. From this result, it appears that although relative contributions of heat between sidewalls and valley

floor are important in boundary layer structure, the redistribution of heat between sidewalls does not have a major influence. The model atmosphere did not tolerate large horizontal potential temperature gradients and reacted quickly to communicate disturbances through gravity wave interactions.

5.0 CONCLUSIONS AND SUGGESTIONS FOR FUTURE RESEARCH

5.1 Conclusions

It has been shown that the CSU Multidimensional Cloud/Mesoscale Model is capable of simulating the morning transition period in narrow mountain valleys. The model accurately reproduces the cross-valley features of morning inversion destruction which were observed in actual valleys. A neutral layer grows under the initially surface based stable air mass and forms a CBL over the heated surfaces. Upslope winds are initiated in sections over the sidewalls shortly after sunrise, but do not become continuous until later in the morning when the heating rate increases. After this occurs, the slope flows carry mass from the CBL to the neutral layer above the valley and the inversion top slowly descends.

In addition, the model results give insight into the microscale physical processes which produce the observed phenomena. Transient circulations which last from 30-60 minutes have a significant role in boundary layer evolution. These patterns develop as very stable pockets of air form overthe sidewall which cannot be penetrated by the upslope flow. As a result, cross-valley circulations develop which create alternating layers of converging and diverging flows in the valley center. The thermodynamic structure is dramatically changed as these flows continue and a variable lapse rate is produced. Once a continuous slope flow is established, the lapse rate of the stable layer becomes more uniform. As this point, the cross-valley circulations diminish and the lapse rate through the stable air mass is much weaker than it was initially.

93

Heat is rapidly redistributed laterally by horizontal mixing and by gravity waves propagating through the stable layer. These disturbances are initiated over the sidewalls where surface heating continually perturbs the overlying air. Large horizontal temperature gradients never can form as these interactions act rapidly to break down even small gradients. This result implies that other scalar quantities, such as moisture and pollutant materials, may be similary diffused rapidly in a horizontal plane above the valley floor. Further, differences in heating rates over opposing sidewalls do not substantially affect boundary layer evolution due to this rapid redistribution.

Heating rates and distribution affect the transition process in a number of ways. Total time required for the valley atmosphere to reach its steady daytime state, typically 3-6 hours after sunrise, depends on total energy input and is unaffected by distribution. However, the structure of the evolving boundary layer is greatly changed when the heat flux form the floor is too weak to establish a deep CBL. This layer is crucial to the formation of the continuous upslope wind, observed 2½-5 hours after sunrise, because the initial heating it provides allows the parcels to remain buoyant longer. This in turn influences the stable layer structure as a continuous upslope flow is important in inhibiting the development of uneven thermal stratification within the stable air. CBL development is also affected by valley width. In wider valleys, deeper CBL development occurs over the valley center where the thermodynamic and dynamic influences of the sidewalls are not as significant.

The results of this research will be useful in other phases of the mountain valley study. They will aid in planning future field programs

in which emphasis will be placed on observation of the controlling microscale processes. Along these same lines, interpretation of existing field data will be easier if comparisons are made to the model results. Also, this type of model study can be helpful in identifying potential air quality problems in valleys in which future development is anticipated.

5.2 Suggestions for Future Research

This highly successful modelling program could be continued to explore other facets of the valley inversion phenomenon. In its present form, the model could be used to examine the effects of sidewall slope, orientation and initial atmospheric stability on the inversion destruction process. With minor modifications, particularly the inclusion of a surface radiation budget, two-dimensional simulations could be run to determine the dominant processes controlling the nocturnal phase of the diurnal cycle, when the stable layer develops. Additionally, passive tracers could be introduced to quantify the dispersion properties of the valley boundary layer. This report leaves unanswered the question of how the along-valley processes interact with the cross-valley thermodynamic and dynamic structures. An existing three-dimensional version of the model could be adapted and run to give insight into this problem as well.

REFERENCES

Ayer, H.S., 1961: On the dissipation of drainage wind systems in valleys in morning hours. J. Meteor., 18, pp. 560-563.

Ball, F.K., 1960: Control of inversion height by surface heating. Quart. J. Roy. Meteor. Soc., 86, pp. 483-494.

Banta, R., and W.R. Cotton, 1979. Horizontal and vertical structure of diurnal boundary layer flow patterns over mountainous terrain. Preprint Volume, Fourth Symposium on Turbulence, Diffusion, and Air Pollution, January 15-18, 1979, Reno, Nevada. Published by American Meteorological Society, Boston, MA, pp. 217-224.

Banta, R. and W.R. Cotton, 1981: An analysis of the structure of local wind systems in a broad mountain basin. To appear in J. Appl. Meteor., 20 (11).

Carroll, J.J. and R.L. Baskett, 1979: Dependence of air quality in a remote location on local and mesoscale transports: A case study. J. Appl. Meteor., 18, pp. 474-486.

Clark, T.L., 1977: A small-scale dynamic model using a terrain following coordinate transformation. J. Comp. Physics, 24, pp. 186-215.

Cotton, W.R., 1975: On parameterization of turbulent transport in cumulus clouds. J. Atmos. Sci., 32, pp. 548-564.

Cotton, W.R. and G.J. Tripoli, 1978: Cumulus convection in shear flow--three dimensional numerical experiments. J. Atmos. Sci., 35, pp. 1503-1521.

Davidson, B., 1961: Valley wind phenomena and air pollution problems. J. Air Poll. Cntl. Assoc., 11, pp. 364-368.

Davidson, B. and P.K. Rao, 1958: Preliminary report on valley wind studies in Vermont, 1957. Final report, Contract AF 19(604)-1971, AFCRC-TR-58-29, College of Engineering, New York University, 54 p.

Davidson, B. and P.K. Rao, 1963: Experimental studies of the valley-plain wind. Int. J. Air Water Pollut., 7(9/10), pp. 907-923.

Deardorff, J.W., 1974: Three dimensional numerical study of the height and mean structure of a heated planetary boundary layer. Boundary-Layer Meteor., 7, pp. 81-106.

Defant, F., 1949: Zur theorie der hangwinde, nebst bermerkungen zur theorie der berg- und talwinde. Arch. Meteor. Geophys. Bioklimat., Ser. A., 1(3-4), pp. 421-450.

Defant, F., 1951: Local winds. Compendium of Meteorology, T.M. Malone, Ed., Boston, American Meteorological Society, pp. 655-672.

Dickerson, M.H. and Gudiksen, P.H., 1980: The Department of Energy's atmospheric studies in complex terrain program. Preprint volume. Second Joint Conference on Applications of Air Pollution Meteorology, March 24-27, 1980, New Orleans, LA. Published by the American Meteorological Society, Boston, MA.

Dirks, R.A., 1969: A theoretical investigation of convective patterns in the lee of the Colorado Rockies. Atmospheric Science Paper No. 145, Colorado State University, Fort Collins, CO, 122 p.

Flohn, H. (Ed.), 1969: World Survey of Climatology, Vol. 2. Elsevier Publishing Co., New York, NY, 266 p.

Fosberg, M.A., 1967: Numerical analysis of convection over a mountain ridge. J. Appl. Meteor., 6, pp. 889-904.

Fox, D.G., G. Wooldridge, T. McKee, and D. Whiteman, 1976: An experimental study of mountain meteorology. Preprint volume, Third Symposium on Atmospheric Turbulence, Diffusion and Air Quality, October 19-22, 1976, Raleigh, NC. Published by the American Meteorological Society, Boston, MA.

Gal-Chen, T. and R.C.J. Somerville, 1975a: On the use of a coordinate transformation for the solution of the Navier-Stokes equations. J. Comp. Physics, 17, pp. 209-228.

Gal-Chen, T. and R.C.J. Somerville, 1975b: Numerical solution of the Navier-Stokes equations with topography. J. Comp. Physics, 17, pp. 276-310.

Geiger, R., 1965: The Climate Near the Ground. Harvard University Press, Cambridge, Mass., 494 p.

Gleeson, T.A., 1951: On the theory of cross-valley winds arising from differential heating of the slopes. J. Meteor., 8(6), pp. 398-405.

Gleeson, T.A., 1953. Effects of various factors on valley winds. J. Meteor., 10(4), pp. 262-269.

Hahn, D.C., 1981: Observed characteristics of turbulence in the atmospheric boundary layer over mountainous terrain. Atmos. Sci. Paper No. 332, Colorado State University, Fort Collins, CO, 104 p.

Hawkes, H.B., 1947: Mountain and valley winds with special reference to the diurnal mountain winds of the Great Salt Lake region. Ph.D. dissertation, Ohio State University, 312 p.

Holton, J.R., 1977: An Introduction to Dynamic Meteorology. New York, Academic Press, 319 p.

Holzworth, G.C., 1980: The EPA program for dispersion model development for sources in complex terrain. Preprint volume, Second Joint Conference on Applications of Air Pollution Meteorology, March 24-27, 1980, New Orleans, LA. Published by the American Meteorological Society, Boston, MA.

Hughes, R.L., 1978: A numerical simulation of mesoscale flow over mountainous terrain. Atmos. Sci. Paper No. 303, Colorado State University, Fort Collins, CO, 123 p.

Klemp, J.B. and R.B. Wilhelmson, 1978: Simulation of three-dimensional convective storm dynamics. J. Atmos. Sci., 35, pp. 1070-1096.

Kuo, H.L. and W.Y. Sun, 1976: Convection in the lower atmosphere and its effects. J. Atmos. Sci., 33, pp. 21-39.

Lenschow, D.H. and P.L. Stephens, 1980: The role of thermals in the convective boundary layer. Boundary-Layer Meteor., 19, pp. 511-532.

Lenschow, D.H., B.B. Stankov and L. Mahrt, 1979: The rapid morning boundary layer transition. J. Atmos. Sci., 36(11), pp. 2108-2124.

Lilly, D.K., 1964: Numerical solutions for the shape preserving two dimensional convection element. J. Atmos. Sci., 21, 83-98.

Lilly, D.K., 1968. Models of cloud-topped mixed layers under a strong inversion. Quart. J. Roy. Meteor. Soc., 94, pp. 292-309.

Louis, J., 1979: A parametric model of vertical eddy fluxes in the atmosphere. Boundary-Layer Meteor., 17, pp. 187-202.

Malkus, J.S. and G. Witt, 1959: The evolution of a convective element: A numerical calculation. The Atmosphere and Sea in Motion. The Rockefeller Institute Press, New York, NY, pp. 425-439.

Moll, E., 1935: Aerologische Unterschung periodischer Gebirgswinde in V-förmigen Alpentälern. Beitr. Physik fr. Atmos., 22(3), pp. 177-197.

Morris, A.L., D.B. Call, and R.B. McBeth, 1975: A small tethered balloon sounding system. Bull. Amer. Meteor. Soc., 56(9), pp. 964-969.

Ogura, Y., 1962: Convection of isolated masses of a buoyant fluid: A numerical calculation. J. Atmos. Sci., 19, pp. 492-502.

Ogura, Y. and N.A. Phillips, 1962: Scale analysis of deep and shallow convection in the atmosphere. J. Atmos. Sci., 14, pp. 173-179.

Orlanski, I., 1975: A rational subdivision of scales for atmospheric processes. Bull. Amer. Meteor. Soc., 56, pp. 527-530.

Orlanski, I., 1976: A simple boundary condition for unbounded hyperbolic flows. J. Comp. Physics, 21, pp. 251-269.

Orville, H.D., 1964: On mountain upslope winds. J. Atmos. Sci., 21, pp. 622-633.

Pielke, R.A., 1974: A survey of fine-mesh modeling techniques Open SESAME, D.K. Lilly, Ed., National Oceanic and Atmospheric Administration, Boulder, CO, pp 219-232.

Pielke, R.A. and Y. Mahrer, 1975: Representation of the heated planetary boundary layer in mesoscale models with coarse vertical resolution. J. Atmos. Sci., 32, pp. 2288-2308.

Prandtl, L., 1942: Flow Theory. Verlay Vieweg and Sohn, Brunswick, pp. 367-375.

Raymond, D. and W. Wilkening, 1980: Mountain-induced convection under fair weather conditions. J. Atmos. Sci., 37, pp. 2693-2706.

Reid, J.D., 1976: Dispersion in a mountain environment. Atmos. Sci. Paper No. 253, Colorado State University, Fort Collins, CO, 150 p.

Revfeim, K.J.A., 1976: Solar radiation at the site of known orientation on the earth's surface. J. Appl. Meteor., 15, pp. 651-656.

Scorer, R.S., 1958: Natural Aerodynamics. Pergamon Press, 313 p.

Start, G.E., C.R. Dickson and L.L. Wendell, 1975: Diffusion in a canyon within rough mountainous terrain. J. Appl. Meteor., 14, pp. 333-346.

Stull, R.B., 1973: Inversion rise model based on penetrative convection. J. Atmos. Sci., 30, pp. 1092-1099.

Stull, R.B., 1976: Mixed-layer depth model based on turbulent energetics. J. Atmos. Sci., 33, pp. 1268-1278.

Sundararajan, A. and S.A. Macklin, 1976: Comments on the heat flux and friction velocity in free convection near the ground. J. Atmos. Sci., 33, pp. 715-718.

Tang, W., 1976: Theoretical study of cross-valley wind circulation. Arch. Meteor. Geophys. Bioklimat., Ser. A, 25, pp. 1-18.

Tennekes, H., 1970: Free convection in the turbulent Ekman layer of the atmosphere. J. Atmos. Sci., 27, pp. 1027-1034.

Tennekes, H., 1973: A model for the dynamics of the inversion above a convective boundary layer. J. Atmos. Sci., 30, pp. 558-567.

Thyer, N.H., 1966: A theoretical explanation of mountain and valley winds by a numerical method. Arch. Meteor. Geophys. Bioklimat., Ser. A, 15(3-4), pp. 318-348.

Tripoli, G.J., 1981: A lateral boundary condition for cumulus models which simulates the mesoscale response to convection. Preprint volume, Fifth Conference on Numerical Weather Prediction, November 2-6, 1981, Monterey, CA. Published by the American Meteorological Society, Boston, MA.

Tripoli, G.J. and W.R. Cotton, 1981: The Colorado State University three-dimensional cloud/mesoscale model--1981. Part I: General theoretical framework. To be submitted to J. de Rech. Atmos.

Tripoli, G.J. and W.R. Cotton, 1980: A numerical investigation of several factors contributing to the observed variable intensity of deep convection over south Florida. J. Appl. Meteor., 19, pp. 1032-1063.

Wagner, A., 1938: Theorie und beobachtung der periodischen gebirgswinde. Gerlands Beitr. Geophys. (Leipzig), 52, pp. 408-449.

Warner, J. and J.W. Telford, 1967: Convection below cloud base. J. Atmos. Sci., 24, pp. 374-382.

Wetzel, P.J., 1978: A detailed parameterization of the atmospheric boundary layer. Atmos. Sci. Paper No. 302, Colorado State University, Fort Collins, CO, 195 p.

Whiteman, C.D., 1980: Breakup of temperature inversions in Colorado mountain valleys. Atmos. Sci. Paper No. 328, Colorado State University, Fort Collins, CO, 250 p.

Whiteman, C.D. and T.B. McKee, 1977: Observations of vertical atmospheric structure in a deep mountain valley. Arch. Meteor. Geophys. Bioklimat., Ser. A, 26, pp. 39-50.

Whiteman, C.D. and T.B. McKee, 1978: Air pollution implications of inversion descent in mountain valleys. Atmos. Environ., 12, pp. 2151-2158.

Whiteman, C.D. and T.B. McKee, 1980: A time-dependent model of temperature inversion structure in mountain valleys. Proceedings, AMS/APCA Second Joint Conference on Applications of Air Pollution Meteorology. March 24-27, 1980, New Orleans, LA. Published by the American Meteorological Society, Boston, MA.

Wilczak, J.M. and J.E. Tillman, 1980: The three-dimensional structure of convection in the atmospheric surface layer. J. Atmos. Sci., 37, pp. 2424-2443.

Zeman, O., and J.L. Lumley, 1976: Modeling buoyancy driven mixed layers. J. Atmos. Sci., 33, pp. 1974-1988.

16. Abstracts

A dry, two-dimensional version of the Colorado State University Multi-Dimensional Cloud/Mesoscale Model was used to simulate the cross-valley dynamic and thermodynamic structure in deep mountain valleys during the morning transition period when the nocturnal inversion is destroyed.

Five simulations were run to examine the effects of valley width, heating distribution and heating rate on the development of the valley boundary layer. The model realistically reproduced the gross features found in actual valleys in both structure and timing. The simulated inversions were destoryed 3½ - 6 hours after sunrise as a result of a neutral layer growing up from the surface meeting a descending inversion top.

All cases revealed the development of strongly stable pockets of air over the sidewalls which form when cold air advected up the slope loses its buoyancy at higher elevations. These stable pockets temporarily block the slope flow and force transient cross-valley circulations to form which act to destabilize the valley boundary layer. Gravity waves acting in conjunction with horizontally travelling eddies and organized cross-valley circulations rapidly redistribute heat across the valley to prevent large horizontal potential temperature gradients from forming. As a result, even large differences in heating rates between opposing sidewalls do not result in significant cross-valley potential temperature differences. Higher surface albedos reulsted in a longer transition period with inversion destruction time dependent on total energy input to the valley atmosphere. The case in which a very high surface albedo over the valley floor prevented the growth of a deep neutral layer, the lapse rate through the stable layer slowly decreased as the inversion top descended. Boundary layers in wider valleys are less influenced by sidewall effects and behave much like boundary layers over flat terrain. Widening the model valley from 1 km to 2 km at the floor produced a 100 m increase in neutral layer depth after two hours.

17 Key Words:

Mountain valley inversion
Complex terrain flow model
mountain boundary layers

17c. COSATI Field/Group